EXPERIMENTAL INVESTIGATION AND PERFORMANCE ANALYSIS OF NANO ENHANCED PHASE CHANGE MATERIAL BASED PHOTOVOLTAIC THERMAL SYSTEM

MOHAMMED MOINUL ISLAM

INSTITUTE FOR ADVANCED STUDIES
UNIVERSITI MALAYA
KUALA LUMPUR

2022

EXPERIMENTAL INVESTIGATION AND PERFORMANCE ANALYSIS OF NANO ENHANCED PHASE CHANGE MATERIAL BASED PHOTOVOLTAIC THERMAL SYSTEM

MOHAMMED MOINUL ISLAM

THESIS SUBMITTED IN FULFILMENT OF THE REQUIREMENTS FOR THE DEGREE OF DOCTOR OF PHILOSOPHY

INSTITUTE FOR ADVANCED STUDIES
UNIVERSITI MALAYA
KUALA LUMPUR

2022

UNIVERSITI MALAYA

ORIGINAL LITERARY WORK DECLARATION

Name of Candidate: **Mohammed Moinul Islam**
Matric No: **17057828/1** (new); **HHD150006** (old)
Name of Degree: **Doctor of Philosophy (PhD)**

Title of Thesis ("this Work"): **Experimental Investigation and Performance Analysis of Nano Enhanced Phase Change Material based Photovoltaic Thermal System**

Field of Study: **Electricity and Energy**

I do solemnly and sincerely declare that:

(1) I am the sole author/writer of this Work;
(2) This Work is original;
(3) Any use of any work in which copyright exists was done by way of fair dealing and for permitted purposes and any excerpt or extract from, or reference to or reproduction of any copyright work has been disclosed expressly and sufficiently and the title of the Work and its authorship have been acknowledged in this Work;
(4) I do not have any actual knowledge nor do I ought reasonably to know that the making of this work constitutes an infringement of any copyright work;
(5) I hereby assign all and every rights in the copyright to this Work to the University of Malaya ("UM"), who henceforth shall be owner of the copyright in this Work and that any reproduction or use in any form or by any means whatsoever is prohibited without the written consent of UM having been first had and obtained;
(6) I am fully aware that if in the course of making this Work, I have infringed any copyright whether intentionally or otherwise, I may be subject to legal action or any other action as may be determined by UM.

    Candidate's Signature   Date: 14/07/2022

Subscribed and solemnly declared before,

    Witness's Signature   Date:

Name:

Designation:

EXPERIMENTAL INVESTIGATION AND PERFORMANCE ANALYSIS OF NANO ENHANCED PHASE CHANGE MATERIAL BASED PHOTOVOLTAIC THERMAL SYSTEM

ABSTRACT

Photovoltaic systems suffer from a paradoxical problem that they need sun light for their operation, but their performance abates with increasing temperature. Commercially available photovoltaic modules (PV) converts less than 20% of the approaching solar energy into power, the rest being dissipated as heat which further affects the conversion efficiency of the module by augmenting its temperature. Co-generation of electricity and heat from a single module, known as photovoltaic thermal (PVT) module, offers a hands-on solution to this problem. However, the major shortcoming with PVT collectors consists in its inefficacy in heat removal and storage of mostly employed heat transfer fluids (HTF) – air and water. As such both fluids suffer from low thermal conductivity and poor specific heat, PVT/air and PVT/water collectors cannot achieve a sustained low cell temperature with considerable electrical efficiency. Phase change materials (PCM) having very good latent heat capacity can be used for thermal control of these collectors, but their poor thermal properties turns out to be barrier in effective heat removal. Hence, incorporation of highly conductive nanoparticles such as carbon nanotube may offer a credible solution to this problem. In the present research, multi-walled carbon nanotube (MWNT) has been used to develop a very new nano enhanced PCM (NePCM) and thus apply this composite material in PVT systems to achieve better thermal control through enhanced thermal properties. Four NePCMs with concentration of functionalized MWNT (f-CNT) ranging from 0.25%wt to 0.01%wt have been synthesized. Detailed characterization of these nano composite materials has been performed by field emission scanning electron microscopy (FESEM), differential scanning calorimetry (DSC), thermogravimetric analysis (TGA) and Fourier transform

infrared (FTIR) spectroscopy and thermal conductivity analysis. With a 3% increase in heat storage capacity and 15% upsurge in thermal conductivity NePCM RT44HC-0.01%fCNT has been confirmed as the best nano composite material for photovoltaic thermal application. Hence, this NePCM has been integrated with a commercially popular parallel-flow PVT and real-time performance of this PVT-NePCM system has been investigated in the outdoor conditions of Kuala Lumpur, Malaysia. To observe whether PVT-NePCM system perform better than other conventional PV and PVT systems four other panels, viz., a reference PV, a PVT with same collector design, a PV-PCM and a PVT-PCM system have been erected in line with the novel PVT-NePCM system to ensure the same ambience. All operating and ambient parameters (different temperatures, solar irradiance, HTF flow rate, wind speed, etc.) have been measured and recorded concurrently by digital data acquisition system from June to September 2019. Thermal performance has been analyzed from both energy and exergy viewpoints. Results show that PVT-NePCM system achieved, at least, 4°C lower cell temperature than other systems and it operates with an energy efficiency of 85.3% and exergy efficiency of 13%. Moreover, PVT-NePCM system extends the cooling period of the solar cells by 37.5% as compared with PVT only system. Extensive application of such system can abate dependence on fossil fuels and help to improve the environment as well.

Keywords: Solar energy; photovoltaic thermal (PVT); nano enhanced phase change material (NePCM); real-time performance investigation; energy-exergy analysis.

PENYELIDIKAN EKSPERIMEN DAN ANALISIS PRESTASI BAHAN PERUBAHAN FASA NANO YANG DITINGKATKAN BERASASKAN SISTEM THERMAL FOTOVOLTAIK

ABSTRAK

Sistem fotovoltaik mengalami masalah paradoks dimana system ini memerlukan cahaya matahari untuk beroperasi, tetapi prestasinya berkurang dengan peningkatan suhu. Modul fotovoltaik (PV) komersial hanya mampu mengubah kurang kurang daripada 20% tenaga suria kepada tenaga elektrik, selebihnya akan hilang sebagai haba yang seterusnya mempengaruhi kecekapan penukaran modul dengan penambahan suhunya. Penjanaan bersama elektrik dan haba dari satu modul, yang dikenali sebagai modul termal fotovoltaik (PVT), menawarkan penyelesaian langsung untuk masalah ini. Walau bagaimanapun, kekurangan utama pengumpul PVT adalah berkaitan dengan ketidakcekapan dalam pemindahan haba dan penyimpanan cecair pemindahan haba (HTF) yang kebanyakannya digunakan di udara dan air. Oleh kerana itu, kedua-dua bendalir mengalami kekonduksian terma rendah dan haba spesifik yang buruk, pengumpul PVT / udara dan PVT / air tidak dapat mencapai suhu sel rendah yang berterusan dengan kecekapan elektrik yang tinggi. Walaupun bahan perubahan fasa (PCM) dapat menawarkan penyelesaian yang boleh dipercayai untuk masalah penyimpanan haba kerana bahan-bahan ini mempunyai kapasiti panas pendam yang sangat baik, sifat haba yang buruk menghalang penyingkiran haba yang berkesan dari modul. Penggabungan nanopartikel yang sangat konduktif seperti nanotube karbon boleh menawarkan penyelesaian yang boleh dipercayai untuk masalah ini. Dalam penyelidikan ini, nanotube karbon multi-dinding (MWNT) telah digunakan untuk mengembangkan PCM nano yang sangat baru (NePCM) dan dengan demikian dapat diterapkan bahan komposit ini di dalam sistem PVT untuk mencapai kawalan terma yang lebih baik melalui sifat terma yang dipertingkatkan. Empat NePCM dengan

kepekatan MWNT fungsional (f-CNT) mulai dari 0,25%wt hingga 0,01%wt telah disintesis. Pencirian terperinci bahan komposit nano ini telah dilakukan dengan mikroskopi elektron pengimbasan pelepasan medan (FESEM), kalorimetri imbasan pembezaan (DSC), analisis termogravimetrik (TGA) dan Fourier transformasi inframerah (FTIR) spektroskopi dan analisis kekonduksian terma. Dengan peningkatan kapasiti penyimpanan haba sebanyak 3% dan peningkatan kekonduksian terma sebanyak 15%, NePCM RT44HC-0,01% fCNT telah disahkan sebagai bahan komposit nano terbaik untuk aplikasi termal fotovoltaik. Oleh itu, NePCM ini telah disatukan dengan PVT aliran selari yang terkenal secara komersial dan prestasi masa nyata sistem PVT-NePCM ini telah diselidik di persekitaran luaran Kuala Lumpur, Malaysia. Untuk memerhatikan sama ada sistem PVT-NePCM bekerja lebih baik daripada sistem PV dan PVT konvensional yang lain, empat panel lain iaitu PV rujukan, PVT dengan reka bentuk pengumpul yang sama, sistem PV-PCM dan PVT-PCM telah didirikan sesuai dengan sistem PVT-NePCM yang baru untuk memastikan suasana sekeliling yang sama. Semua parameter operasi dan persekitaran (suhu yang berbeza, pancaran matahari, kadar aliran HTF, kelajuan angin, dan lain-lain) telah diukur dan direkodkan secara serentak oleh sistem pemerolehan data digital dari bulan Jun hingga September 2019. Prestasi telah dianalisis dengan menggunakan kedua-dua hukum termodinamik yang pertama dan kedua. Hasil kajian menunjukkan bahawa sistem PVT-NePCM baru mencapai, sekurang-kurangnya, suhu sel 4°C lebih rendah berbanding sistem lain. Sistem ini beroperasi dengan kecekapan tenaga keseluruhan sebanyak 85.3% dan kecekapan eksergi 13%. Sistem PVT-NePCM ini memanjangkan tempoh penyejukan sel suria sebanyak 37.5% berbanding dengan sistem PVT sahaja. Penggunaan sistem sedemikian secara meluas dapat mengurangi kebergantungan pada bahan bakar fosil dan juga dapat membantu memulihara alam persekitaran.

Kata kunci: Tenaga solar; termal fotovoltaik (PVT); bahan perubahan fasa nano dipertingkatkan (NePCM); penyiasatan prestasi masa nyata; analisis tenaga-tenaga.

ACKNOWLEDGEMENTS

TABLE OF CONTENTS

LIST OF FIGURES

LIST OF TABLES

LIST OF SYMBOLS AND ABBREVIATIONS

A	:	Area of the collector (m^2)
a	:	Reduced environment temperature ($\equiv T_a/T_s$)
$\dot{B}_e$	:	Rate of electrical exergy (W)
$\dot{B}_{dest}$	:	Exergy destruction rate (W)
$\dot{B}_s$	:	Rate of exergy from solar radiation reaching module surface (W)
$\dot{B}_{wi}$	:	Rate of exergy influx with inlet water (W)
$\dot{B}_{wo}$	:	Rate of exergy outflux with outlet water (W)
$\dot{B}_{th}$	:	Rate of thermal exergy (W)
C_g	:	Geometric concentration ratio of concentrator solar modules
C_p	:	Specific heat capacity of heat transfer fluid (water) (J/kg.K)
$C_{p,s}$	:	Specific heat of phase change material in solid phase (J/kg.K)
$C_{p,l}$	:	Specific heat of phase change material in liquid phase (J/kg.K)
d	:	Day of the year
$\dot{E}_e$	:	Rate of electricity generation (W)
$\dot{E}_l$	:	Conversion losses (W)
$\dot{E}_{wi}$	:	Rate of heat influx with inlet water into the system (W)
$\dot{E}_{wo}$	:	Rate of heat outflux with outlet water (W)
$\dot{E}_s$	:	Solar radiation intercepting the module surface (W)
FF	:	Fill factor
G	:	Solar irradiance (W/m^2)
IP	:	Improvement potential (W)
I_{mpp}	:	Current at maximum power point (A)
I_{sc}	:	Short circuit current (A)
L_{NePCM}	:	Latent heat of nano enhanced phase change material (J/kg)
$\dot{m}$	:	Mass flow rate of heat transfer fluid (water) (kg/s)
m_{NePCM}	:	Mass of nano enhanced phase change material (kg)
P_{max}	:	Maximum power output (W)
Q_{ch}	:	Heat required to change the phase (J)
$\dot{Q}_{gain}$	:	Heat gain by heat transfer fluid (water) (W)
$\dot{S}$	:	Entropy generation (W/K)
T_a	:	Ambient temperature (K)
T_{wi}	:	Inlet water temperature (K)
T_{wo}	:	Outlet water temperature (K)
T_s	:	Temperature of the Sun (K)

| V_{mpp} | : | Voltage at maximum power point (V) |
| V_{oc} | : | Open circuit voltage (V) |

Greek symbols:

α	:	Absorptance of the photovoltaic module glass cover
β	:	Angle of inclination of the module
δ	:	Solar declination angle
ε	:	Exergy efficiency
η	:	Energy efficiency
φ	:	Latitude of the experimental site
τ		Transmittance of the photovoltaic module glass cover
i		Interaction factor

Subscripts:

a	:	ambient
e	:	electrical
f	:	final
i	:	initial
l	:	liquid phase
o	:	overall
s	:	solid phase
th	:	thermal
wi	:	water inlet
wo		water outlet

LIST OF APPENDICES

None

CHAPTER 1: INTRODUCTION

1.1 Background

Energy from the Sun can be harnessed by two fundamental techniques: firstly, capturing thermal energy by means of solar thermal collectors (STC); secondly, converting sunlight into electricity through photovoltaics. While photovoltaic (PV) technology is considered as a superior method for solar energy conversion it works with a paradox that it requires sunbeams to produce electricity but the efficiency declines with the increase in cell temperature. In fact, cell temperature is one of pivotal factors that govern the amount of power exploitable from a PV module. For each degree increase in cell temperature power output of a crystalline silicon (c-Si) solar cell drops by 0.45 to 0.65% and the energy conversion efficiency drops by 0.08% (Kalogirou & Tripanagnostopoulos, 2006; Radziemska, 2003a). Commercial crystalline silicon PV modules, at their maximum power point, can transform around 15 to 20% of the incoming sunbeams into electricity, the remnants being dissipated as heat to the ambience (van Helden et al., 2004). This heat can be partly recovered through suitable heat extraction system. Such PV modules equipped with heat removal facility are called photovoltaic thermal (PVT) modules. While natural or forced convection of air is the simplest way to take away unwanted heat, liquid-based heat exchangers demonstrate more efficacy in heat removal.

Both PV and STC have reached certain technological maturity and are employed on commercial basis around the globe. Photovoltaic thermal (PVT) technology, in contrast, is still going through research and development (R&D) phase for reaching the technological transcendence adequate to claim commercial success. Being a thermal and electrical energy co-generation system PVT efficiency enhancement involves

ameliorating both thermal and electrical efficiency. Interestingly, enhancement of both efficiencies basically depends on a single issue, that is, efficient removal of heat from the PV module. Effectual heat removal from the PV module depends on several factors including the type of heat transfer fluid (HTF) employed for heat extraction, module and thermal collector geometry, application of heat transfer enhancement devices, using phase change materials (PCM), etc.

Heat transfer fluids play the central role in extracting heat from a body or a surface. From the early development phase of PVTs, researchers are widely using air (Aste et al., 2008; Bambrook & Sproul, 2012; Tripanagnostopoulos et al., 2006) and water (Aste et al., 2015; Mishra & Tiwari, 2013; Yazdanpanahi et al., 2015) as the two major HTFs. While air-cooling is a cheaper solution for removing heat from the PV modules poor thermo-physical properties of air makes it quite inefficient. On the other hand, water is considered as one of the best HTFs for PVT application because of its higher thermal properties like high specific heat, substantial thermal conductivity and high enthalpy of vaporization. Most importantly, being non-toxic hot water collected from the PVT can directly be utilized for domestic, hospital and industrial purposes. In recent years, researchers are working with different nanofluids such as Al_2O_3-water, TiO_2-water, ZnO-water, MWNT-water with a view to enhance heat transfer rate (Al-Waeli et al., 2019; Nasrin et al., 2018; Sardarabadi et al., 2016). Furthermore, mineral and synthetic thermal oils have been tried with PVT and found conducive in some cases.

Apart from working on HTFs, endeavors have been made to improve the design aspects of this hybrid system (both module and thermal collector) in order to enhance the efficacy of heat removal. While vast majority of the PV panels are of flat surface configuration researchers also proposed parabolic configuration and/or usage of reflectors and lenses (Akrami et al., 2018; Elsafi & Gandhidasan, 2015) to facilitate

interception of concentrated solar irradiance to endorse improved electrical efficiency. On the other hand, a good number of research works have been dedicated on the upgrading of thermal collector design. Researchers around the globe are working to develop an optimum design for thermal collector that would be instrumental to enhance heat transport. There have been proposed many collector designs, out of which parallel-flow, oscillatory-flow, spiral-flow, serpentine-flow, parallel serpentine-flow, web-flow (Ibrahim et al., 2009), two-sided serpentine flow (Hossain et al., 2019), quad-core flow (Fayaz et al., 2018) designs are a few to be named. The purpose of all these designs was to get larger contact area between the module and the collector so that amount heat transported would be maximized.

Effective thermal management of PV systems is related to its heat transfer potential; however, this potential needs to be harvested efficaciously. In order accelerate the heat transfer rate heat transfer equipment like heat pipe (Alizadeh et al., 2018), thermoelectric generator (TEG) (Borkar et al., 2014; Kane et al., 2017), passive heat sink (Natarajan et al., 2011), microchannel heat sink (Yang & Zuo et al., 2015), etc. have been integrated with PV panels. Apart from this, specialized cooling techniques such as radiative cooling (Safi & Munday, 2015; Zhu et al., 2014), jet impingement cooling (Royne & Dey, 2007), liquid immersion cooling (Sun et al., 2014; Zhu et al., 2011), etc. have also been implemented to regulate module temperature within a workable limit and thereby boost PV performance.

In recent years, phase change materials (PCM) have emerged as an innovative and practicable solution for heat storage and thermal management in diverse sectors including thermal comfort in buildings, preservation of food and pharmaceutical products, heat or cold storage, electronic device cooling, etc. PV researchers also found these materials as a potential solution to control solar cell temperature. Huang et al.

(2006) integrated paraffin wax filled aluminum container with internal fins with a PV module to limit its cell temperature and claimed to maintain it below 29°C for more than two hours under 750 W/m^2 solar irradiance and 32°C ambient temperature. In a ensuing work, same research group employed a blend of two dissimilar PCMs with unalike phase transition temperatures contained in an aluminum vessel with internal triangular fins and affirmed to attain extended thermal regulation period (Huang, 2011). In the meantime, PV researchers were facing the tricky issue of usage between thermally conductive or thermally insulated PCM container. To address this issue, Hasan et al. (2010) proposed four different PCM containers, two made from highly conductive metal aluminum and the other two made from thermally insulating perspex and examined their performance with five different PCMs. The best cooling effect was achieved with salt hydrate PCM contained in aluminum casing.

Despite of the adjuvant feature of high heat storage capacity poor thermal properties like low thermal conductivity, wide range of phase transition, etc. came out as the major shortcomings of using PCM in PV thermal regulation. A few attempts have been reported to address this problem. While some researchers inserted metal chips into PCM to improve thermal conductivity other proposed the usage of metal encapsulated PCM. However, each idea suffered from their own shortcomings. For example, metal chips inserted into the PCM gets accumulated at the bottom of the container during the melt phase and tends to initiate corrosion. Moreover, they promote leakage current flow across the metal frame which could otherwise instigate potential induced degradation (PID) of the PV module. On the other hand, although metal encapsulation is the possible best way for PCM containment it is economically impracticable. Therefore, to address this critical issue, the present research aims to enhance the thermal properties of PCM by incorporating highly conductive nanoparticles with a view to improve its efficacy in limiting PV cell temperature and extend heat storage period.

1.2   Research Problem

Photovoltaic modules work with the enigma that they require sunlight to generate power, but their efficacy dwindles with rise in temperature. Like many other sectors, PCM has opened a horizon in thermal regulation of photovoltaic devices. PCMs can maintain body temperature of any object within desired limit by means of passive cooling. Through efficacious integration of these materials with PV modules solar cell temperature can be kept close to their phase transition temperature. However, effectual engagement of this technology in PV cooling could not be materialized yet due to several shortcomings with the integration and containment method as well as the materials themselves.

Generally, PCMs are contained in thermally conductive metal casings to facilitate sharp and aggregate phase change and joined on PV backside through thermal paste. The two intricate problems continue to exist with PCM casings or box are: 1) irregular solidification pattern of the material from liquid phase and uneven distribution inside the box creating a non-uniform temperature distribution throughout the solar cells, 2) inhomogeneous and unsound contact between PV backside and the PCM container causing poor heat removal from the solar cells to PCM.

However, the crucial problem of using PCMs in PV thermal regulation consists in their poor thermal conductivity, low specific heat and wide phase transition range. Though most of the PCMs possess high latent heat (wherefore they gained popularity in thermal storage applications), most of them suffer from the drawback of poor thermal conductivity that deters efficient heat transfer and causes delay in leveling solar cell temperature during phase transition. Besides that, most of the PCMs, especially the organic (carbon-bearing) ones have considerably lower specific heat than water, which indicates their impotency in storing a substantial amount of heat. Another problem with

organic PCMs is that they don't melt at a specific point or even over a narrow range of phase transition temperature; rather they start phase transition at a certain temperature and completes the transformation beyond $2 - 6^{\circ}C$ of the starting point. As a result, the heat storage period is cut down and cell temperature cannot be maintained low for desired span of time.

Endeavors of applying PCM in photovoltaic thermal (PVT) systems to attain higher water outlet temperature in application end and extend the heat storage beyond sunset are not seeing that much success because of the prevailing problems as pointed out above. The purpose of this thesis is to incorporate highly conductive multi-walled carbon nanotubes (MWNT) into the matrix of an organic paraffin wax PCM and synthesize a new nano enhanced phase change material (NePCM) with improved thermal properties and integrate it with PVT with a view to enhance its thermal performance. The specific problems as identified in this research can be stated as follows:

1. There is an urging to explore and examine the nanomaterials appropriate for enhancing the thermal properties of organic PCMs.

2. Effect of incorporation of nanoparticles in PCMs in their heat storage capacity and, thereby extending the heat availability period needs to be clarified.

3. Effect of integration of NePCM in PVT collectors needs to be investigated to confirm whether such merger improves system efficiency or not.

1.3   Research Objectives

Based on the research questions as identified in the preceding section, the following objectives have been set for the present research work:

1. To synthesize and characterize new nano enhanced phase change materials (NePCM) and determine an optimum composition of NePCM suitable for PV thermal management.

2. To analyze the potential of the PVT-NePCM system through experimental performance investigation.

3. To evaluate the thermal and electrical performance of the PVT-NePCM system based on energy and exergy approach.

4. To compare the performance of PVT-NePCM system with PV, PVT, PV-PCM and PVT-PCM systems.

1.4 Scope of the Present Research

The aim of the present research proposal is to develop a susceptible PVT system using nano enhanced PCM (NePCM) to get the better output in the form of enhanced thermal efficiency as well as better electricity conversion efficiency. In order to accomplish this, aim the following scopes of work have been set:

1. To prepare and optimize a proper proportion of nano particles and PCMs, and thereby ascertain the best composition for nano enhanced PCM (NePCM).

2. To integrate the newly developed NePCM in PVT through proper integration method and carry out performance study of the PVT-NePCM system.

3. To compare the performance of the proposed PVT-NePCM system with existing other thermal management systems for photovoltaics in order to assess its relative merit.

1.5   Research Methodology

The aim of the present research is to develop a novel nano enhanced phase change material (NePCM) to replaces organic PCMs with better thermal properties and suit photovoltaic thermal application. Hence, the research goal is achieved in two distinct phases:

Phase – I: Four (04) nano composite materials have been synthesized by incorporating MWNT at different concentrations (wt%) in paraffin wax PCM matrix. Thereafter, all the new composite materials (NePCM) are characterized using differential scanning calorimetry (DSC), thermogravimetric analysis (TGA), Fourier transform infrared (FTIR) spectroscopy and field emission scanning electron microscopy (FESEM). Hence, the material that offers the best thermal property set is confirmed through comparative analysis and this NePCM is selected for PVT application.

Phase – II: The selected NePCM is employed as thermal storage material on the PVT panel. For this purpose, the amount of material required to control the module temperature to a certain limit has been estimated through energy balance equation. Hence, these materials have been packed in small thermally conductive and leakproof aluminum pouches, wherein enough space is kept for volume expansion upon fusion. The NePCM loaded pouches have been integrated on the backside of the PVT panel by means of aluminum tapes and secured through aluminum channels. Outdoor experimental investigations have been carried out with five systems installed side by side, namely PV, PVT, PV-PCM, PVT-PCM and PVT-NePCM. Then, comparative performance of all five systems have been carried out by using both energetic and exergetic approach.

1.6   Significance of the Research

The research presented in this thesis builds on the recent advancements in the area of photovoltaic thermal (PVT) technology. It focuses on analyzing the real-time energetic and exergetic performance of a nano enhanced phase change material (NePCM) based PVT (PVT-NePCM) system, wherein usage of nano composite PCM for thermal regulation has been tried for the first time in PV and PVT research.

Generally, the thesis makes a significant contribution towards effective thermal regulation and heat storage solution for PVT systems by introducing a novel heat storage material. More specifically and from the perspective of material science, a new nano composite material has been synthesized out of organic PCM and nanoparticle and, the material is thus integrated with PVT module with a view to achieve better control over cell temperature, improve and maintain augmented electrical performance, enhance heat removal rate from the module and extend heat storage potential of PCM.

This investigation provides an insight into the tracts of overheating sources of the solar cells and presents practicable ways for effective heat removal. Better understanding on efficient heat storage materials will enable manipulations of cell temperature more controllable, which in turn pave the way to achieve better enhancement in electrical and thermal performance of the PVT system.

The findings of this research are anticipated to have a substantial impact on thermal regulation of PV and PVT systems. Finally, the research aims to open a new horizon of the possibilities of nighttime applications of PVT through engaging nanomaterials enhanced phase change materials as an effective thermal storage.

1.7   Thesis Structure

The background, methodology and outcomes of the present research has been detailed in five chapters, **Chapter 1** being a general introduction along with specific objectives and scope. The rest of the chapters are organized as follows:

Chapter 2: This chapter is the summary of the previous literature on PV thermal management, PVT technology, PCM and its application in thermal control and nanoparticles and nanocomposite materials and their application in thermal control, etc. This chapter is ended up by re-counting with a summary of the research gap.

Chapter 3: The detail research methodology along with the meteorological condition of the PV plant site, specifications of different PV modules used to conduct the experiment, experimental setup, instrumentations and lastly the experimental testing conditions are described in this chapter.

Chapter 4: The experimental results along with corresponding explanation have been discussed in this chapter. The outcomes of the material characterization and, energetic and exergetic performance have been detailed thoroughly.

Chapter 5: The thesis wraps up with some concluding remarks and recommendations of future work in this chapter.

CHAPTER 2: LITERATURE REVIEW

2.1   Introduction

Literature reviews are imperative in building perception about the current research and disputes pertinent to a research question. One of the basic purposes of literature review is to refine and precisely define the research questions, which is vital for adopting apt research protocol and scheming appropriate research methodology. As the present research is centered around some specific research questions narrative or traditional literature review method has been adopted to produce a well-found knowledge base with a view to highlight the developments accomplished so far in photovoltaic thermal research, synthesize the information and ultimately find research gaps. The data and information related to the research aim have been procured from ScienceDirect, Springer Link, Taylor and Francis, Nature, Web of Science, Google Scholar, etc. Search string keywords used were, etc. Peer reviewed research articles, reviews, grey literatures (including technical reports) from 1978 (the year the first paper about PVT was published) to 2020 have been taken into consideration. The number of selected articles was 200. In course of the literature review, relevant key theories have been examined and emphasis is given how different authors applied these theories. The focus was to synthesize the theme arising from a paper with an aim to answer the key research questions put forward in chapter 1.

2.2   Photovoltaic Thermal Technology

The concept of photovoltaic thermal (PVT) technology evolved with a view to co-generate both electricity and heat from the same solar module and maximize the harvest from a single unit. A PVT (Figure 2.1) is a merger of photovoltaic (PV) module and solar thermal collector (STC) wherein that waste heat generated by the former one is

collected by the later device and transported to thermal application end through heat exchanger. To represent of the phenomenon of synchronized conversion of solar energy into power and heat some researchers termed it as 'photo thermo conversion' (Kumar et al., 2015).

The heat generated in the PV modules in course of their operation can be utilized in heating applications like in space heating, household works and low-temperature industrial process heat (IPH) applications (Tyagi et al., 2012). In addition, PVT modules can be retrofitted to buildings (known as building integrated PVT or BIPVT) without any major alteration of the structure. Clarke et al. (1998), Moshfegh and Sandberg (1998), Brinkworth et al. (2000), etc. testified efficacious integration of PVT systems with buildings.
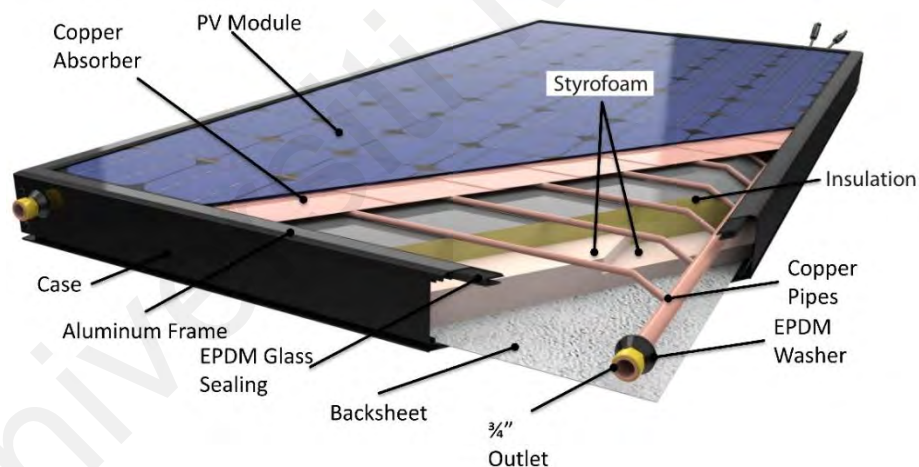
Figure 2.1: Sectional image of a PVT collector
(https://www.solarmastertech.com)

In 1970s, the early works of Florschuetz (1975), Wolf (1976), Kern and Russell (1978), Florschuetz (1979), and Hendrie (1979) placed the basis in PVT research (Chow, 2010). Thereafter, research works by Garg and Adhikari (1997, 1998, 1999), Garg and Agarwal (1995), Garg et al. (1994), Sopian et al. (1996), Sopian et al. (2000), Tiwari and Sodha (2006), Tiwari et al. (2006), Tyagi et al. (2012a), etc. built the

methodological base of this budding technology. Bergene and Løvvik (1995) first presented a workable physical model of flat-plate PVT where water was used as the heat transfer fluid (HTF). On the other hand, Luque et al. (1997) designed a concentrator PVT (CPVT) using heat-pipe technology. The same author group, in an ensuing work, presented an electrical and thermal model for unevenly irradiated solar cells (Luque et al., 1998). Despite of research and development (R&D) works in the last three decades, commercialization of this technology is still in its nascent phase due some technical issues like leakproof containment, effective heat removal, etc.

Table 2.1 presents different types of PVTs reported so far in literature. Based on geometry, PVTs can be of simple flat-plate structure or they can have concentrating feature. On the other hand, based on heat transfer fluid (HTF) there can be PVT/water, PVT/air and PVT/nanofluid systems (Bosanac et al., 2003).

Table 2.1: PVT classification

Basis of classification	PVT collector
Design	- Flat-plate PVT (FPVT) - Concentrator PVT (CPVT)
Erection mode	- Standalone PVT - Building integrated PVT (BIPVT)
Heat transfer fluid	- PVT/air collector (PVT/a) - Unglazed - Single glazed - Double glazed - Glazed dual pass - PVT/water collector (PVT/w) - PVT/nanofluid
Heat transfer equipment	- Heat pipe-based PVT - Micro-channel-based PVT - Heat spreader-based PVT - Jet impingement-based PVT

2.3 Thermal Management of PVT Systems

A PVT system yields two discrete types of energy, namely heat and electricity. Hence, the purpose of thermal management of the PVT systems involves two distinct purposes: 1) to maintain a low cell temperature in order to sustain electrical efficiency

and 2) to ensure efficient harvest and usage of the waste heat from the module. (Machniewicz et al., 2015; Radziemska, 2003b). While standard operating condition (STC: 25°C and 1000 W/m^2) is hard to maintain in practice cell temperature must be kept as near as conceivable to hold onto a considerable electrical efficiency. On the other hand, efficient heat removal from the module is indispensable to enhance system thermal efficiency. In the following sections, various schemes adopted by the researchers for thermal management and effective heat removal from PVTs have been delineated.

2.3.1 Air cooling

The most hands-on method to remove heat from PVT modules is to flow air beneath the panel either by natural convection (passive air-cooling) or forced convection (active air-cooling). Brinkworth et al. (1997) studied the passive cooling induced by buoyancy in a rectangular duct attached behind a vertically erected PV module. Under a solar irradiance of 620 W/m^2 and an ambient temperature of 15 – 22°C, the cell temperature could be maintained below 40°C when air was flown at velocities between 1.8 – 3.2 m/s. On the other hand, Valeh-e-Sheyda et al. (2014) reported to hold the cell temperature of a rooftop PV at 48.7^{o}C under 1000 W/m^2 by passive air-cooling while air was flowing between 4.13 – 5.0 m/s.

Reduction in cell temperature primarily depends on air flow speed and ambient temperature. Teo et al. (2012) claimed to keep solar cell temperature below 48°C under 1000 W/m^2 through active air-cooling at a flow rate of 0.05 kg/s. Similarly, a simulation study showed that cell temperature below 40°C was attained when the air speed was raised as high as 5.0 m/s (Cuce & Cuce, 2014).

Poor heat transfer coefficient of air and need for additional power for the fan/blower in active air-cooling are the main drawbacks of this method. That is why, researchers like Tripanagnostopoulos (2007), Mazón-Hernandez et al. (2013), etc. recommended active air-cooling exclusively for large-scale PV power plants.

2.3.2 Water Cooling

Water is a considered as the best HTF for PVT systems. Because, in one hand, water possesses better thermal properties than air; on the other hand, water itself can be used as a product.

Wu and Xiong (2014) proposed a natural way of water cooling, wherein rainwater collected in a closed chamber expands as solar radiation intensifies and flush out to flow over the module top surface. Effect of active water cooling on PVT electrical and thermal performances have been studied by Dorobantu et al. (2013), Rahman et al. (2015); Moharram et al. (2013), Zhu and Si (2012), Rodgers and Eveloy (2013) and Matsuka (2012). Some researchers presented numerical models of the water-cooling technique and some of them carried out experimental investigations to support simulation results. Vera et al. (2014) proposed an optimization model for water-cooling system. It predicted the optimum limits for the control parameters like water flow rate, collector dimension, etc. to attain optimum efficiency under certain ambient.

2.3.3 Liquid Immersion Cooling

Liquid immersion cooling is mainly practiced in cooling computer components, wherein components are submerged in thermally (but not electrically) conductive fluids. Researchers have tried this technique for PV cooling, too. Immersion cooling reportedly alleviate thermal stress on module top cover glass as well as solar cells (Zhu et al., 2011). However, Merhotra et al. (2014) indicated an inadequacy of such cooling system

that being a conductive liquid water is ionized and affect the electrical performance of the module. Authors recommended deionized (DI) water as a substitute.

Xiang et al. (2012) detected that there is a certain limit for depth of immersion which is conducive for PV efficiency augmentation. Another study investigating the effect of position of the module under water on its efficiency reports that electrical efficiency reaches to its maximum when the module is submerged 5 cm below the water free surface and cell temperature at this position holds around 40ºC under a solar irradiance of 805 W/m^2 (Tina et al., 2012).

Apart from water, attempt has been made to cool PV cells by immersing into dielectric fluid such as dimethyl-silicone oil. Sun et al. (2014) experientially inspected the cooling effect on the cell temperature of a CPV module by means of flowing dimethyl-silicone oil over its surface. Authors observed that cell temperature drops by 11ºC (from 31º to 20ºC) as the oil flow is increased by five times (from 0.22 m/s to 1.09 m/s).

2.3.4 Thermoelectric Cooling

Thermoelectric cooling (TEC) works on Peltier effect. In simple words, during electricity flow through two alongside conductors there creates a heating or cooling effect. While this approach has already been applied of electronics (like microprocessors) cooling, researchers engaged it for PV cooling, too. Najafi and Woodbury (2013) built a MATLAB model of a TEC based PV cell cooling system. Authors reported to achieve a robust control over cell temperature at the minimum power consumption. Cui et al. (2016) devised a TEC on top of PCM for concentrating photovoltaic (CPV) modules, wherein thermoelectric generator exhibited its efficacy in inhibiting high temperatures of the concentrating PV.

2.3.5   Heat-pipe Cooling

Heat-pipes are two-phase system used to cool sections or elements. Beach and White (1981), Feldman et al. (1981), Akbarzadeh and Wadowski (1996), Anderson et al. (2008) and several other researchers employed heat-pipe technology in PV cooling, especially in concentrator photovoltaics (CPV). Application of heat pipes has been found to elevate PV efficiency by 15 – 30% (Kumar et al., 2015).

2.3.6   Jet Impingement Cooling

Jet impingement is a dynamic cooling technique that cools down the heated body by high heat transfer rates arising from cooling fluid shot from the nozzles. This method was originally used in industries for metal annealing, cooling of the gas turbine blades, and cooling in the grinding processes.

Royne and Dey (2007) proposed a jet impingement method for cooling a CPV module with densely packed solar cells. In the case that jet flow emitted from four nozzles (each diameter: 1.4 mm) vertically hits on the bottom surface of the solar cell receiver (aperture area: 50×50 mm^2), the optimal heat transfer coefficients are 28×10^3 and 37×10^3 W/(m^2.K) under the conditions of I_{cell} = 200 kW/m^2 and 500 kW/m^2, respectively. Further, cooling effects were simulated under these optimal conditions. Results showed that T_{cell} was decreased to 30°C (ΔT_{cell} =30°C) and 40°C (ΔT_{cell} =70°C) under the conditions of I_{cell} = 200 kW/m^2 and 500 kW/m^2, respectively.

2.3.7   Passive Heat Sink

Araki et al. (2002) studied a copper sheet on a heat-conductive epoxy printed aluminum baseplate as a passive and simple heat sink for cooling CPV modules with C_g = 500× using a square imaging Fresnel lens. A solar cell was placed on the heat sink and the cooling performance was evaluated, wherein temperature difference between

the solar cell and ambient air was found only 18°C under $I = \sim 600$ W/m^2 ($I_{cell} = \sim 300$ kW/m^2).

2.3.8   Microchannel Cooling

Reddy et al. (2014) have designed a copper microchannel heat sink for active cooling of CPV modules with $C_g = 500\times$ using a square parabolic dish reflector. The microchannel attached beneath the solar cell has a rectangular through hole (height: 4 mm, width: 0.5 mm, pitch: 0.5 mm) cooling down the solar cell by water flowing through the holes. The solar cell temperature was simulated assuming that the six microchannels linked in series and placed in the flow parallel to the hole. As a result, cell temperature (T_{cell}) reached 40.0°C and 49.09°C at the inlet and outlet sides, respectively, under an irradiance of $I = 550$ W/m^2 ($I_{cell} = 275$ kW/m^2) and water flow rate of 0.0176 L/s.

2.3.9   Radiative Cooling

Radiative cooling of PV modules is a passive cooling technique that enhances the radiative cooling effect by modifying the emissivity spectrum of the module surface for spectrally selective thermal radiation/absorption.

The Earth's atmosphere has a transparent window in the infrared spectrum range of 8–14 μm. Within this atmospheric window, thermal radiation from terrestrial bodies can be transmitted to outer space almost without being absorbed by the atmospheric air. Thus, the terrestrial bodies can release their heat into outer space. However, in the spectrum range outside of the atmospheric window, the atmosphere is not transparent and emits the thermal radiation to the Earth's ground, heating the terrestrial bodies. Radiative cooling of the terrestrial body occurs once the radiative heat flux release exceeds the incoming heat flux, including radiative, conductive, and convective heat.

Zhu et al. (2014) have reported that a micro-structured silica pyramid formed on the solar cell modifies the emissivity spectrum, enhancing radiative cooling performance. The pyramid shape was optimized to give the solar cell high emissivity in the entire infrared spectrum region. Considering convective heat transfer under an irradiance level of $I = I_{cell}$ = 800 W/m^2, air temperature of T_a =27°C, and wind velocity of v = 3.0 and 1.0 m/s for top and bottom surface respectively, cell temperature (T_{cell}) was reduced by ΔT_{cell} = 17.6°C and 13.1°C from the case of untreated silicon cell surface for silica pyramid and 5 mm thick uniform silica surface, respectively.

After developing the coupling electrical-thermal model for simulating various cases and conducting field trial, this paper aims to elucidate the consequence of radiative cooling on the temperature of normally installed PV modules, and the influence of factors such as thermal convection and thermal emissivity. The increased thermal emissivity results in only an average temperature drop less than 1.0°C, while the ventilation conditions have an impact of over 10°C. The simulation study also reveals that a limit of around 2.0°C in temperature reduction is all the value of an additional radiative cooling coating on PV modules. To make an additional radiative cooling coating on existing PV panels cost-effective, Li et al. (2021) suggests using multifunctional coatings.

2.3.10 Phase Change Material Cooling

The prime barrier in implementing any solar device is the detachment between demand and supply. This issue can be mitigated to some extent through the usage of effective energy storage materials like phase change materials (PCM). PCMs can accumulate 5 to 14 times additional energy per unit volume than water, concrete or rock (Sharma et al., 2009). Through the storage of large amount of heat these materials can extend heat availability period (Telkes, 1980). However, these materials were not tried

in thermal energy storage before mid-1970s (Pielichowska & Pielichowski, 2014). The early applications of PCM in PV temperature control was stated in 1978 by Stultz and Wren (1978). Huang et al. (2004) first attempted the application of PCM in thermal regulation of photovoltaic thermal (PVT) systems. Thereupon, Hasan et al. (2010), Browne et al. (2016), Sharma et al. (2016) and many other researchers worked on integrating PCM in controlling PV cell temperature and solar energy storage.

Table 2.2 outlines the strong points and shortcomings of the PV thermal management systems discussed as above.

Table 2.2: Comparative features of different PV cooling methods

Cooling technology	Merits	Demerits
Natural convection of air	- Low expenditure - No maintenance - Easy to implement - Extended life - Almost silent - No electricity required - Passive heat transfer	- Poor heat removal rate owing to poor thermal properties of air and low mass flow rates - Accretion of dust in inlet grating further worsens heat transfer - Reliant on wind speed and course
Forced convection of air	- Higher heat transfer rates compared to natural convection - Independent of wind direction and speed - Higher mass flow rates result in better heat removal	- Expenditure on devices. - Additional power required - Clamorous - Maintenance cost required
Water cooling	- Higher heat transfer compared to both natural and forced convection of air - Commendable heat capacity and thermal conductivity of water result in better heat removal	- Need a pumping system to circulate water, hence electricity consumption is significant - Higher maintenance cost - Short life of the water conducting lines due to corrosion
Heat-pipe cooling	- Good temperature drop - Passive heat exchange - Low cost - Easy to install	- Poor heat removal - Dust accumulation on inlet grating - Reliant on wind speed and direction.

Table 2.2, continued

Cooling technology	Merits	Demerits
Thermoelectric cooling	• No moving parts • Soundless • Compact size • Easy to install • Low maintenance cost	• Heat transfer depends on ambient conditions • Needs electricity to operate • Poor consistency • No heat storage capacity • Requires efficient heat removal from hot side
PCM cooling	• Higher heat storage capacity due to latent heating • Isothermal heat removal • No electricity required • Passive heat exchange • Soundless • No maintenance cost	• High cost of PCM • Some PCMs are toxic, corrosive and flammable • Disposal issue after life cycle completion

2.4   Phase Change Materials

Phase change materials (PCM) can accumulate and discharge a significant amount of energy during the phase change process. Therefore, they are widely popular as a thermal energy storage (TES) materials (Sharma et al., 2009). During phase transformation these substances do not admit sensible heat, rather they absorb latent heat from the vicinities experiencing an endothermic process over a certain temperature range. As can be seen from Figure 2.2, PCMs primarily heat up sensibly up to their melting point, thereafter it absorbs latent heat and liquefy progressively with time and this heat absorption continues until melting completes. The fusion period is the function of the volume and thermal conductivity of the PCM and occurrence of any matter that boosts heat transfer rate. PCMs' phase transition temperatures vary markedly with material type, thermal properties and chemical structure (Cabeza et al., 2011; Oró et al., 2013).

Use of PCM in the sun-oriented energy systems is astoundingly predominant in the cogeneration equipment, where the power expenses can be reduced during the greatest long stretches of utilization. Application of PCM requires fewer equipment leading to diminish the need for extra power which is the prime vantage point of this technology

(Zalba et al., 2003). Stultz et al. (1978) first used icosane or eicosane ($C_{20}H_{42}$) for PV temperature control, which is an alkane with a melting temperature, latent heat and thermal conductivity of 36.7°C, 246.50 kJ/kg and 0.491 W/m.K, respectively.
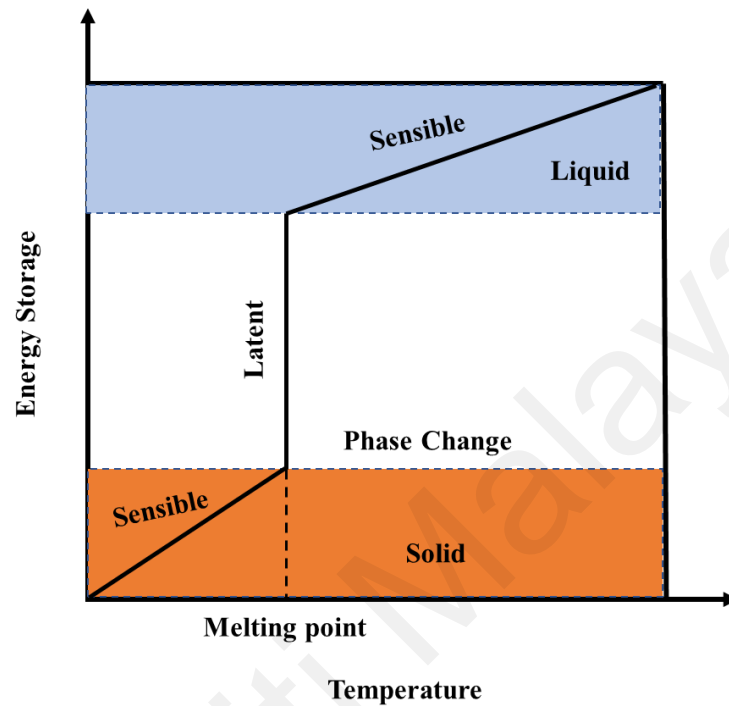
Figure 2.2: Graphical illustration the phase changing phenomenon
(Gao & Deng, 2013)

Basically, PCMs are of three kinds: organic, inorganic and eutectic. While organic PCMs are paraffin or non-paraffin carbon-containing compounds, inorganic PCMs include salt hydrates and metallics, and eutectics are blends of either organic-organic or inorganic-inorganic or inorganic-organic compounds (Sharma et al., 2009). Figure 2.3 shows a classification of the PCMs.
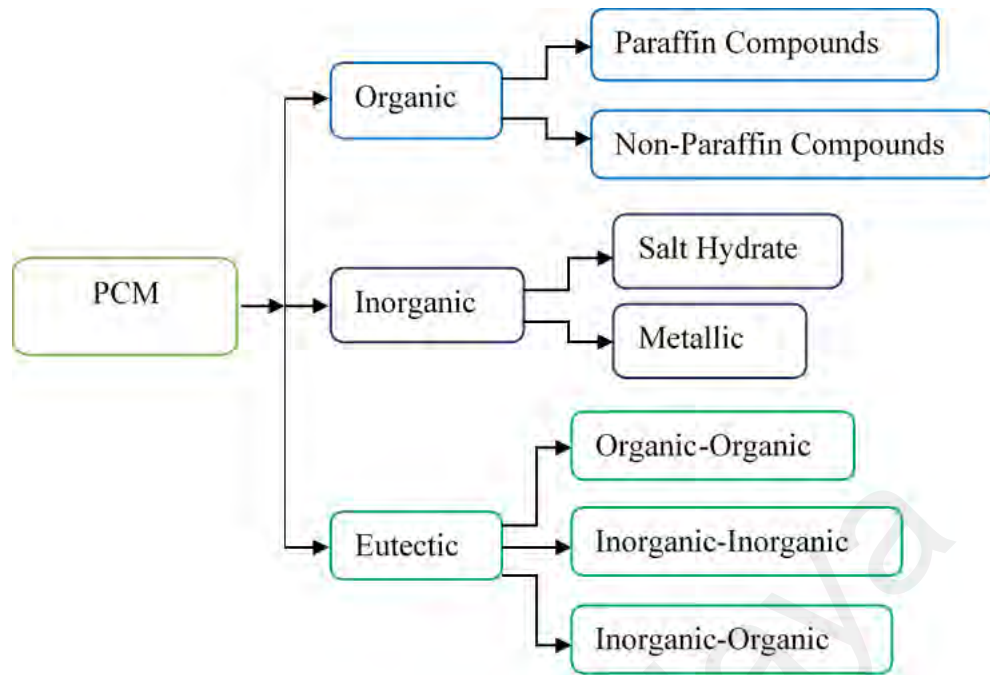
Figure 2.3: Classification of phase change materials

Among the organic PCMs, paraffin wax and fatty acids are mostly popular in industry. Paraffin wax is a blend of high molecular weight linear chain n–alkanes with melting point over 37ºC (Mozes, 1982) and latent heat of fusion from 200 to 220 kJ/kg. These are soft, uncolored, chemically stable, non-toxic and non-corrosive materials having self-nucleating feature. These materials congeal without much under cooling, melt congruously and do not segregate on solidification. Besides, paraffins are biodegradable. However, low thermal conductivity and moderate flammability are the main weaknesses of paraffin wax (Sharma et al., 2009). On the other hand, fatty acids are saturated or unsaturated carboxylic acids with extended aliphatic chain with melting point between $-5º$ to 71ºC and latent heat of fusion ranging from 45 to 210 kJ/kg (Kenisarin & Mahkamov, 2007). Saturated fatty acids like capric acid ($CH_3(CH_2)_6COOH$), lauric acid ($CH_3(CH_2)_{10}COOH$), palmitic acid ($CH_3(CH_2)_{14}COOH$), etc. are some of the examples of good PCMs. Low thermal conductivity, instability at high temperatures and high cost are the major drawbacks in implementation of these materials.

Inorganic PCMs amount to salt hydrates and metallics. Salt hydrates are favorable PCMs for thermal storage despite their dehydration in thermal cycling process and higher super cooling (Kenisarin & Mahkamov, 2007). But the expedient side of salt hydrates includes the constancy of latent heat upon cycling, high latent heat of fusion per unit volume and minor volume changes on phase transformation. Above all, their thermal conductivity is nearly twice as that of the paraffins (Sharma et al., 2009). Glauber's salt (sodium sulfate decahydrate, $Na_2SO_4.10H_2O$) is the most renowned salt hydrate PCM (Nagano et al. 2000) with manganese nitrate hexahydrate, $Mn(NO_3)_2.6H_2O$ (melting range 7.7^o to 25.3^oC) another good PCM (Nagano et al., 2003).

Metallics PCM are low melting point metals and metal eutectics with high heat of fusions per unit volume, high thermal conductivities and low specific heats. Examples of metallics include Ga, Bi-In eutectic, Bi-Pb eutectic, Bi-Cd-In eutectic, Bi-Pb-In eutectic, etc. Bulk of metallic substances is the main impotence in application of these materials (Sharma et al., 2009). Figure 2.4 demonstrates that, while paraffin wax is fit for relatively low thermal storage salt hydrates and eutectics are better choices for middle-high range of thermal storage (Gao & Deng, 2013).
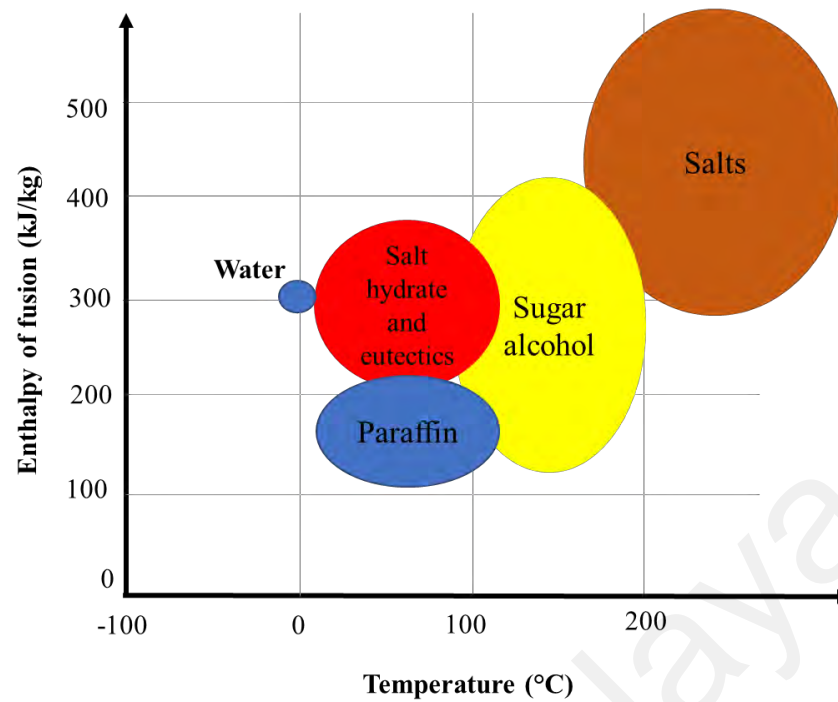
Figure 2.4: Melting points and latent heat of some PCMs
(Gao & Deng, 2013)

2.4.1 PCM Selection

Solar thermal energy harvested by STC or PVT collectors is typically collected as sensible heat as warm water, wherein large volume of water is necessary to supply a substantial amount of heat. However, PCM can accumulate greater amount of thermal energy per unit volume by exploiting both sensible and latent heat storage. Moreover, these materials can keep the temperature of the stored hot water more stable.

Selection of PCM for PV thermal regulation needs a methodical approach. Hasan et al. (2014a) and Gao and Deng (2013) independently worked out the lists of properties desirable in a PCM for PV applications. A summary of the criteria for selecting PCMs for PV thermal control is enumerated in Table 2.3. High thermal conductivity of the PCM is desirable in order to facilitate rapid heat transfer from a PV-PCM system. Malvi et al. (2011) reported in a numerical study that a 10% upsurge in the thermal conductivity of the PCM enhances the output of a PV-PCM system by 3%. To boost the

heat removal rate, some researchers used of fins on the PCM container (Huang et al., 2006), while others inserted metal shreds into the PCM to augment thermal conductivity (Maiti et al., 2011).

Table 2.3: Property requisites for PCM selection in PV thermal application
(Gao & Deng, 2013; Hasan et al., 2014a)

Properties	Requisite	Argument
Thermal	- Elevated latent heat - High heat capacity - High thermal conductivity - Reversible phase change - Stable melting temperature	- Maximum heat absorption - Minimum sensible heating - Effectual heat transfer - Daytime response - Congruent behavior
Kinetic	- High nucleation rate - No super cooling - High crystal growth	- Suppress super cooling - Easy to freeze - Faster solidification to meet heat retrieval demands
Physical	- Reasonable phase equilibrium - Minor volume modification on phase transition - High density - High specific heat	- Stable thermal storage - Avoid overdesign - To ensure low containment
Chemical	- Chemical stability - Congruent melting - Non-corrosive - Non-flammable and non-explosive - Non-toxic	- Long PCM life cycle - Minimum thermal gradient - Long container life - To ensure safety - Human and environment protection
Environmental	- Biodegradable/reusable - Odor free	- Easy for disposal - For dwelling comfort
Economic	- Abundant - Low cost - Cost effective	- Easy accessibility and affordability - Market penetration - Economic feasibility

In solar applications, the commonly exploited PCMs are sodium sulfate decahydrate (Glauber's salt), calcium chloride hexahydrate and paraffin wax (Demirbas, 2006). Glauber's salt is white crystalline sodium sulfate decahydrate ($Na_2SO_4 \cdot 10H_2O$) with a density of 1.464 gm/cm^3 and melting points of 32.38°C. It is nonflammable, chemically stable and absorbs and liberates most of its heat at a constant temperature. Most importantly, it needs only one-eighth of the space of rocks and two-fifth of the space of

water for equivalent heat storage (Telkes, 1980). The drawback points of this salt include poor thermal conductivity, corrosiveness and relatively high cost. Apart from Glauber's salt, another salt hydrate calcium chloride hexahydrate ($CaCl_2.6H_2O$) is also popular in solar thermal applications. It is a hygroscopic, achromatic acicular trigonal crystalline material with melting point 302.2 K and heat of fusion 190.8 kJ/kg and heat capacity 150 kJ/kg (Demirbas, 2006). On the other hand, paraffin wax is the largely employed PCM in thermal storage applications.

The PCMs employed most in PV system thermal management are listed in Table 2.4.

Table 2.4: Features of the PCMs typically used in PV and PVT systems

PCM (Organic/Inorganic) [Ref.]	Density (kg/m³ or kg/L or kg/dm³)	Melting temperature (ºC)	Solidification temperature (ºC)	Latent Heat of Fusion (kJ/kg)	Specific Heat Capacity (kJ/kg.K)	Thermal conductivity (W/m.K)	Kinematic viscosity (m²/s× 10⁻³)	Thermal expansion coefficient (K⁻¹)	Volumetric expansion (%)
Rubitherm RT20 (organic) (Hasan et al., 2010)	0.88 kg/L (*s*) 0.77 kg/L (*l*)	21.23 (onset) 25.73 (peak)	-	140.3	1.8 – 2.4 (*s*)	0.2	-	-	14%
Rubitherm RT21 (organic) (Huang, 2011)	840 kg/m³ (*s*) 760 kg/m³ (*l*)	21	-	134	-	0.2	0.02571	-	-

PCM (Organic/Inorganic) [Ref.]	Density (kg/m³ or kg/L or kg/dm³)	Melting temperature (°C)	Solidification temperature (°C)	Latent Heat of Fusion (kJ/kg)	Specific Heat Capacity (kJ/kg.K)	Thermal conductivity (W/m.K)	Kinematic viscosity (m²/s× 10⁻³)	Thermal expansion coefficient (K⁻¹)	Volumetric expansion (%)
Rubitherm RT25 (organic) (Biwole et al., 2013)	785 kg/m³ (*s*) 749 kg/m³ (*l*)	26.6	-	232	1.8 (*s*) 2.4 (*l*)	0.19 (*s*) 0.18 (*l*)	1.7970	0.001	-
Rubitherm RT27 (organic) (Hendricks & Sark, 2013; Huang et al., 2011; Lo et al., 2013)	880 kg/m³ (*s*) 750 kg/m³ (*l*)	26-28	-	184 (179)	2.0 (1.8 – 2.4)	0.2	0.02632	-	-
Rubitherm RT31 (organic) (Huang, 2011)	840 kg/m³ (*s*) 750 kg/m³ (*l*)	29	-	169	-	0.2	0.02632	-	-
Rubitherm RT35 (organic) (Huang et al., 2011)	880 kg/m³ (*s*) 760 kg/m³ (*l*)	35	-	157	1.78 (*s*) 2.37 (*l*)	0.2 (*s & l*)	0.033	-	10%
Rubitherm RT42 (organic) (Sharma et al., 2016)	880 kg/m³ (*s*) 760 kg/m³ (*l*)	38-43	-	174	2.0	0.2	-	-	12.5%
Rubitherm RT44 (organic) (Pakrouh et al. 2015)	780 kg/m³ (*s*) 760 kg/m³ (*l*)	41 - 45	-	255	2.0	0.2	-	-	-
Rubitherm RT60 (organic) (Huang, 2011)	950 kg/m³ (*s*) 780 kg/m³ (*l*)	60	-	144	-	0.2	0.03705	-	-

PCM (Organic/Inorganic) [Ref.]	Density (kg/m³ or kg/L or kg/dm³)	Melting temperature (°C)	Solidification temperature (°C)	Latent Heat of Fusion (kJ/kg)	Specific Heat Capacity (kJ/kg.K)	Thermal conductivity (W/m.K)	Kinematic viscosity (m²/s× 10⁻³)	Thermal expansion coefficient (K⁻¹)	Volumetric expansion (%)
Rubitherm RT10HC (organic) (Machniewicz et al., 2015)	-	9	10	126	2	0.2 (*s & l*)	-	-	-
Rubitherm RT18HC (organic) (Machniewicz et al., 2015)	-	17	19	222	2	0.2 (*s & l*)	-	-	-
Rubitherm RT25HC (organic) (Machniewicz et al., 2015)	-	22	26	177	2	0.2 (*s & l*)	-	-	-
Rubitherm RT35HC (organic) (Machniewicz et al., 2015)	-	34	36	197	2	0.2 (*s & l*)	-	-	-
Thermusol HD35 (Hendricks & Sark, 2013)	780 kg/m³	35	-	160	2.5	0.2	-	-	-
GR 40 (Huang et al., 2006)	710 kg/m³ (*s*)	43	-	82	1.5	0.15	-	-	almost zero
BASF Micronal DS5001 (Hendricks & Sark, 2013)	300 kg/m³	26	-	110	-	-	-	-	-
Rubitherm SP22 (Hasan et al., 2010)	1.49 kg/L (*s*) 1.43 kg/L (*l*)	22.97 (onset) 24.6 (peak)	-	213.12	2.5	0.6	-	-	4%

PCM (Organic/Inorganic) [Ref.]	Density (kg/m³ or kg/L or kg/dm³)	Melting temperature (°C)	Solidification temperature (°C)	Latent Heat of Fusion (kJ/kg)	Specific Heat Capacity (kJ/kg.K)	Thermal conductivity (W/m.K)	Kinematic viscosity (m²/s× 10⁻³)	Thermal expansion coefficient (K⁻¹)	Volumetric expansion (%)
Rubitherm SP224A (Sari & Kaygusuz, 2002; Tyagi & Buddhi, 2008; Xiao et al., 2013; Zalba et al., 2003)	1.49 kg/L (*s*) 1.44 kg/L (*l*)	23	-	150	1.4 (*s*) 1.95 (*l*)	0.6 (*s*) 0.4 (*l*)	1.23	0.0008	-
Waksol A (Huang et al., 2011)	770 kg/m³ (*s*) 760 kg/m³ (*l*)	32-36	-	162	2.3 (*s*) 2.43 (*l*)	0.33 (*s*) 0.31 (*l*)	-	-	-
Capric-palmitic acid (eutectic) (Hasan et al. 2015)	0.87 kg/dm³ (*s*) 0.79 kg/dm³ (*l*)	22.5	-	173	2.0 (*s*) 2.3 (*l*)	0.14 (*s*) 0.14 (*l*)	0.0023	0.00078	4.8%
Capric-lauric acid (eutectic) (Hasan et al., 2010)	0.88 kg/L (*s*) 0.863 kg/L (*l*)	20.78 (onset) 24.66 (peak)	-	171.98	-	0.139	-	-	2.3%
Calcium chloride hexahydrate, CaCl₂.6H₂O (salt hydrate) (Hasan et al., 2015)	1.71 kg/dm³ (*s*) 1.56 kg/dm³ (*l*)	29.8	-	191	1.4 (*s*) 2.1 (*l*)	1.08 (*s*) 0.56 (*l*)	1.84	0.0005	-

*s =solid, l = liquid

2.4.2 PCM Characterization Techniques

Characterization of the PCM comprises of morphological analysis, microstructural analysis, thermal analysis, functional group analysis, and so on (Chen et al., 2018;

Karaipekli et al., 2017). To study the morphology and the microstructure, scanning electron microscopy (SEM or FESEM) is mainly utilized (Zhang et al., 2016; Zhang & Liu, 2017). Sometimes, transmission electron microscopy (TEM) is further utilized for more definite analysis. Functional group analysis is carried out with Fourier-transform infrared spectroscopy (FT-IR) (Alkan et al., 2009). In PCM characterization, differential scanning calorimetry (DSC) is utilized for thermal analysis (Groenewoud, 2001). On the other hand, thermogravimetric analysis (TGA) is carried out to identify the weight loss of the PCM with increase in operating temperature (Sharma & Shukla, 2015). Thermal stability of the pure or composite PCM must be resolved through TGA. One of the main purposes to go for composite PCM is to improve its thermal conductivity. Hence, thermal conductivity analysis is significant for nano enhanced PCM (composite of nanoparticle and PCM). The hot plate method which depends on the transient plane source procedure is the most mainstream and utilized by specialists around the world (Ivanov, 2012; Lee et al., 2012).

2.4.3   Research on PV-PCM and PVT-PCM Systems

Phase change materials have been employed by many researchers to limit PV cell temperature and augment system efficiency. The vantage points of using PCM is that they possess good heat absorption capacity and need no moving parts to run a thermal control system. Therefore, no extra electricity is consumed, and no maintenance cost is required (Hendricks & Sark, 2013). Although Horne (1993) proposed the use of PCM to protect PV cells the first successful PV-PCM system was designed and developed by Häusler & Rogaß. (1998).

Machniewicz et al. (2015) numerically studied the effect of transition temperature of PCM on PV-PCM system efficiency. Four different paraffin wax PCMs with different phase transition temperatures were confined in 2-cm aluminum honeycomb structure

kept amid two aluminum panes. Paraffin wax with very low transition temperature was found to persist in melted state for the longest period and the best thermal performance was achieved with the PCMs with transition temperatures between 18º to 25ºC (Figure 2.5).
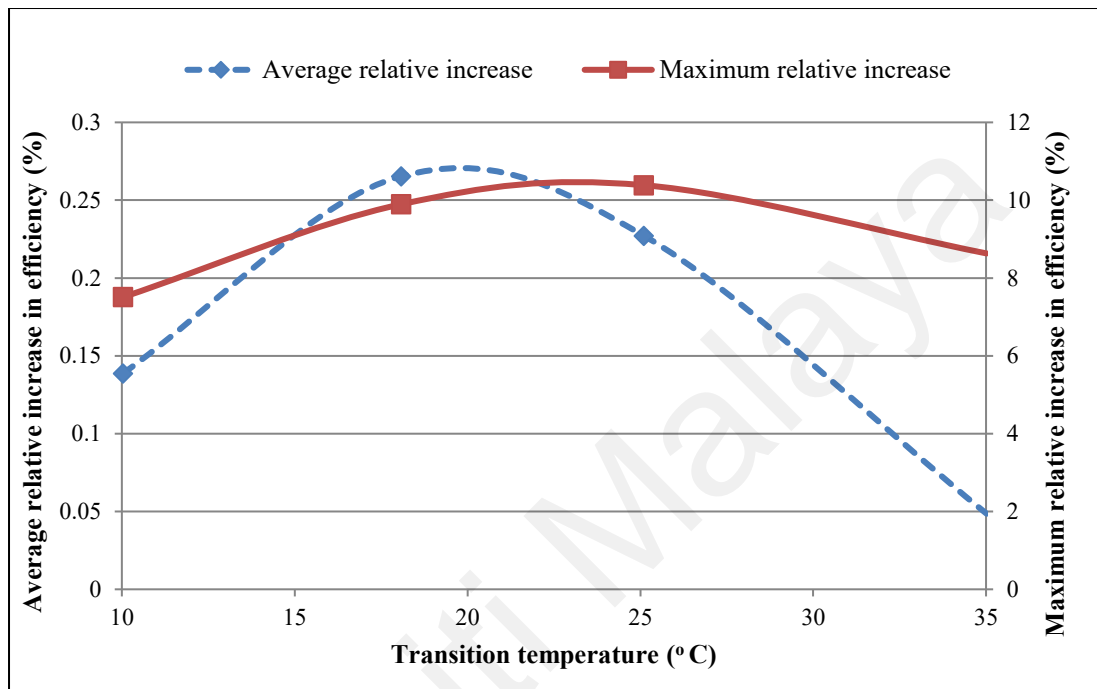
Figure 2.5: Average and maximum relative increase in efficiency for various transition temperatures
(Machniewicz et al., 2015)

A numerical model of a PV-PCM scheme, based on finite difference method, was built by Brano et al. (2014), where the system comprised of five different layers including glass and plastic layers, PV cell layer, PCM layer, etc. The phase change process was assumed isothermal and the model was validated by an in-situ experimental study using PCM RT27. The model faithfully predicted cell temperature for both sunlit and cloudy days.

The possibility of using PCM in building integrated photovoltaic (BIPV) system in the hot and arid weather of UAE was studied by Hassan et al. (2014). Authors reported

a maximum drop in peak temperature of 5°C on a cloudy day and 11°C on sunny day. It was projected that better temperature regulation is conceivable in hot summer days.

Hasan et al., (2014a) tested five different PCMs from the three classes, *viz.*, salt hydrate (SP224A and $CaCl_2.6H_2O$), paraffin (RT22) and eutectic mixture of fatty acids (capric-lauric acid and capric-palmitic acid) through differential scanning calorimetry (DSC) and temperature history method (THM). Capric-palmitic acid was testified as a good choice for PV-PCM application due to its higher heat of fusion, reasonable range of melting and solidification between 19° and 25°C.

Hasan et al. (2014b) employed solid-liquid PCM in PV panels to stabilize its operating temperature and assessed their efficacy under dissimilar climates of Dublin, Ireland and Vehari, Pakistan. Eutectic of capric-palmitic acid (PCM_1) and calcium chloride hexahydrate, $CaCl_2.6H_2O$ (PCM_2) were used in this study, wherein experimental results show that PCM_2 proved more effective in shaving peak temperature of the panel. A curtailment in cell temperature of 7°C in Dublin and 17°C in Vehari was realized with PCM_1, whereas PCM_2 lessened up to 10°C in Dublin and 21°C in Vehari. The significant findings have been summarized in Table 2.5. Cost-benefit analysis reveals that PV-PCM systems are more cost effective in the hot climatic conditions than rather cold environment.

Hasan et al. (2015), in an ensuing study, reported that daily average power savings at Dublin, Ireland was 1% with PV-PCM_1 and 1.8% with PV-PCM_2, whereas in Vehari, Pakistan these values were 4.4% and 7.7%, respectively.

Table 2.5: Temperature regulation, short-circuit current, open-circuit voltage, etc. for reference PV, PV-PCM₁ and PV-PCM₂ systems in Dublin and Vehari (Hasan et al., 2014b)

Measured Data	Time	Reference PV		PV-PCM₁		PV-PCM₂	
		Dublin	Vehari	Dublin	Vehari	Dublin	Vehari
Insolation G (W/m²)	At peak	970	950	970	950	970	950
	Average	674	660	674	660	674	660
Temperature (°C)	At peak	49	63	43	51	40	42
Temperature Regulation (°C)	At peak	-	-	7	17	10	21
Fill factor (%)	Average	-	69.64	72.82	71.26	73.22	72.24
V_{oc} (V)	At peak	20.1	18.32	20.81	19.71	20.95	20.15
	Average	20.41	18.72	20.52	19.42	20.81	19.92
I_{sc} (A)	At peak	3.74	3.42	3.70	3.35	3.68	3.33
	Average	2.82	2.45	2.77	2.41	2.78	2.39

Alenei et al. (2014) developed a numerical model of the BIPV-PCM installed in a building façade and examined its thermal performance both numerically and experimentally. Authors reported a thermal efficiency of around 10% with an overall efficiency of 20% (Figure 2.6).
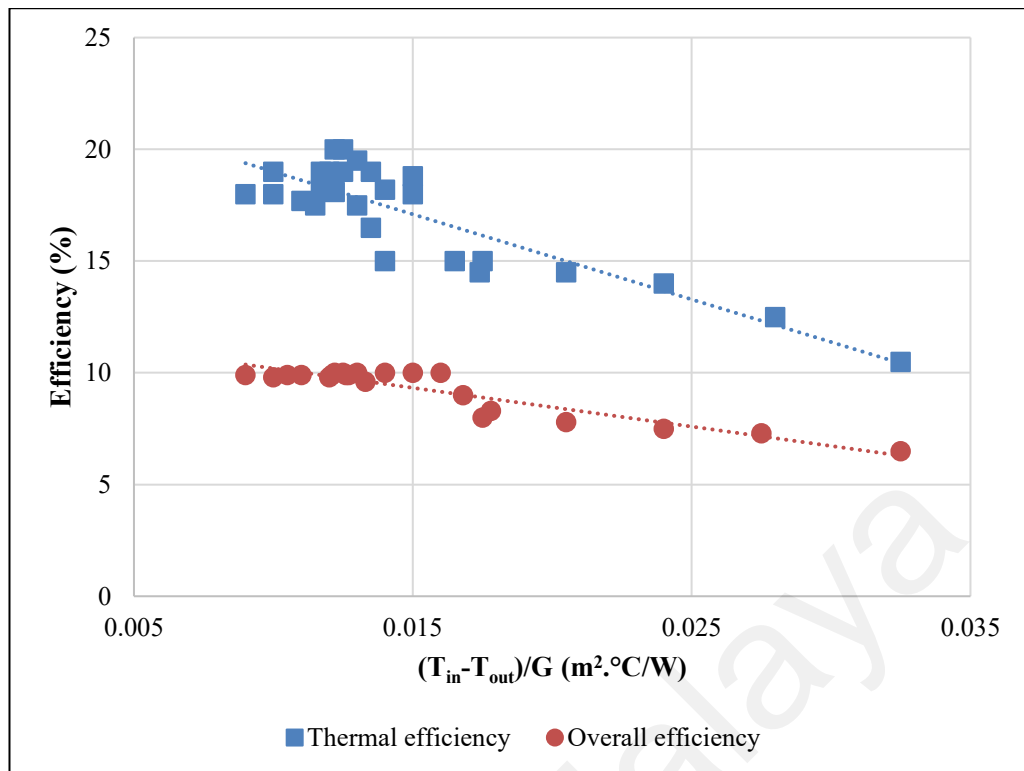
Figure 2.6: Thermal performance of the BIPV-PCM system
(Aelenei et al., 2014)

Biwole et al (2013) developed a computational model of the SP/PCM system (authors used this acronym to signify PV-PCM), wherein five different sizes of the PCM container (designated as a, b, c, d, e containing PCM RT25 and design c with cooling fins) were examined. Figure 2.7 shows that superior performance was observed with a vessel size of 13.2 cm × 4.9 cm having 3 cm long fins (design c), where the panel temperature was regulated within 34.9°C even after one hour whereas solar panel without PCM reached this temperature in only 5 minutes.
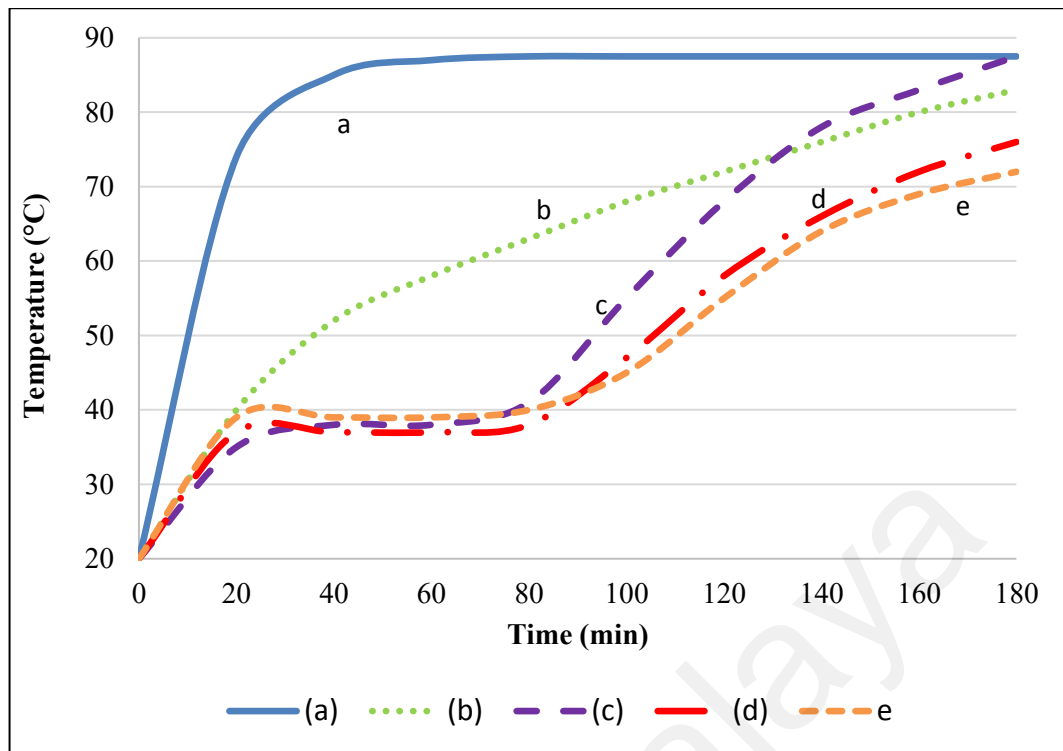
Figure 2.7: Effect design and size of PCM container on panel's operating temperature (design a, b, d, e are SP/PCM system of four different sizes; design c with cooling fins)
(Biwole et al., 2013)

Hendricks and Stark (2013) investigated the performance improvement of a BIPV-PCM module on a yearly basis using numerical model built on MATLAB. Experimental studies were conducted in moderate climate of Utrecht, Netherlands and hot weather of Malaga, Spain. While the energy gain with PV-PCM system in the summer is observed the same for both moderate and hot climates, PV-PCM system in hot region (Malaga) demonstrated fairly a higher energy gain in winter. In Figure 2.8, the temperature profile of the PV module with and without PCM shows that use of PCM ensures a steady cell temperature all day long.
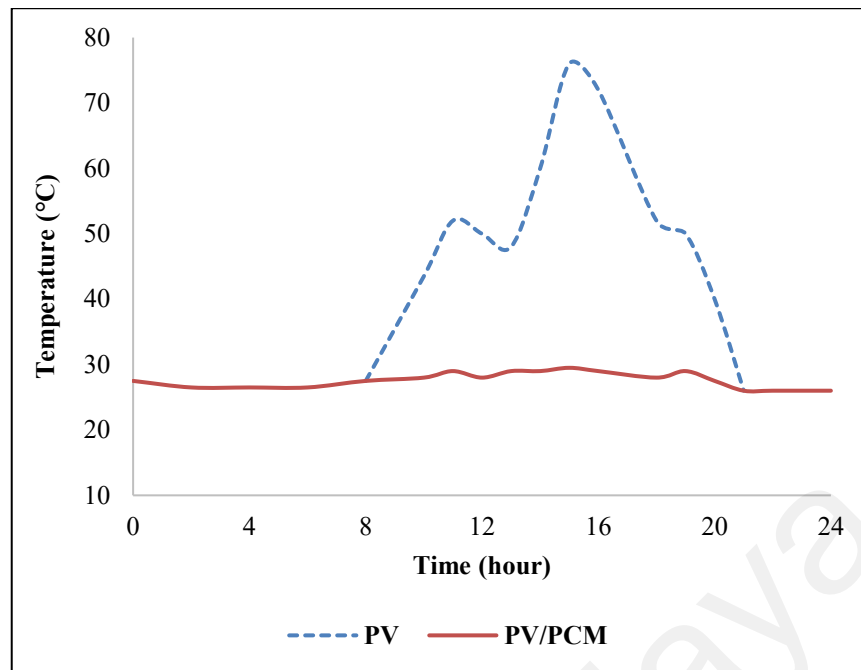
Figure 2.8: PV and PV-PCM temperature profile
(Hendricks & Sark, 2013)

A finite difference-based energy balance of a PV-PCM system proposed by Lo et al., (2013) and numerical analysis was carried out for four different cases, *viz.* Case I: no phase change, Case II: phase change, Case III: just started phase change and Case IV: just ending phase change. Brano et al. (2014), in a succeeding research, verified and validated the numerical model by experimental investigation where paraffin was used as PCM. Paraffin demonstrated meager performance as a thermal storage medium which might be due to its low thermal diffusivity.

Huang (2011) investigated a PV-PCM system composed of two PCMs with dissimilar phase transition temperatures. Two geometrical configurations of the containers, *viz.*, triangular and half circle were used to examine five different combinations of PCMs. The triangular cells containing RT27-RT21 were observed to offer more electrical energy supply and longer thermal regulation time (Figure 2.9).
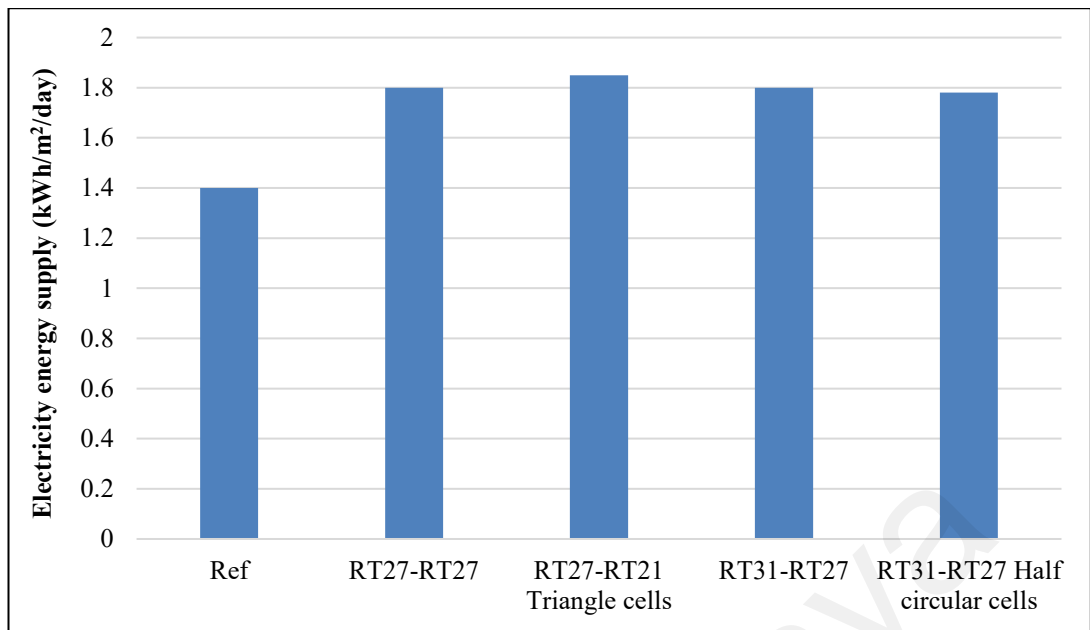
Figure 2.9: Electrical output of different PCM pairs in PV-PCM system
(Huang, 2011)

Huang et al. (2011) studied the effect of convection and crystalline segregation of PCM on the performance of a BIPV-PCM system. Authors noticed that due to crystal segregation there produced porosity in PCMs creating resistance to heat transfer. Application of fins in the PCM container was suggested as potential solution to crystal dissociation problem.

Hasan et al. (2010) assessed the potential of five selected PCMs (all with a melting temperature of $25\pm4^{\circ}C$) to regulate the BIPV-PCM temperature. Thermal conductivity of the PCM and the whole PV-PCM system turned out to be the prime controlling factor in temperature regulation. Salt hydrate PCM $CaCl_2$ accomplished the highest temperature reduction of $10^{\circ}C$ for the longest period of 5 hours under 1000 W/m^2.

Cellura et al. (2008) performed theoretical and numerical analysis of the thermal treatment of a PV-PCM system in COMSOL Multiphysics® considering hot ambiance. The average conversion efficiency was found 12% for a PV system without PCM, while it reached 26% with PV-PCM system. Figure 2.10 clearly manifests that PV-PCM system sustains lower temperatures all over the process.
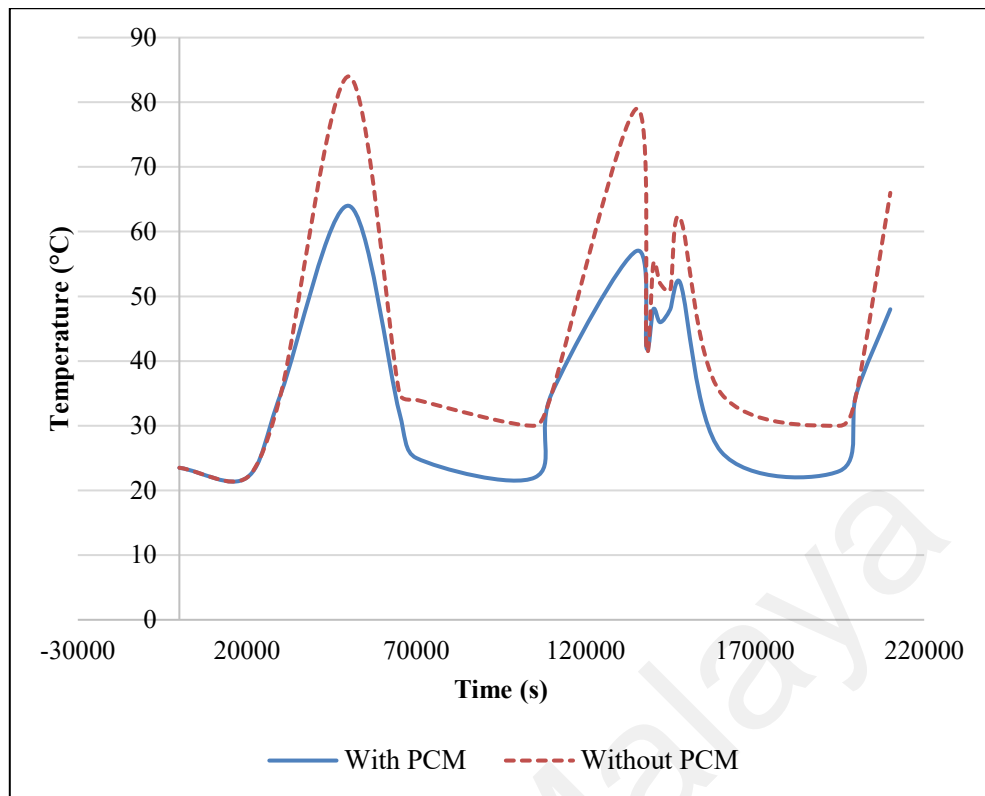
Figure 2.10: Temperature profiles with PV-only and PV-PCM systems (Cellura et al., 2008)

Huang et al. (2007) built three different 3D simulation models to simulate the functioning of PCM integrated with PV: $3D_1$ with heat transfer coefficient of 5 W/m^{2}K at two edges of PV-PCM system, $3D_2$ with adiabatic edges and $3D_f$ with attached pin fin configuration. Despite of the fact that pin fins improve thermal consistency, they were found to restrict natural convection.

Huang et al. (2004) used an aluminum box PCM container with a front surface coating of solar selective absorbing material to emulate a BIPV-PCM system holding PCM RT25. It was found that for the PV-PCM system with two fins the PV front surface temperature could be maintained below 36.4°C for 1 hour 20 minutes using a PCM thickness of 20 mm, whereas the temperature was sustained at 33°C for 2.5 hours when PCM thickness was doubled.

Cui et al. (2016) employed PCM in concentrating photovoltaic-thermoelectric (CPV-TE) system (Figure 2.11) with a view to assuage the fluctuation in temperature of the

39

PV cell and TE module, thereby maintain a fixed operating point for the CPV-TE system. Working with four types of PV cells (c-Si, CIGS, single junction GaAs and GaInP/InGaAs/Ge (III-V)) it was confirmed that use of PCM helps to maintain a moderately even temperature around 330K for five hours during mid-day and results in daily total efficiency of 26.75%. Li et al. (2014) also worked with integrating PCM in CPV-TE system and reported a 30% enhancement in the system efficiency.
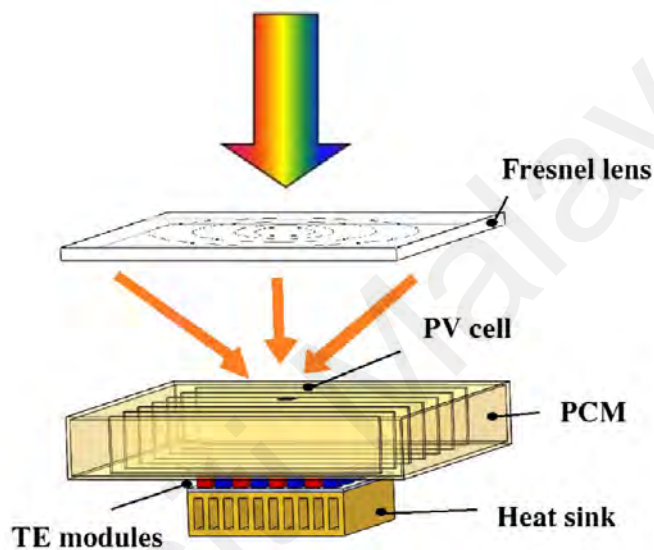
Figure 2.11: Schematic of hybrid PV-TE-PCM system
(Cui et al., 2016)

Sharma et al. (2016) experimentally investigated the thermal performance of PCM based building integrated concentrator PV (BICPV-PCM) system and compared the results with a naturally aerated BICPV-only system. Organic PCM RT42 was selected for this comparative study. Under an irradiance level of 1000 W/m^2, electrical efficiency was augmented by 7.70% with a 3.8°C reduction in module temperature.

Maiti et al. (2011) used metal-wax composite PCM (1-mm aluminum chips embedded in paraffin wax) for temperature regulation of a PV module. The predicted and experimental values of temperature rise for metal implanted PCM and PCM without metal chips is shown in Figure 2.12. In outdoor trial, the maximum temperature of the

PV-only system reached $78^\circ - 80^\circ C$, whereas with PV-PCM system this was limited to $64 - 65^\circ C$ leading to overall energy gain of 55%.
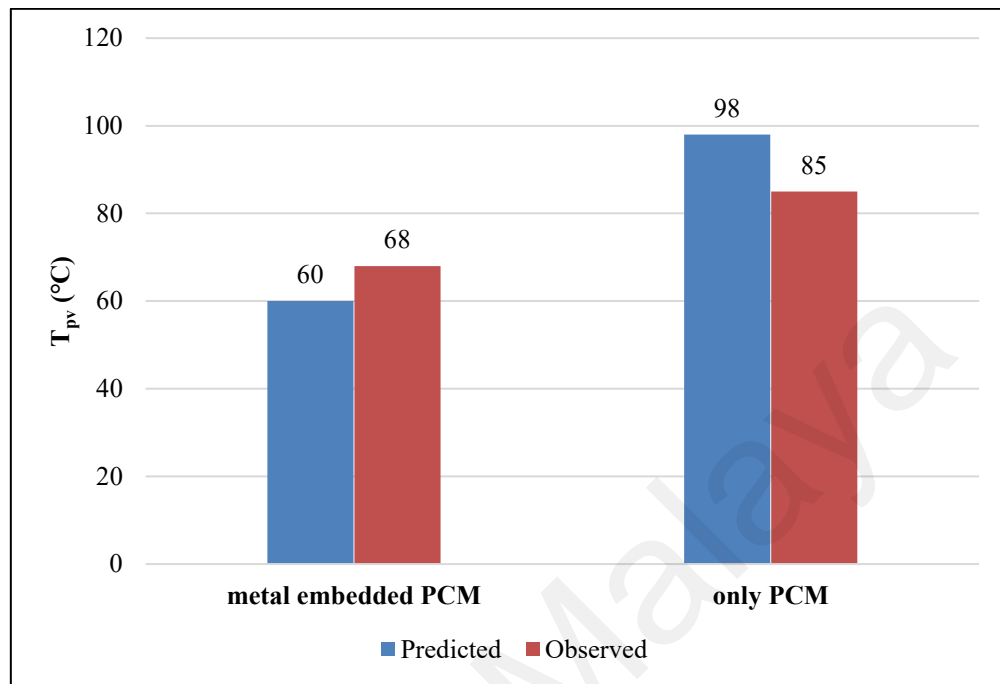
Figure 2.12: Predicted and observed values for PV module surface temperature
(Maiti et al., 2011)

Lillo et al. (2011) carried out performance investigations of CPV modules at twelve sites around the world using PCMs of four different phase transition temperatures, congruously *viz.*, 25°, 35°, 45° and $55^\circ C$. CPV-PCM system installed in Cairo, Egypt yielded 37.2% more power than that with a CPV-only system as compared to same arrangements in London, England. This finding suggests that PCMs are more adjuvant in thermal regulation in hot climates.

The endeavors of applying microencapsulated phase change materials (MPCM or MEPCM) slurry in the thermal regulation of PVT collectors are quite new. A PVT collector with MPCM slurry as the working fluid has been studied both theoretically and experimentally by Qui et al. (2016) and Qui et al. (2015). The effect of the slurry concentration on electrical output was studied and reportedly electrical yield is better when MPCM concentration was kept within 10%.

Ho et al. (2015) studied the performance of a PV-MPCM module which floats on water and rejects the heat carried by MPCM from the PV back surface. Two sizes of MPCM, *viz.*, 3 cm and 5 cm with corresponding melting points of 28ºC and 30ºC were considered. A 1.8ºC reduction in module temperature was detected with 2.1% increase in power generation compared to PV-only system by using 5-cm water saturated MPCM layer in the PV-MPCM system. Prior to this study, Ho et al., (2013) performed a numerical study on a BIPV-MPCM system using water saturated MPCM layer as passive thermal control medium. At elevated summer temperatures, BIPV-MPCM system with 3-cm water saturated MPCM layer (melting point 30ºC) was able to maintain a surface temperature of 34.1ºC whereas a PV-only system gained 38.5ºC under the same conditions.

2.5   Nanoparticles as PCM Property Enhancer

Although application of PCM in PV and PVT has brought improvement in their efficiency, significant outcome is still impalpable due to poor thermal properties of the PCM. Hence, for successful implementation of the PV-PCM or PVT-PCM systems, it is important to enhance the thermal conductivity of the PCM. Thermal conductivity of the base PCM can be upgraded utilizing various ways, such as metal chips impregnation into the PCM, microencapsulation, etc. However, the first method is electrically delinquent for the PV module and the later one is very expensive to implement. On the other hand, incorporation of nanoparticles (nano powders, nanowires, nanotubes) opens a new horizon in meaningful upgradation of PCM thermal conductivity (Javani et al., 2014; Khodadadi & Hosseinizadeh, 2007). It has been reported that besides enhancing the thermal conductivity insertion of nanoparticles retards the melting phase and extends the solidification phase of a PCMs, thereby improves thermal homogeneity to the base PCM (Murugan et al., 2018). In addition, nanoparticles improve the dynamic

thickness of the PCM which counteractively affects the convective heat transfer (Kant et al., 2017). Nanoparticles noticeably increase thermal cycling stability of the PCMs (Qiu et al., 2019).

2.5.1 Selection Criteria of Nanoparticles

Nanoparticle selection depends on thermal conductivity, particle size, cost, volume fraction and type of base PCM, etc. Particle size plays an important role in nanoparticle applications since nano scale particles increases the surface area relative to volume and provide better dispersion into the base material. Experimental evidence indicates that effective thermal conductivity increases with decrease in particle size (Ho & Gao, 2009). Also, time required for melting increases with nanoparticles concentration (Hajare & Gawali, 2015). This is because dynamic viscosity increases pointedly as nano particle concentration increases. Enhancement in dynamic viscosity may play an important role in natural convection dominated melting of nano composite PCM. If natural convection governs the heat transfer rate in melting process, higher viscosity reduces the buoyancy more that, in turn, slower the melting process (Hajare et al., 2014).

2.5.2 Nanomaterials in Energy-intensive Applications

The impregnation of nanoparticles into the PCM lattice adds incredible thermal conductivity (Ling et al., 2015). It can prolong the time length of the energy storing/discharge process (Mills et al., 2006). Incorporation of nanoparticles reportedly solves some other problems with PCM like leakage during liquid phase to some extent (Zhang & Fang, 2006). Nanoparticles utilized for energy applications are chiefly metals, oxides, and carbon materials. The mostly utilized metal nanoparticles are Cu, Ag, and Al nanoparticles. Qian et al. (2015) demonstrated that the expansion of Ag nanoparticle on polyethylene glycol (PEG) can improve its thermal conductivity by 127%.

Moreover, time required for the melting and solidification process is reduced, principally because of the improvement in the heat transfer. Nanoparticles like Cu, Al, Ag nanowire improve the thermal conductivity of the base PCM (Chen et al., 2017). Metal oxide nanoparticles are thermally steadier than its base metal and some even display thermal conductivity more noteworthy than metal nanoparticles (Zeng et al., 2010). Thermal conductivity of the base PCM reportedly increased by around 1-80 % through the incorporation of metal oxide nanoparticles depending on the type of the nanoparticle (Wu et al., 2010). The metal oxide nanoparticles that are most normally utilized for PV and solar thermal applications are Al_2O_3 (Colla et al., 2017), TiO_2 (Sharma & Shukla, 2015), and Fe_3O_4 (Şahan et al., 2015).

The carbon-based nanoparticles are progressively getting focus because of the benefit of the better thermal strength as compared with metal and metal oxides nanoparticles. The major carbon-based nanoparticles those are used in solar applications include multi-walled carbon nanotubes (MWNT), graphene, and graphite. It has been seen that the thermal conductivity of the natural PCMs can be multiplied by utilizing these carbon-based nanoparticles. Choi et al. (2014) have indicated that heat transfer rates in stearic acid PCM can be improved to about 3.35 times with the graphite nanoparticles. Harish et al. (2015) found that dispersion of only 1.0 vol.% of graphene into lauric acid PCM can improve the thermal conductivity to about 230%. It has been observed that nanoparticle agglomeration does not significantly influence the enthalpy and melting temperature of base PCM. Li (2013) observed that the dispersion of graphite nanoparticles into paraffin can improve the thermal conductivity to about 741%. The colloidal suspension of nanoparticles, nanotubes, and nanofibers have attracted specialists especially because of high thermal energy storing properties, high thermal conductivity, and incredible diffusion characteristics. A genuine case of a nanoparticle-based colloidal suspension is liquid KNO_3 blended in with some oxide

nanoparticles like SiO_2 or Al_2O_3 (Chieruzzi et al., 2015). Authors observed an enhancement in heat transfer by around 5.0 to 9.5 % and that in heat storage capacity by 16%.

Wang et al. (2017) have demonstrated that dispersion of 2.0 wt% graphite nanoparticles increases thermal stability up to 300 melt-freeze cycles. Dispersion of multi walled CNT (MWNT) into the palmitic acid reportedly improved the thermal conductivity by 30% (Wang et al., 2010). According to Zou et al. (2018) thermal conductivity can be improved by 128% in the MWNT/graphene-based composite. Cui et al. (2011) indicated that dispersion of 10 wt% nanofibers into liquid soy wax can augment the thermal conductivity by 44.8 % which is greater than that attained with CNTs. Yu et al. (2013) have detailed that thermal conductivity can be improved by 13.3 % in paraffin by incorporating 4.0 wt% carbon nanofibers.

Nano composite PCMs impregnated with metal nanoparticles gives brilliant thermal conductivity. Additionally, inclusion of metal structure helps to conform a firm shape of the composite material (Mahmoud et al., 2013). Cu, Ni, and TiO_2 are mostly used metal and metal oxide nanoparticles in solar applications (Chen et al., 2016; Huang et al., 2017; Li et al., 2016). Wang et al. (2016) found the thermal conductivity of paraffin wax/Cu composite to be 2.88 W/mK which is 491% greater than paraffin wax. Karthik et al. (2015) have indicated that impregnation of graphite nanoparticle into erythritol PCM can improve the thermal conductivity by 3.77 W/mK which is multiple times greater than the base material. The honeycomb structure of nanotubes helps thermal efficiency increase with a decrease in time taken for melt-freeze cycle (Kabeel et al., 2017). Abdelrahman et al. (2019) have used $RT35HC/Al_2O_3$ nanocomposite to reduce PV module temperature and reported a 52.3% decrease in the top surface temperature. Zarma et al. (2019) reported that in a concentrator PV system application of nano

composite of Al_2O_3 nanoparticle (5.0 wt%)/PCM can prompt the achievement of electrical efficiency up to 8% and abate the cell temperature by 12°C.

Kant et al. (2020) have examined the impact of nano enhanced PCM (NePCM) on the BIPV system. The base PCM picked was the n-octadecane which was mixed with various types of nanoparticles, viz., Cu, Al_2O_3, CuO, and TiO_2. Results show that the NePCM lessen the working temperature of BIPV for a longer period as compared to pure PCM n-octadecane. The cooling period (i.e., to maintain BIPV temperature below 40°C) was observed 60 minutes with Cu, 55 minutes with CuO, 50 minutes with Al_2O_3, and 49 minutes with TiO_2, whereas pure n-octadecane could maintain this limit only for 41 minutes.

2.5.3 Research Works on the Application of Nanoparticles in PVT

The suspension of nanoparticles (1 – 100 nm) in common carrier fluids is known as nanofluid. Nanofluids can be effective coolants for PV modules since they reportedly enhance thermal properties (especially, thermal conductivity) of the common heat transfer fluids (HTF) like water, ethylene glycol, etc. (Mahian et al., 2013).

Elmir et al. (2012) reported that use of Al_2O_3/water nanofluid on silicon solar cell increases the average Nusselt number. Yun and Qunzhi (2012) applied layers of MgO/water nanofluid with different concentrations on the top of PV cells and observed that increase in film thickness distresses thermal and electrical efficiencies of the PV module.

Rejeb et al (2016) developed a finite volume based 2D FORTRAN model to study the effect concentration of nanofluids, types of nanoparticles and carrier fluids on PVT electrical and thermal performances. The best thermal and electrical performance was realized with Cu/water nanofluid. It was also detected that increasing the weight

fraction of nanoparticles from 0 to 4% enhances the thermal conductivity of Cu/water by 11.82% and that of Al_2O_3/water by 11.23%.

Jing et al. (2015) prepared a well dispersed SiO_2/water nanofluids with different particle sizes and applied in PVT collectors. As compared to deionized (DI) water, thermal conductivity was enhanced by 20% by using 5-nm particle size and 2% volume fraction of nanofluid. Authors also built a 2D numerical model of the PVT with nanofluid using CFD technique. With the optimal light concentration of 40 and a flow velocity of 0.015 m/s the maximum improvement of exergy efficiency of 7.0% was achieved by using nanofluid instead of DI water.

Ghadiri et al. (2015) used distilled water and a ferrofluid (Fe_3O_4/water) with 1.0 wt% and 3 wt% concentrations, the ferrofluids being subjected to constant and alternating magnetic fields in the cooling section of a PVT system. Application of 50-Hz frequency alternating magnetic field prompted about 4 – 5% increase in overall efficiency with an overall exergy output of 48 W. As compared to an overall efficiency of only 52% with distilled water coolant ferrofluid accomplished a remarkable 76% overall efficiency.

Karami and Rahimi (2014) employed different concentrations of boehmite ($AlOOH \cdot xH_2O$) for the PV cooling, where two geometries of flow channel were used: a straight rectangular channel and a helical channel. The highest temperature drops (18.33ºC for the straight channel and 24.22ºC and helical channel) were attained for 0.1 wt% concentration of nanofluid and the corresponding electrical efficiency accomplishment was 20.57% and 37.67%. Helical geometry resulted in better heat transfer as confirmed by high Nusselt number.

Sardarabadi et al. (2014) employed SiO_2/water nanofluid as the HTF for PVT collectors and observed that as compared to plain water 1.0 wt% of SiO_2/water

nanofluid enhances the thermal and overall energy efficiency by 7.6% and 3.6%, while 3.0 wt% of SiO_2/water nanofluid augments these margins by 12.8% and 7.9%. The exergy efficiency with 1.0 wt% and 3.0 wt% of SiO_2/water was 22.61% and 24.31% respectively, whereas with plain water this value was 19.36%.

Xu and Kleinstreuer (2014) made use of dilute nanoparticle suspensions in liquids to ameliorate the efficiency of concentrating photovoltaic thermal (CPVT) collector. An outlet temperature of 62°C was observed with nanofluid and under controlled flow rate the overall efficiency of the system reached 70%.

2.6 Summary of Literature Review and Research Gaps

The main objective of the present research is to develop a susceptible PVT system using nano enhanced PCM (NePCM) to control the cell temperature below a practicable limit and to get better electrical and thermal efficiency. From the literature review, it is found that most of the conventional thermal regulation methods could not achieve a cell temperature below 40°C, rather in most cases it was around 48°C. On the other hand, though thermal efficiency accomplishment (> 70%) with some cooling methods were satisfactory electrical efficiency (< 10%) is still far below a considerable mark. Another major issue with PVT systems is their ineffectiveness to provide heat for nighttime application. While deep-cycle or other sorts of batteries provide a solution for electrical energy storage for PV systems, workable heat storage is still far from success. Some researchers proposed the usage of PCM as heat storage solution for PVT applications and reported significant results. However, such research initiatives are in a nascent phase and more extensive works with every possible materials and deployment methods should be investigated. Possibility of using nanomaterials in conjunction with phase change materials should also be investigated thoroughly.

CHAPTER 3: RESEARCH METHODOLOGY

3.1 General

This chapter presents a systematic, theoretical analysis of the methods applied to resolve the present research questions. The various steps that are involved in studying the research problem will be discussed and appraised in detail. Research techniques espoused for the present research are basically data-based experimental or empirical along with limited simulation works, wherein conclusions will be drawn based on verified observation or experimentation. Assumptions underlying these research techniques will also be examined rigorously in order to retrench experimental errors and uncertainties.

3.2 Experimental

In the present research, a novel framework of photovoltaic thermal (PVT) system has been proposed that employs nano enhanced PCM (NePCM) for thermal regulation and heat storage. This is basically an experiment-based research and the research protocol is described as follows. In the first phase, a few organic PCMs is primarily selected considering their phase change (transition) temperature (PCT) and the mean daytime temperature of Kuala Lumpur, Malaysia; thereafter, the best materials is confirmed through differential scanning calorimetry (DSC) characterization method. Hence, nanoparticles with high thermal conductivity has been incorporated in the selected PCM matrix to form nano enhanced PCM (NePCM) and the newly synthesized material is characterized through differential scanning calorimetry (DSC), thermogravimetric analysis (TGA), Fourier transform infrared (FTIR) spectroscopy and field emission scanning electron microscopy (FESEM). In the second phase of the research, this newly developed material has been integrated with PVT module to

fabricate PVT-NePCM system. To facilitate a comparative performance evaluation a PV-PCM and a PVT-PCM module has been fabricated using the selected PCM and real-time experimental performance investigation is carried with five systems, namely a reference PV, a PV-PCM, a PVT, a PVT-PCM and the newly developed PVT-NePCM. The detailed research protocol is shown in Figure 3.1.
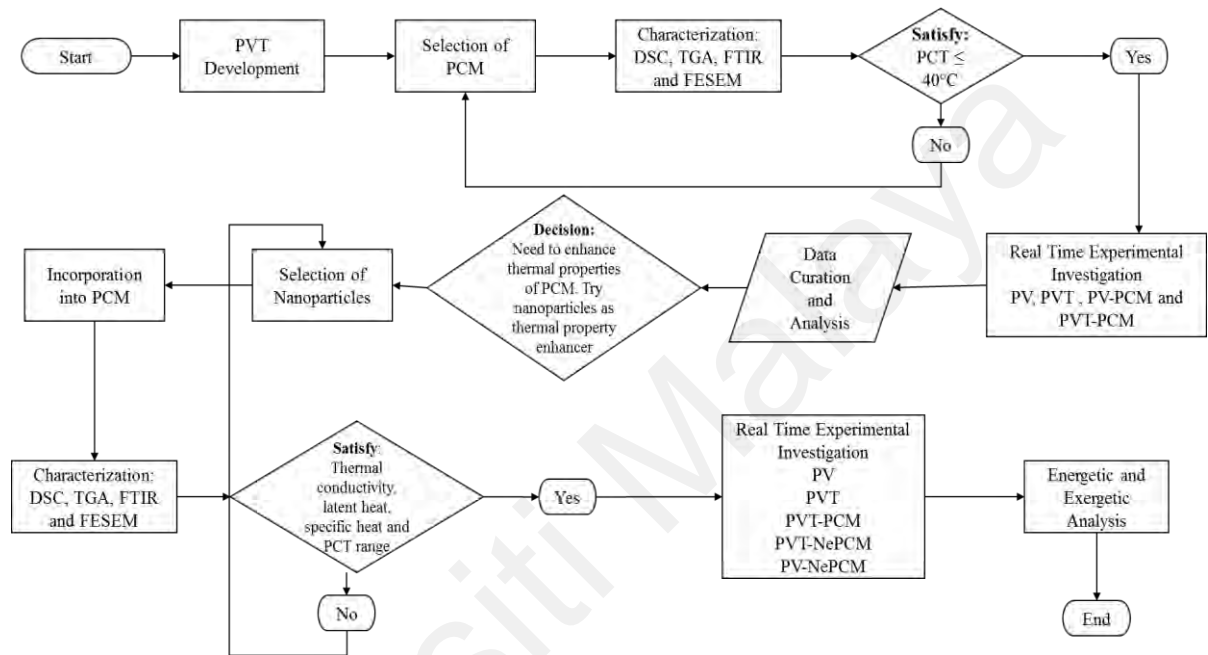
Figure 3.1: Research protocol for the present investigation

The electrical and thermal performance of the newly developed PVT-NePCM system has been studied and contrasted with those of PV, PVT, PV-PCM and PVT-PCM systems. To ensure the same environs, all the modules have been erected side by side in the same outdoor experimental site and data is recorded concurrently from the five modules in digital data loggers. Figure 3.2 shows the schematic of the PVT module. Table 3.1 enumerates the electrical specification of the five 36-cell polycrystalline silicon (p-Si) PV and PVT modules chosen for the experimental investigation. Thermal collector of the PVT is designed in line with commercially available parallel circular pipe configuration so that the efficacy of using NePCM may well verified for the regular systems. Detail specification of the thermal collector is given in Table 3.2. The

schematic of the outdoor experimental set up along with the instrumentation and data acquisition arrangement is illustrated in Figure 3.3.
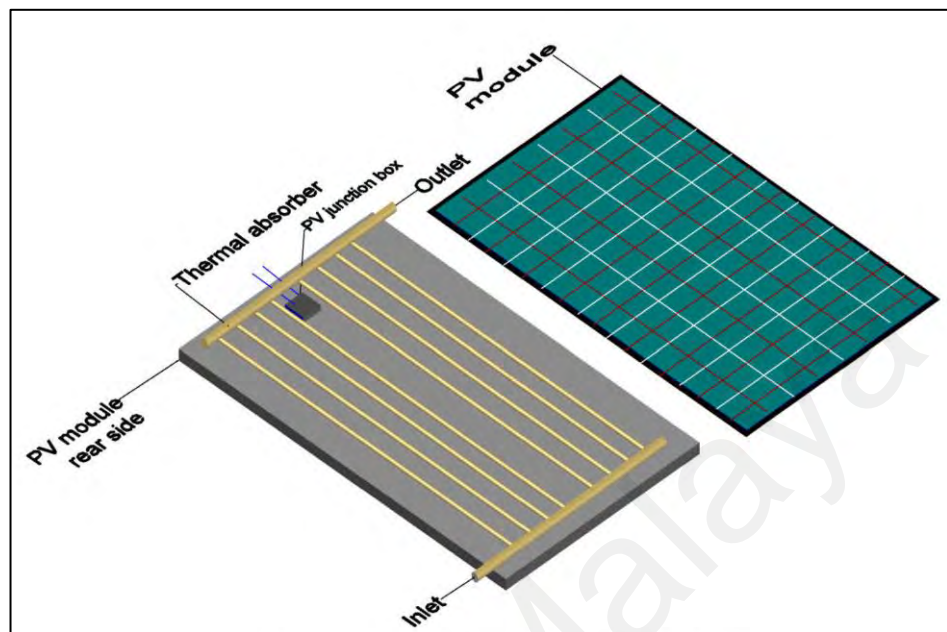
Figure 3.2: Schematic design of the PVT module

Table 3.1: PV and PVT modules' specification

Model: CENTSYS (SFPVP – 100)	
Maximum power (P_{max})	100 W
Power tolerance	+/- 3%
Number and type of cells	36; polycrystalline silicon
Open-circuit voltage (V_{oc})	21.6 V
Short-circuit current (I_{sc})	6.11 A
Maximum power voltage (V_{mpp})	18 V
Maximum power current (I_{mpp})	5.55 A
Module efficiency	14.9%
Solar cell efficiency	17.2%
Maximum system voltage	1000 V DC
Operating temperature	$- 40^o$ to 85^oC
Module dimension	1025 mm × 671 mm × 30 mm
Cell dimension	156 mm × 104 mm
Tested at	1000 W/m^2, 25°C, AM 1.5 (STC)

Table 3.2: Thermal collector specification

Configuration: Parallel circular pipe	
Material (both collector & absorber)	Copper
Number of riser pipes	8
Spacing between risers	40 mm
Header pipe diameter	20 mm
Riser pipe diameter	12 mm
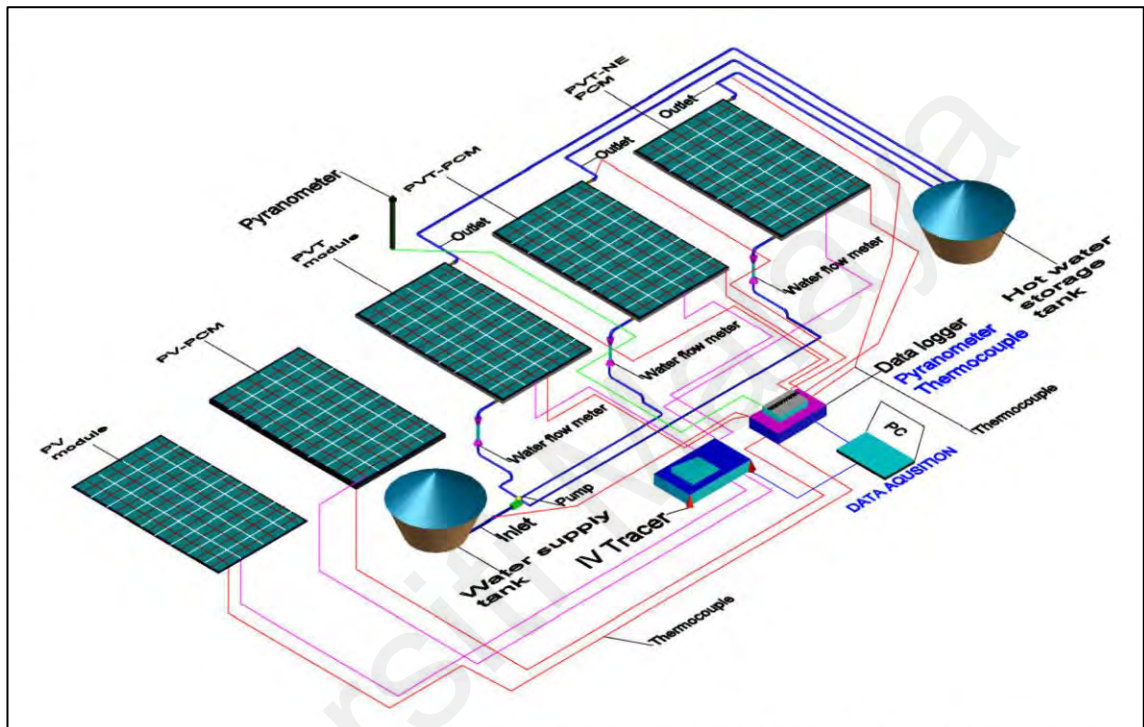
Figure 3.3: Schematic of the experimental arrangement

At this stage, synthesis and characterization of the new nano enhanced phase change material (NePCM) has been elucidated in the subsequent sections.

3.3 Synthesis and Characterization of Nano Enhanced Phase Change Material

3.3.1 Selection of Phase Change Material

Selection of PCM for PVT applications depends on the ambient temperature where the module is installed. The regular daytime temperature of Kuala Lumpur, Malaysia is 33ºC (MetMalaysia, 2020) and an allowance of 10º to 15ºC is considered enough to captivate the major amount of heat from the module. Hence, four organic PCMs with

melting points around 42º to 50ºC has primarily been selected for the current application since organic PCMs possess more heat storage capacity within this temperature range (Figure 3.4). The latent heat and phase transition temperatures of the selected organic PCMs have been ascertained through differential scanning calorimetry (DSC) test. From Table 3.3, it is apparent that RT44HC is the best PCM for the present application with the highest latent heat capacity of 241.584 kJ/kg. Moreover, its narrow phase transition range, which is only 2.35ºC (from 44.55º to 46.90ºC), makes it suitable for solar application. The thermal properties of RT44HC as reported by Rubitherm GmbH, Germany are given in Table 3.4.

| RT47 | RT55 | RT50 | RT44HC |
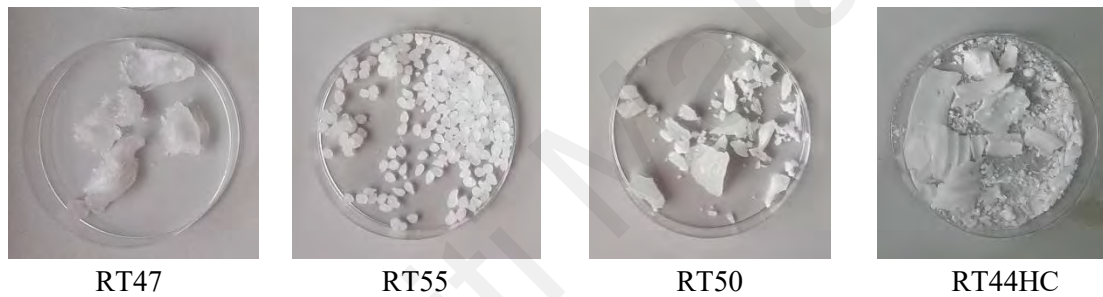
Figure 3.4: Physiognomy of four primarily selected PCMs

Table 3.3: DSC test results of the selected organic PCMs

PCM	Onset temperature (ºC)	Peak temperature (ºC)	End temperature (ºC)	Latent heat (kJ/kg)
RT44HC	44.55	45.69	46.90	241.584
RT47	39.95	45.67	47.25	139.224
RT50	44.72	49.62	50.92	144.888
RT55	49.81	54.97	57.17	142.400

Table 3.4: Thermal properties of RT44HC (Rubitherm, 2020)

Phase change temperature (ºC)	44.0
Density (kg/m^3)	805
Latent heat capacity (kJ/kg)	242
Specific heat capacity (kJ/kg.K)	2.15
Thermal conductivity (W/m.K)	0.18

3.3.2 Selection of Nano Particles

Despite their extensive latent heat storage capacity organic PCMs possess very low thermal conductivity. Supplement of nanoparticles in PCM matrix has been found to enhance their thermal conductivity (Rosen et al., 2004). Such composite materials, known as nano enhanced PCM (NePCM), employ various nanoparticles like aluminum (III) oxide (Al_2O_3), copper (Cu), copper (II) oxide (CuO), titanium (IV) oxide or titania (TiO_2), zinc oxide or zinc white (ZnO), silicon carbide (SiC), titanium carbide (TiC), gold (Au), silver (Ag), single-walled carbon nanotubes (SWNT) and multi-walled carbon nanotubes (MWNT), graphene, graphene oxide (GO), exfoliated graphene (ExG) are the most frequently used nanomaterials for thermal applications (Trisaksri & Wongwises, 2007).

It has been reported that thermal and electrical conductivity of MWNT is very near to that of copper (Ebbesen et al., 1996; Treacy et al., 1996) and assimilation of only 1% functionalized nanotubes doubled the thermal conductivity of the base material (Khalid, 2013; Kim et al., 2001). Therefore, in the present research, MWNT is preferred as thermal conductivity enhancer for PCM RT44HC. The 98% pure laboratory grade MWNT (OD: 10 – 20 nm; L: 10 – 30 μm) was procured from TMM Disruptive Advanced Materials, Brooklyn, NY, USA. The physiognomies of PCM RT44HC and pure MWNT are shown in Figure 3.5.
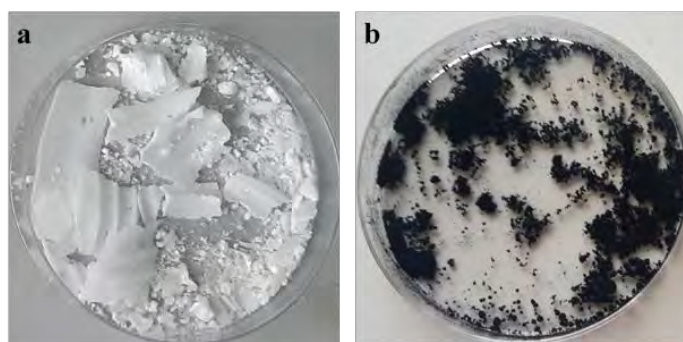

Figure 3.5: Physiognomy of (a) RT44HC and (b) MWNT

3.3.3   Preparation of NePCM

The NePCM was prepared by means of the following procedure. Primarily, MWNT nanotubes were desiccated at 105°C for 24 hours to dissipate moistness and then flown through a 100-mesh sieve. Then, surface modification of pure MWNT was accomplished in the following process to produce functionalized multi-walled carbon nanotube (f-CNT) (Ngo et al., 2013; Saito et al., 2002). For this purpose, 0.5 gm of nanotubes were absorbed in 80 ml H_2SO_4/HNO_3 (3:1, v/v) mixture and sonicated at 70°C a few times in a ultrasonication bath for 30 – 45 minutes. The acid treated MWNTs were filtered through a 500-nm polytetrafluoroethylene (PTFE) filter and the black precipitate assimilated after filtration was washed thrice with distilled water and methanol and dried at 80°C in vacuum for eight hours. The black lumps formed upon drying were then crushed into ultra-fine powder in a high energy ball mill.

In the next phase, 0.025 gm f-CNT was dispensed into 10 gm (i.e., 0.25 wt% f-CNT) of molten RT44HC and swung for one hour on a hot plate cum magnetic stirrer at 50°C (Figure 3.6 (a)). Afterwards, the mixture was sonicated (Figure 3.6 (b)) at 50°C for one hour to lay out the nanotubes evenly all over the PCM matrix. After sonication, the solution was cooled in room temperature forming a solid NePCM cake of RT44HC-0.01%f-CNT. In the same manner, three other NePCMs, namely RT44HC-0.10%f-CNT, RT44HC-0.05%f-CNT and RT44HC-0.01%f-CNT were synthesized.
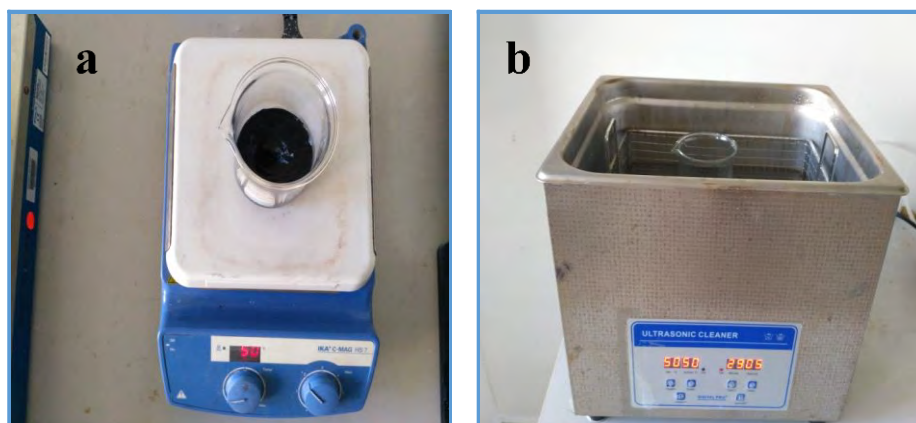
Figure 3.6: (a) Magnetic stirring of nanotubes in molten PCM and (b) Ultra sonication of the mixture

3.3.4 Characterization of NePCM

The four synthesized NePCMs have been characterized for their microstructural features, phase transition properties, thermal and chemical stability.

3.3.4.1 Field emission scanning electron microscopy

Microstructural analyses of the pure and nano composite materials have been carried out by a field emission scanning electron microscopy (FESEM). A FESEM of model: Quanta FEG 250 manufactured by Thermo Fisher Scientific, USA (Figure 3.7) is used to capture the micrographs of the pure PCM, MWNT nanoparticles and NePCM samples. The high-resolution electron microscope can characterize both conductive and non-conductive materials and particularly suitable for nano-characterization with a wide magnification range of 6 to 1000000×. In the present research, non-conductive PCM, conductive MWNT and NePCM samples were observed under magnifications ranging from 5000× to 100000× with a view to reveal the changes in microstructure due to insertion of nanoparticle in the PCM matrix.

Figure 3.7: Field emission scanning electron microscope (FESEM) set up at INFRA lab, Universiti Malaya, Malaysia

3.3.4.2 Differential scanning calorimetry (DSC)

In order to detect the transitions of the PCM and NePCM along with their heat capacity and heat content change the heat flow, the DSC method was employed in the present study. A double furnace PerkinElmer DSC-8000 calorimeter (Figure 3.8) with heating rates from $0.01°$ to $300°C/min$ was used for this purpose. Thermal analyses of all the samples were carried out within the temperature range from $-10°$ to $150°C$, wherein a ramp rate $5°C/min$ was maintained. To remove moisture or oxygen from the furnace nitrogen (N_2) was flown as an inert purge gas at a rate of 20 ml/min.

Figure 3.8: Differential scanning calorimeter (DSC) at INFRA lab, Universiti Malaya, Malaysia

3.3.4.3 Simultaneous thermal analyzer

Thermal stability of the materials was studied by thermogravimetric analysis (TGA) in a simultaneous thermal analyzer (STA) of Model: STA 6000 manufactured by PerkinElmer (Figure 3.9) for examining the weight degradation of the samples from 30° to 500°C at 5°C/min. Similar to DSC, nitrogen (N_2) gas was supplied into the furnace at a rate of 20 ml/min.
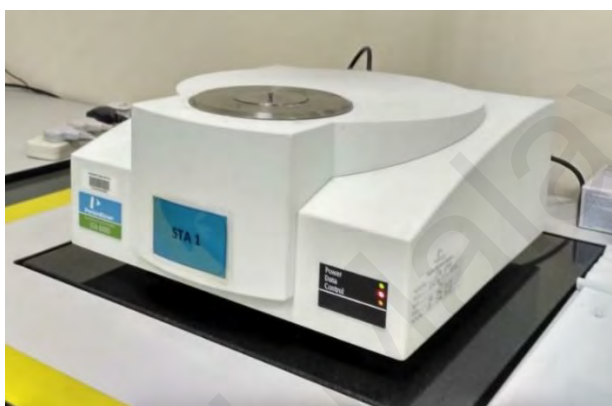

Figure 3.9: Simultaneous thermal analyzer (STA) at INFRA lab, Universiti Malaya, Malaysia

3.3.4.4 Fourier transform infrared (FTIR) spectroscopy

The functional groups play an important role on the chemical compatibility of PCM (Alkan et al., 2009). Chemical stability of the pure and composite materials was ascertained through Fourier transform infrared (FTIR) spectroscopy using a PerkinElmer Spectrum 400 FTIR spectrometer wherein GladiATR brand attenuated total reflectance (ATR) accessory manufactured by Pike Technologies was employed (Figure 3.10). The measuring range of the apparatus is from wave number 4500 cm^{-1} to 400 cm^{-1} under static atmosphere. Table 3.5 gives the measurement ranges of all the instruments used for material characterization.
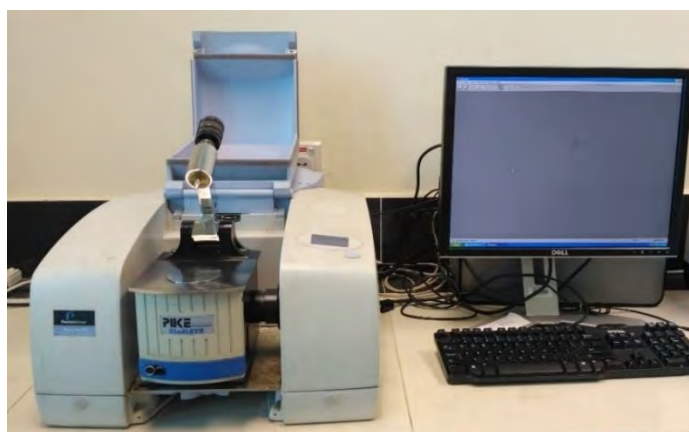
Figure 3.10: Fourier transform infrared (FTIR) spectrometer at CenFac lab, Universiti Malaya, Malaysia

Table 3.5: Measuring ranges of the instruments used for characterization

Instrument	Measuring Range
FESEM (Model: Quanta FEG 250, Thermo Fisher Scientific)	Magnification range: 6× to 1000000×
DSC (Model: DSC-8000, PerkinElmer)	−50° to 600 °C
STA (Model: STA 6000, PerkinElmer)	30° to 1000 °C
FTIR (Model: Spectrum 400, Perkin Elmer)	400 cm^{-1} to 4500 cm^{-1}

3.3.5   Thermal Conductivity Measurement

Thermal conductivity of the pure PCM and NePCM has been measured in order to observe how incorporation or functionalized MWNT (f-CNT) into PCM matrix influence this property. The transient hot bridge (THB) method has been adopted in the present research to measure the thermal conductivity of PCMs and NePCMs because it allows the measurement of solid, melt and liquid samples and ensures temperature regulation with highest precision. Figure 3.11 (a) shows the THB furnace used to measure thermal conductivity.
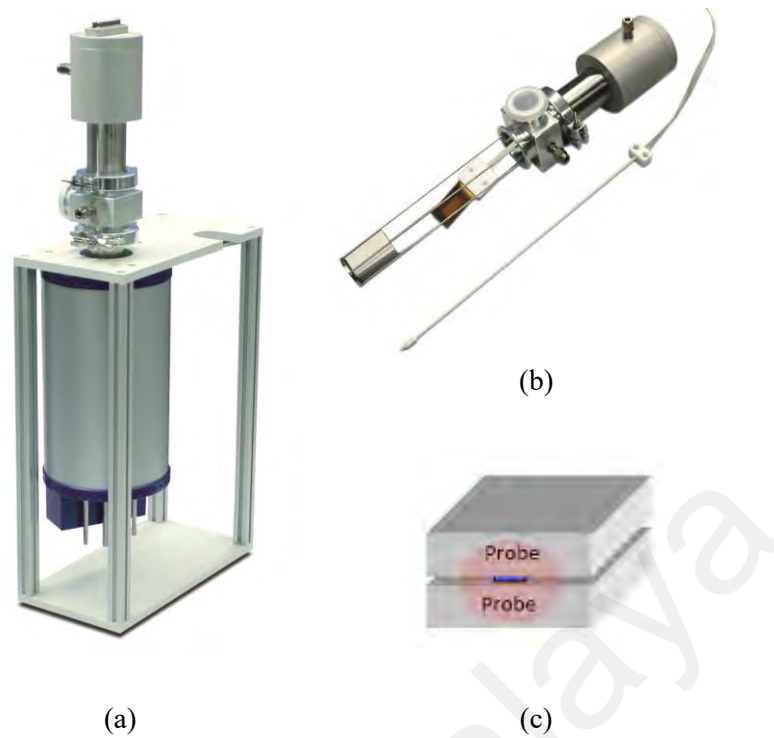
Figure 3.11: Transient hot bridge (THB) furnace

The most important part of THB method is a strip shaped conductor as shown in Figure 3.11 (b) (yellow strip at the middle). This strip serves as a heat source and a temperature sensor as well. A dainty rectangular metallic foil was embedded between two pieces of PCM samples (Figure 3.11 (c)). It was heated by the electric flow and the temperature in the region was optically estimated as the capacity of time. This procedure gives both the thermal conductivity and the thermal diffusivity of the sample. By precisely watching the temperature the different thermal properties can be handily decided (Gustafsson, 1991; He, 2005).

3.3.6   Thermal Cycling Stability Test

Phase change materials are generally used in such applications where they undergo many melt-freeze cycles every day, which deteriorate their thermal stability and efficacy to control temperature precisely. A thermal cycling stability test is designed to determine the cycling stability of a phase change material. During the study, a PCM goes through specified number of cycles (several hundreds to thousands) as quickly as

possible to see if any thermal or chemical degradation occurs. The results help to set the useful lifetime of a PCM and its suitability for different applications.
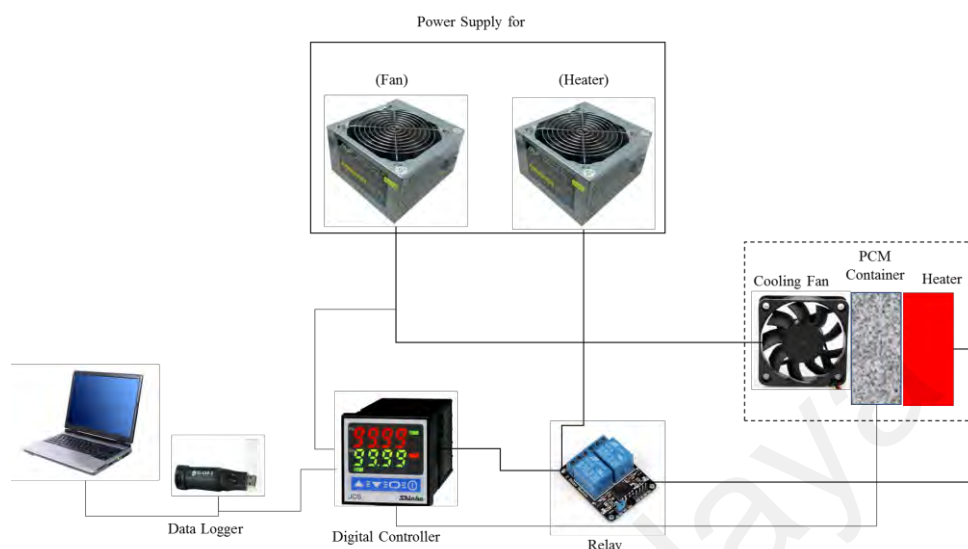

Figure 3.12: Thermal cycling stability test set up

In the present research, a custom-made thermal cycling tester (Figure 3.12) has been used to study the stability of the newly synthesized NePCMs. The basic components of the set up comprise of an electric heating plate attached to a material holder and a cooling fan. A relay circuit controls the ON/OFF of the cooling fan and the heater based on two cut-off temperatures: the upper cut-off and the lower cut-off. As soon as the heating plate reaches the upper cut-off temperature (phase transition starting temperature of the material) its circuit is automatically open and at the same time cooling fan switch is closed. Upon cooling, temperature of the heating plate falls and the moment it reaches the lower cut-off (generally set 10°C below the upper cut-off) the cooling stops and the electrical circuit gets ON again. Any number of ON/OFF cycles can be set by means of digital controller that otherwise perpetrate melt-freeze cycles of the NePCM. The temperature and time lapse data are logged continuously in computer through a digital data acquisition device, which helps to ascertain how many cycles are in progress at any moment.

3.4   Outdoor Experimental Investigation

In solar research, outdoor investigations are preferred over indoor experimentations because of the inadequacy of the solar simulators to imitate the real-time conditions. Virtually, only outdoor studies can faithfully depict the real-time performance of a solar device. Fabrication of PVT-NePCM module and erection of the outdoor experimental set up have been detailed in the subsequent sections.

3.4.1   Fabrication of PVT-NePCM Module

As mentioned earlier, since the objective of this research is to examine the efficacy of nano enhanced PCM in reducing PV cell temperature and provide better PVT thermal efficiency, therefore the commercially available parallel circular pipe configuration for the thermal collector has been chosen. To fabricate a parallel circular pipe collector, a certain number of riser pipes of relatively lower diameter (12 mm in present study) are connected to pipes header on both ends at right angles that are of relatively bigger diameter (20 mm in this case). The number of riser pipes depends on the width of the PV module and the designed inter-pipe spacing (40 mm in this case). In order to ensure better thermal contact between the thermal collector and PV backside, each riser pipe is placed into a specially designed channel. These channels are designed such that one side tightly encircles the outer periphery of the riser pipe and the other flat side closely touches the PV backside; moreover, thermally conductive adhesive is used to make the contact further thermally efficient. Figure 3.13 shows the steps in fabrication of PVT-NePCM system.

(a) Cooling channel attached to PV backside

(b) NePCM packets lay over the channel

(c) NePCM packets secured by net and aluminum channels

(d) PVT-NePCM module with cover

Figure 3.13: Fabrication steps (a to d) of the PVT-NePCM module

The major challenges for PCM/NePCM based PVT systems are leakproof containment of the material and ensuring a well dispersal after freezing. The later problem is very difficult to solve with larger containers because upon solidification materials tend to agglomerate at lower corners as a result of gravity. To solve this problem, small aluminum foil pouches have been chosen in the present research to ensure equitable distribution of the latent heat storage material all over the panel. At first, the total amount of material required to maintain a certain cell temperature is calculated by applying equation 3.3. Then, it has been estimated that how many small

aluminum pouches can cover the whole thermal collector. Thus, the total amount of NePCM needed for a panel is divided equally and filled up into the pouches in such a manner that enough space is left for volume expansion during melt cycle. Hence, opening of the aluminum pouches are sealed by using a heat-sealing machine. To ensure leakproof, the sealed edge is further secured by using aluminum tape. Thereafter, the NePCM contained pouches are integrated with the thermal collector by means of aluminum tape and secured by aluminum T-slot channels and wire net.

3.4.2 Experimental Setup

The experimental setup is composed of five PV and PVT panels, namely PV, PV-PCM, PVT, PVT-PCM, PVT-NePCM. The setup has been built to test the effect of one or more independent variables on the behavior of several dependent variables. The control mechanisms are designed to regulate the independent variables and the instrumentations are set in accordance the requirement to measure the dependent variables. The independent variables involved in the present study are inlet flow velocity, incident solar irradiance, water inlet temperature and ambient temperature while the dependent variables are electrical and thermal energy. The incident solar irradiance (measured with a silicon pyranometer) and different temperatures (measured with K-type thermocouples) have been recorded uninterruptedly in a digital data logger. On the other hand, an *I-V* tracer with maximum power point tracking (MPPT) circuit was engaged to measure and record the electrical parameters (open-circuit voltage, V_{oc}; short-circuit current, I_{sc}; maximum voltage, V_m; maximum current, I_m; maximum power, P_{max}; fill factor, *FF*) of the PV and PVT modules. The onsite experimental setup and the data acquisition system are shown in Figure 3.14.

The present experimental investigation has been carried out in the Solar Garden, UM Power Energy Dedicated Advanced Centre (UMPEDAC), University of Malaya, Kuala

Lumpur, Malaysia. This integrated outdoor solar research facility is situated at 3.1169°N and 101.6669°E. Average ambient temperature of the experimental site is 27.63°C, the maxima and minima being 32.67°C and 24.24°C respectively. Annual rainfall ranges from 1800 to 3900 mm with an average humidity over 80%. Average wind speed ranges from 6.44 km/h in December to 7.56 km/h in January. Maximum daily global solar irradiance and direct normal irradiance values are 1068 W/m^2 and 915 W/m^2 respectively (MetMalaysia, 2020).

(a)

Figure 3.14: (a) Experimental setup for onsite comparative performance study, (b) Data acquisition system
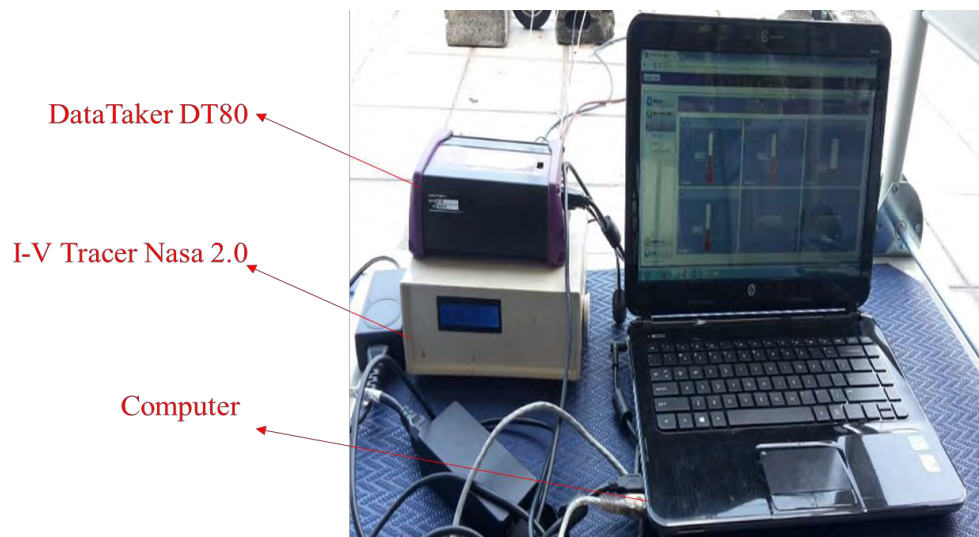
(b)

Figure 3.14, continued

3.4.3 Instrumentation

The instruments used to measure and record experimental data have been described in the subsequent sections. All the instruments have been calibrated as per standard procedure.

3.4.3.1 Pyranometer

A photodiode-based silicon pyranometer of LI-COR brand, USA, model PY82186 (Figure 3.15) has been used in this experiment to measure the solar irradiance. Despite of its limitation to produce a uniform response the measurements of silicon pyranometer are as faithful as the first-class thermopile pyranometer in visible solar spectrum which controls the photoelectric effect. It is capable of measuring irradiance from 0 to 1280 W/m^2 within the spectral range of 300 to 1100 nm and can operate well from 40° to 75^oC temperature.

Figure 3.15: Pyranometer (Model: LI-COR, PY82186)

3.4.3.2 Flow meter

The flow meter (Figure 3.16) used in this experimental setup to measure the flow rate of the heat transfer fluid (HTF) is a variable-area meter (also known as rotameter). The measuring range of the flow meter is 16 to 160 L/hr with a resolution of 8 L/hr. As water is employed as the HTF in the experimental study, so rotameter of model LZB-10B is selected to ensure the use with fluids having specific gravity 1.0 at normal operating temperature range. The basic independent or control variable in this experimental study is water inlet velocity. Although differential gate valve has been used for gross level flow control, the precise control of flow velocity is achieved by the flow control knob of the flow meter.

Figure 3.16: Flow meter (Model: LZB-10B)

3.4.3.3 Thermocouple

The type K thermocouple probe (Figure 3.17) has been used to measure the inlet and outlet temperatures of water along with top and bottom surface temperatures of the PV and PVT modules. Type K thermocouple is the most rugged in temperature measurement with the widest measuring range. This thermocouple is a bimetal wire of chromel (90% nickel and 10% chromium) and alumel (95% nickel, 2% manganese, 2% aluminum and 1% silicon).

Figure 3.17: K-type thermocouple

3.4.3.4 Data logger

Solar experimental data are stochastic by nature and the experiments are run for a whole day or even for days together. So, there is a need for continuous data acquisition in order to follow the real trend of a particular variable. A digital data logger of brand DataTaker, model DT80 (Figure 3.18) has been used to measure and store different temperatures and irradiation level continuously for a long period of experimental run. The real-time data is viewed and downloaded through a web-based graphical user interface (GUI) that defines basic measurement tasks. Logged data is then extracted by a USB memory device or downloaded using the web interface into files ready for import into spreadsheets and data analysis tools.

Figure 3.18: Data logger (Model: DataTaker DT80)

3.4.3.5   I-V tracer

An *I-V* tracer with MPPT facility (Figure 3.19) is used to measure the current-voltage relationship (*I-V* curve) of photovoltaic modules. The *I-V* tracer NASA 2.0 used in the present experimental study is developed at UM Power Energy Dedicated Advanced Centre (UMPEDAC), University of Malaya, Malaysia. It is used for measuring and controlling short circuit current (I_{sc}), open circuit voltage (V_{oc}), maximum current (I_m), maximum voltage (V_m) and maximum power (P_{max}) generated by module. This *I-V* tracer can trace power up to 2000 W.

Figure 3.19: *I-V* tracer (Model: NASA 2.0)

3.5   Mathematical Formulation

3.5.1   Installation of the Modules

Malaysia is located in north hemisphere of the globe; hence, solar modules have been mounted facing to the south. The orientation angle of the PV and PVT modules towards the equator have been calculated using equations 3.1 and 3.2 (Cooper, 1969):

$$\delta = 23.45 \ \sin[(\tfrac{360}{365}) \ (d + 284)] \tag{3.1}$$

$$\beta = (\varphi - \delta) \tag{3.2}$$

where δ is solar declination, d is the day of the year (e.g., $d = 1$ on 1st January), φ is the latitude of the experimental site and β is the alignment angle of the modules towards the equator.

3.5.2   Estimation of NePCM Required

Amount of nano composite phase change material required to absorb the heat produced by a PV module is estimated by (El Khadraoui et al., 2016; Hossain et al., 2019):

$$m_{NePCM} = \frac{Q_{ch}}{L_{NePCM} + + \int_{i}^{m} C_{p,s} \ (T) \ dT + \int_{m}^{f} C_{p,l} \ (T) \ dT} \tag{3.3}$$

where $C_{p,s}$, $C_{p,l}$ are specific heats of solid and liquid phase of the NePCM, respectively. Q_{ch} is heat requisite for phase change, i, m and f denote initial, melting and final temperature. The mass of PCM required for PVT-PCM system is also estimated using the same equation.

3.5.3 Energy Analysis

The energy balance equation for the PVT-NePCM system under equilibrium state is given as (Li et al., 2020; Sardarabadi et al., 2017):

$$\dot{E}_s + \dot{E}_{wi} = \dot{E}_{wo} + \dot{E}_e + \dot{E}_l \tag{3.4}$$

where $\dot{E}_e$ is the rate of electricity generation, $\dot{E}_{wi}$ rate of heat influx to the system with water, $\dot{E}_{wo}$ rate of heat outflux with water, $\dot{E}_l$ is the conversion losses, $\dot{E}_s$ is the rate of solar irradiance reaching the module surface and is given by:

$$\dot{E}_s = \tau \times \alpha \times A \times G \tag{3.5}$$

where A is the module surface area, G incident solar irradiance, τ and α are the transmittance and absorptance of PV glass cover.

Heat gain by the PVT-NePCM system can be calculated as:

$$\dot{Q}_{gain} = \dot{m}\, C_p (T_{wo} - T_{wi}) \tag{3.6}$$

where $\dot{m}$ is mass flow rate of water, C_p is specific heat of water, T_{wi} and T_{wo} are water inlet and outlet temperature.

Thermal, electrical and overall efficiencies of the PVT-NePCM system are given by:

$$\eta_{th} = \frac{\dot{Q}_{gain}}{\dot{E}_s} = \frac{\dot{m}\, C_p (T_{wo} - T_{wi})}{\tau \alpha\, A\, G} \tag{3.7}$$

$$\eta_e = \frac{P_{max}}{A \times G} \tag{3.8}$$

where maximum electrical power output is calculated by:

$$P_{max} = I_{SC} \times V_{OC} \times FF = V_{mp} \times I_{mp} \tag{3.9}$$

$$\eta_o = \eta_{th} + \eta_e \tag{3.10}$$

Energy parameters for the other four systems, i.e. PV, PVT, PV-PCM and PV-NePCM have been calculated based on the same above principle.

3.5.4 Exergy Analysis

In order to explore the functional energy available for conversion, second law of thermodynamics has been employed in the present analysis. Exergy balance equation in equilibrium state is given by (Fudholi et al., 2018; Park et al., 2014; Sardarabadi et al., 2017):

$$\dot{B}_s + \dot{B}_{wi} = \dot{B}_{wo} + \dot{B}_e + \dot{B}_{dest} \tag{3.11}$$

where $\dot{B}_{wi}$, $\dot{B}_{wo}$ signify rate of exergy influx and outflux with inlet and outlet water, and $\dot{B}_{dest}$ denotes exergy destruction rate during the process. As electricity is a high-grade of energy, the rate of electrical exergy $\dot{B}_e$ can practically considered equal to the electricity generation by PV module.

Before reaching the Earth surface solar radiation is absorbed in different layers of the atmosphere and gets diluted. Therefore, solar radiation touching the ground is considered as diluted black body radiation (dilute BBR). Hence, rate of exergy from solar radiations $\dot{B}_s$ reaching the module surface (as dilute BBR) has been estimated by applying Badescu's equation (Badescu, 2018):

$$\dot{B}_s = A \times G \times \alpha \times [1 - \frac{4}{3}\left(\frac{a}{i}\right) + \frac{4}{3}\left(\frac{a}{i}\right)^4] \tag{3.12}$$

where α is absorptance of the photovoltaic module glass cover, a is ratio of ambient temperature (T_a) and sun surface temperature (T_s) and i is the interaction factor. Sun surface temperature is taken as 5777 K.

Electrical, thermal and overall exergy efficiencies of the PVT-NePCM system along with exergy destruction, improvement potential and entropy generation are given by (Kumar et al., 2021):

Electrical exergy efficiency:

$$\varepsilon_e = \frac{\dot{B}_e}{\dot{B}_s} \tag{3.13}$$

Thermal exergy efficiency:

$$\varepsilon_{th} = \frac{\dot{B}_{th}}{\dot{B}_s} = \frac{\dot{m}\, C_p [(T_{wo} - T_{wi}) - T_a \ln(\frac{T_{wo}}{T_{wi}})]}{A \times G \times \alpha \times [1 - \frac{4}{3}(\frac{a}{i}) + \frac{4}{3}(\frac{a}{i})^4]} \tag{3.14}$$

where $\dot{B}_{th}$ is the rate of thermal exergy.

Overall exergy efficiency:

$$\varepsilon_o = \varepsilon_{th} + \varepsilon_e \tag{3.15}$$

Exergy destruction rate:

$$\dot{B}_{dest} = \dot{B}_s - \dot{B}_{th} - \dot{B}_e \tag{3.16}$$

Improvement potential:

$$IP = \left(1 - \frac{\varepsilon_o}{100}\right) \times \dot{B}_{dest} \tag{3.17}$$

Entropy generation rate:

$$\dot{S} = \frac{\dot{B}_{dest}}{T_a} \tag{3.18}$$

Exergy parameters for the other four systems have been calculated following the above fundamental equations.

3.5.5 Uncertainty Analysis

In this section, an uncertainty analysis of the PV and PVT electrical and thermal parameters has been performed. The total uncertainty δu of a parameter u is composed of the uncertainty of repetition error (δu_r) and the uncertainty from equipment error (δu_e) (Sardarabadi et al., 2014).

$$\delta u = \sqrt{(\delta u_r)^2 + (\delta u_e)^2} \tag{3.19}$$

If U is a function of n independent linear parameters as $U = U\ (u_1, u_2, u_3, .. u_n)$ and let the parameters $u_1, u_2, u_3, .. u_m, u_{m+1} .... u_n$ are measured with uncertainties $\delta u_1, \delta u_2, \delta u_3, .., \delta u_m, \delta u_{m+1,}, ... \delta u_n$ where U is defined as: $U = \frac{u_1 \times u_2 \times u_3,.. \times u_m}{u_{m+1} \times .... \times u_n}$, then the uncertainty of U will be (Kline, 1953):

$$\delta U = \sqrt{(\frac{\partial U}{\partial u_1} \delta u_1)^2 + (\frac{\partial U}{\partial u_2} \delta u_2)^2 + (\frac{\partial U}{\partial u_3} \delta u_3)^2 + \cdots + (\frac{\partial U}{\partial u_n} \delta u_n)^2} \tag{3.20}$$

where δU is the uncertainty of the function U, δu_i the uncertainty of u_i and $\frac{\partial U}{\partial u_1}$ is the partial derivative of U with respect to u_i.

Therefore, fractional uncertainty of U (given that uncertainties in $u_1, u_2, u_3, .. u_m, u_{m+1} .... u_n$ are independent of each other) will be (Taylor, 1997):

$$\frac{\delta U}{U} = \sqrt{(\frac{\delta u_1}{u_1})^2 + (\frac{\delta u_2}{u_2})^2 + (\frac{\delta v_2}{u_3})^2 + \cdots (\frac{\delta u_m}{u_m})^2 + (-\frac{\delta u_{m+1}}{u_{m+1}})^2 + (-\frac{\delta u_n}{u_n})^2} \tag{3.21}$$

Using equation 3.21 and recalling equations of energy and exergy efficiency fractional uncertainties from both energetic and exergetic viewpoints can be estimated.

From the above analysis, the maximum absolute uncertainty for all parameters is estimated and found less than 5% in all trials. Uncertainty values within this bound assert the consistency of the measured data (Sardarabadi et al., 2014). Table 3.6 gives the model, range of measurements and uncertainties associated with different sensors and instruments used in the experimental setup.

Table 3.6: Measurement ranges and uncertainty of the instruments

Instrument	Range	Maximum uncertainty in measurement
Data logger (Model: DataTaker DT80)	− 270 to 1372°C	±2%
Silicon Pyranometer (Model: LICOR LI200R)	0 to 2000 W/m^{-2}	±3%
Flow meter (Model: LZT M-6)	0.5 to 4.0 L/min	±0.5%
I-V tracer (Model: NASA 2.0)	0 to 50V & 0 to 16A	±4.5%
Thermocouple (Model: RS pro; type K)	−200 to 1000°C	±0.5%

3.6 Summary

The aim of the present research is to examine the efficacy of employing nano composite materials in thermal management of PV and PVT. For this purpose, the new nano composite material has been developed and characterized in this research following the standard operating procedure as practiced in materials science. On the other hand, outdoor experimental research protocol, erecting all the PV and PVT systems under the same ambience, has been preferred for comparative performance investigation, because actual performance of solar devices can only be captured under real-time conditions that cannot be accurately realized at indoor.

CHAPTER 4: RESULTS AND DISCUSSION

4.1 Introduction

This research has been accomplished in two major phases: synthesis and characterization of a novel nano enhanced phase change material (NePCM) that is compatible for PVT application and performance investigation of a NePCM based PVT (PVT-NePCM) system. Findings of both phases of the work has been delineated in the following sections.

4.2 Characterization of Nano Enhanced Phase Change Material

The basic motive of this research is to synthesize a nano enhanced phase change material (NePCM) which would be appropriate for thermal management of photovoltaic thermal modules. For this purpose, several PCMs and nano particles have primarily been selected and from this set the best combination is discerned. The trials and their outcomes in course of this selection process have been enunciated in the following sections.

4.2.1 Base Material Characterization

4.2.1.1 Phase change material

Selection of PCM for photovoltaic thermal applications depends on the ambient temperature where the module is installed. The regular day temperature of Kuala Lumpur is 33ºC (MetMalaysia, 2020) and an allowance of 10º to 15ºC is considered enough to captivate the major amount of heat from the module. Hence, PCMs with melting points around 42º to 50ºC has been selected for the current application. Organic PCMs, in general, possess more heat storage capacity within this temperature range.

Four organic PCMs, namely RT44HC, RT47, RT50, RT55, manufactured by Rubitherm GmbH, Germany, have primarily been nominated and their latent heat and phase transition temperatures have been ascertained through differential scanning calorimetry (DSC). The DSC curves of the four PCMs are presented in Figure 4.1, which confirms that RT44HC exhibits the highest heat storage capacity among the four PCMs. With a heat storage capacity of 241.584 kJ/kg RT44HC leads the other three PCMs by around 100 kJ/kg. Moreover, from Table 4.1 it is apparent that phase transition of RT44HC occurs within the narrowest range of temperature (44.55° – 46.90°C). Therefore, it is the best choice among the four primarily selected organic PCMs.
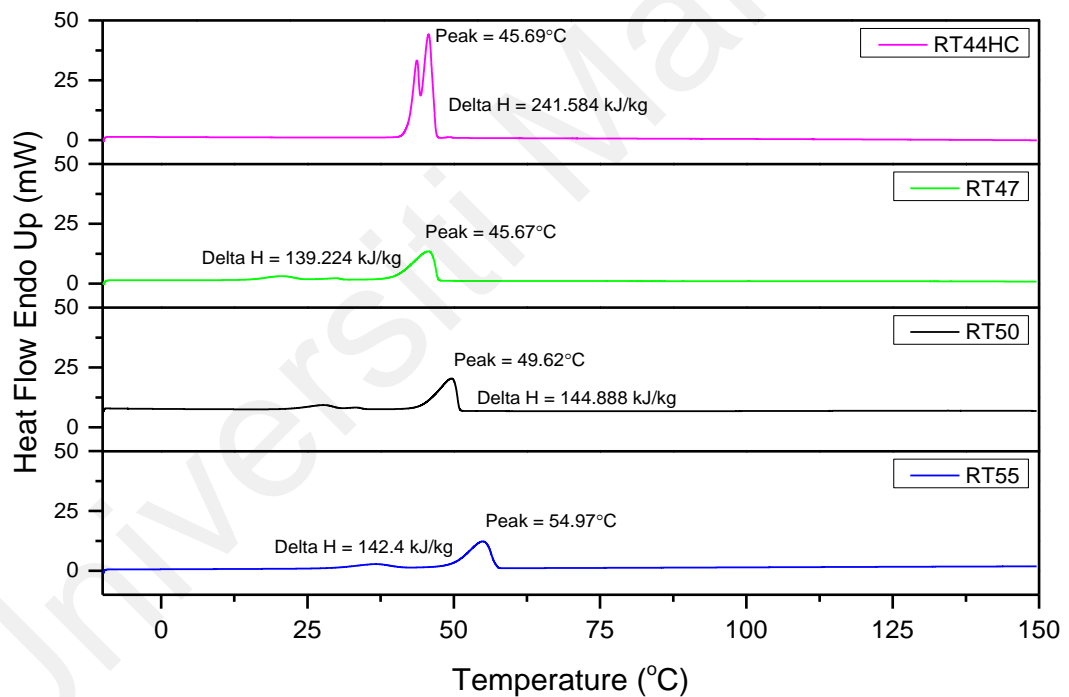
Figure 4.1: DSC heating curve for four PCMs

Table 4.1: Phase transition range of the PCMs as obtained from DSC test

PCM	Phase transition range (°C)
RT44HC	44.55 - 46.90
RT47	39.95 - 47.25
RT50	44.72 - 50.92
RT55	49.81 - 57.17

The selected organic PCM RT44HC is characterized for phase transition behavior, thermal stability, functional group and interior morphology through DSC, TGA, FTIR and FESEM analyses, respectively.

Figure 4.2 shows the DSC heating curve of RT44HC wherein the material is seen to have a narrow transition range, the peak of the transition temperature being 45.69°C with the onset and endset at 44.55° and 46.90°C, respectively. This test also confirms a considerable latent heat storage capacity of 241.6 kJ/kg for this pure PCM.
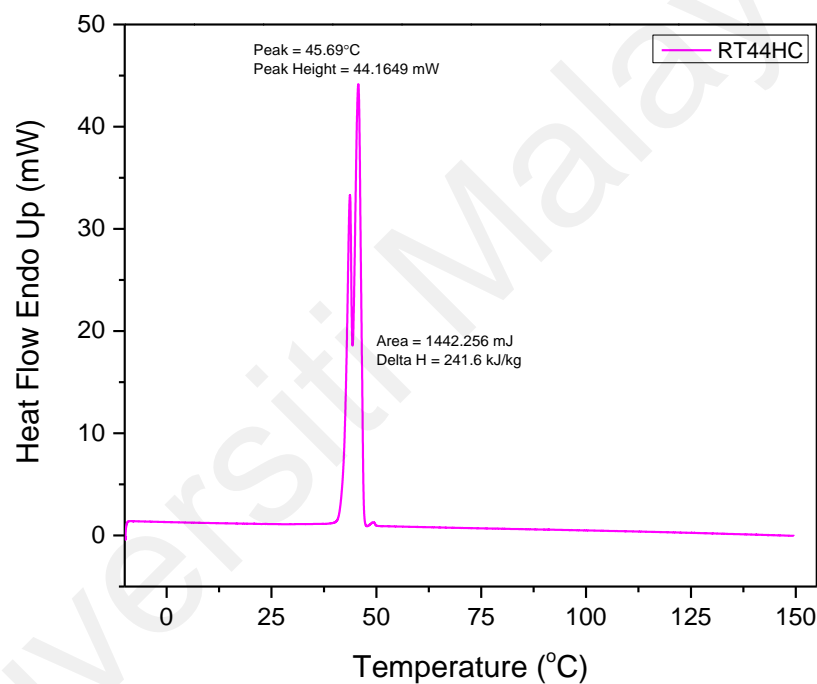
Figure 4.2: DSC heating curve for pure RT44HC

Pure PCM RT44HC exhibits a good constancy upon heating. It is apparent from Figure 4.3 that up to around 175°C there is almost zero weight loss (weight 100%) of the material, even at 200°C it retains 95% of its weight and noticeable degradation starts near 250°C. As the maximum operating temperature of this material in PVT application will not exceed 65°C RT44HC can be considered thermally stable within the working range.
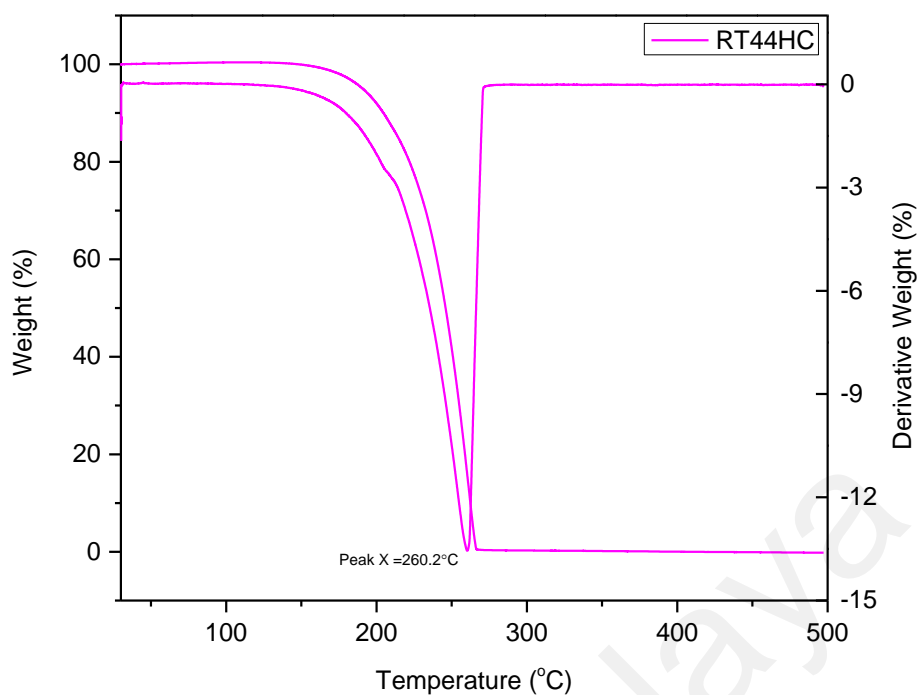
Figure 4.3: TGA curve for RT44HC

The characteristic peaks in the FTIR spectra of pure RT44HC is presented in Figure 4.4. A C–H stretching observed in the region of 3000 cm $^{-1}$, C–H symmetric & bending near 1470 cm^{-1}, a C–H rocking near 725 cm^{-1}.
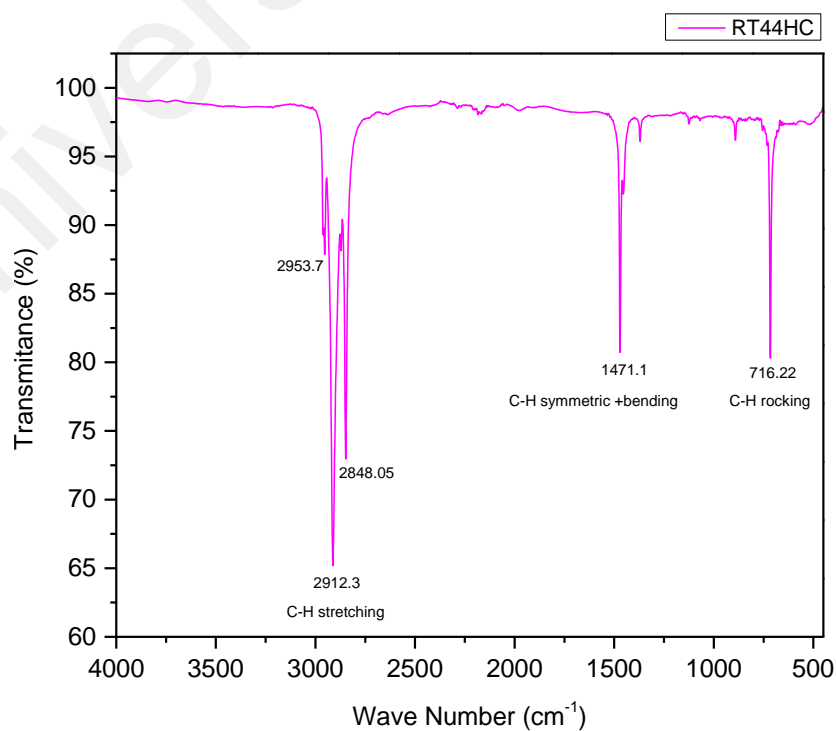

Figure 4.4: FTIR curve for RT44HC

The FESEM micrograph of pure PCM RT44HC in Figure 4.5. It can be noticed that pure PCM has a wide range of pore size distribution from 1.441 to 7.131 μm. Previous studies also show that industrial grade pure paraffin wax contains similar porous structure (Silakhori et al., 2013).
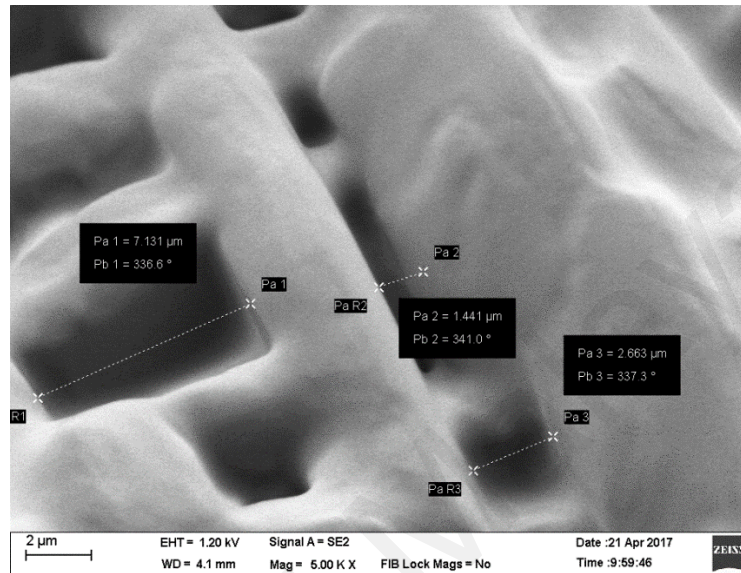
Figure 4.5: FESEM micrograph of RT44HC

4.2.1.2 Multi-walled carbon nanotube

Carbon nanotubes (CNTs) are cylindrical molecules consisting of rolled-up sheets of hexagonally ordered carbon atoms (i.e., graphene). While such nanotubes formed as single-walled (SWNT) is very expensive to synthesize, multi-walled (MWNT) consisting of several concentrically interlinked nanotubes offer relatively low-cost solution with almost same physical and chemical features. Hence, laboratory grade MWNT is selected as reinforcement material for pure PCM RT44HC. In the present research, basically the observational techniques are used for characterizing MWNT.

The FESEM microstructural study has been carried out to depict its morphological attribute. The highly tangled tubes of MWNT is displayed in Figure 4.6, from which it is apparent that there is no major defect in shape. In addition, TGA analysis is

performed to estimate the residual mass, the temperature at the onset of oxidation and the temperature of the maximum oxidation rate. Figure 4.7 shows that up to around 575°C MWNT retains 100% of its mass, oxidation starts near 600°C and after that oxidation occurs at a sharp rate resulting in a 35% weight loss at 1000°C. Since the working temperature of a PVT system is far below the oxidation onset temperature of MWNT so it can safely be used in PCM matrix as a property enhancer. Furthermore, DSC heating curve of MWNT (Figure 4.8) also confirms no phase transition up to 400°C. On the other hand, FTIR spectra of pure MWNT (Figure 4.9) shows the major peaks near wave numbers 2940, 2850 and 1580 cm^{-1}, which confirms the presence of carbon-based functional group, particularly C-H.
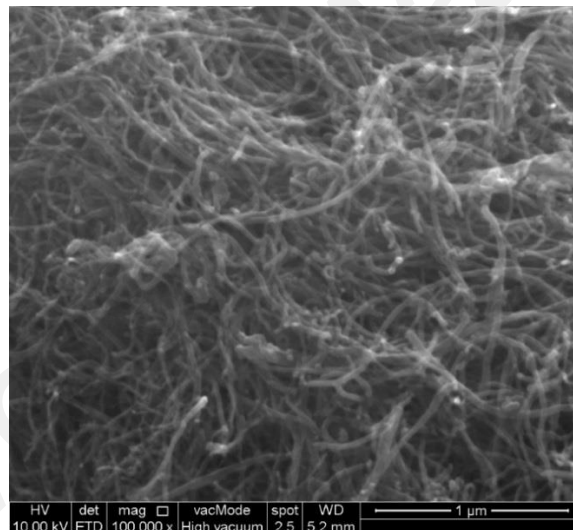
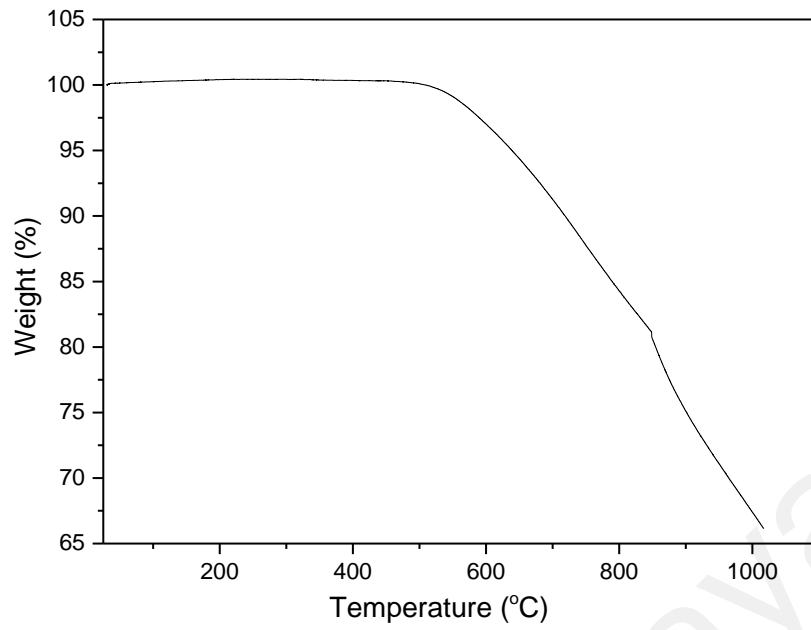**Figure 4.6:** FESEM micrograph of pure MWNT
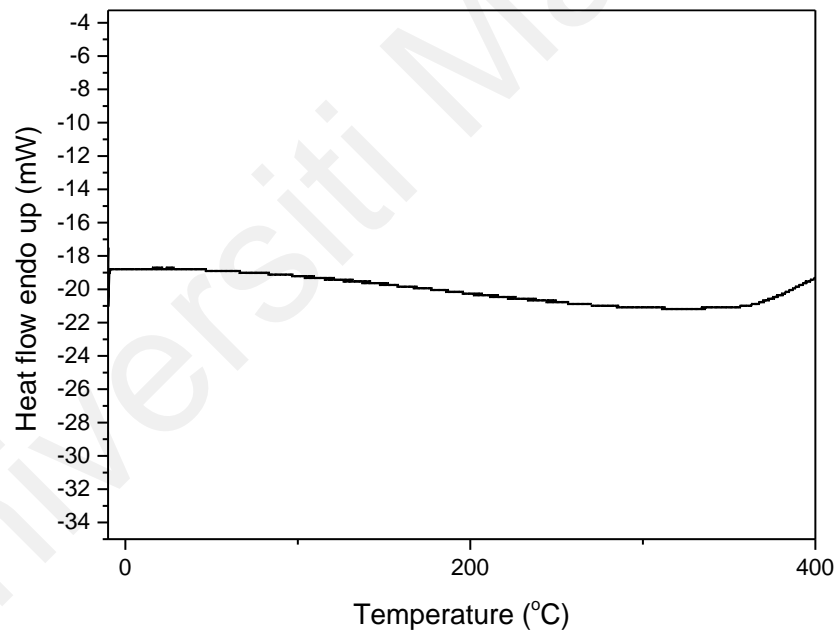
Figure 4.7: TGA curve for pure MWNT

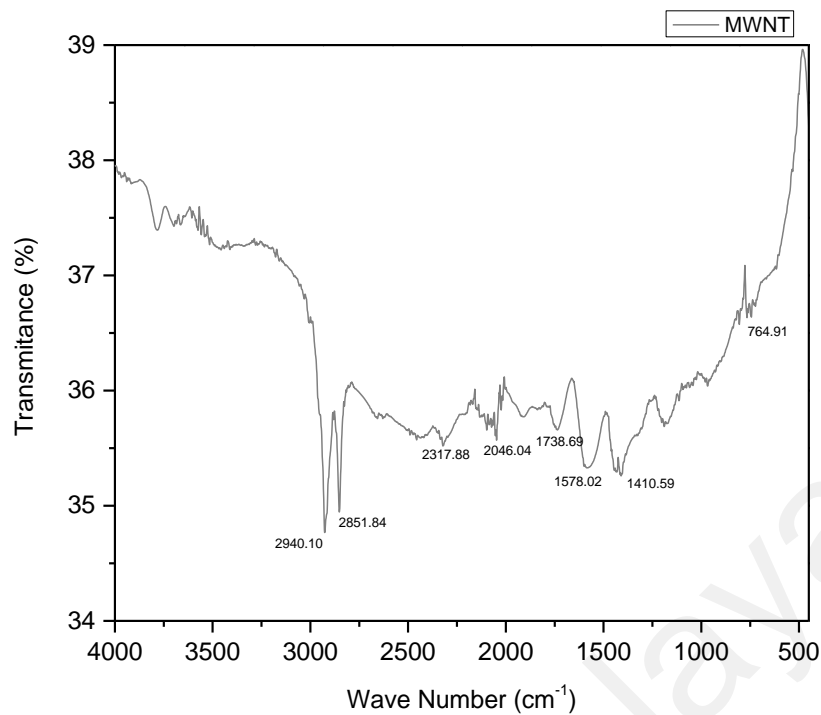**Figure 4.8:** DSC heating curve for pure MWNT

Figure 4.9: FTIR spectra for pure MWNT

4.2.2 NePCM Characterization

In the present research, four NePCMs have primarily been synthesized by incorporating 0.25, 0.10, 0.05 and 0.01 wt% functionalized MWNT (f-CNT) into pure RT44HC matrix. The following sections delineate different thermal, morphological and chemical features of these nanocomposites.

4.2.2.1 DSC analysis

The DSC heating curve of the four NePCMs have been shown in Figure 4.10. A comparative deliberation on the four graphs reveals that RT44HC-0.01%fCNT exhibits the highest peak transition temperature of $46.83^{\circ}C$, which is $1.14^{\circ}C$ higher than that of the pure PCM (refer to Figure 4.2). Moreover, it exhibits the narrowest phase transition range among other samples. Hence, this NePCM fits better for PVT application.
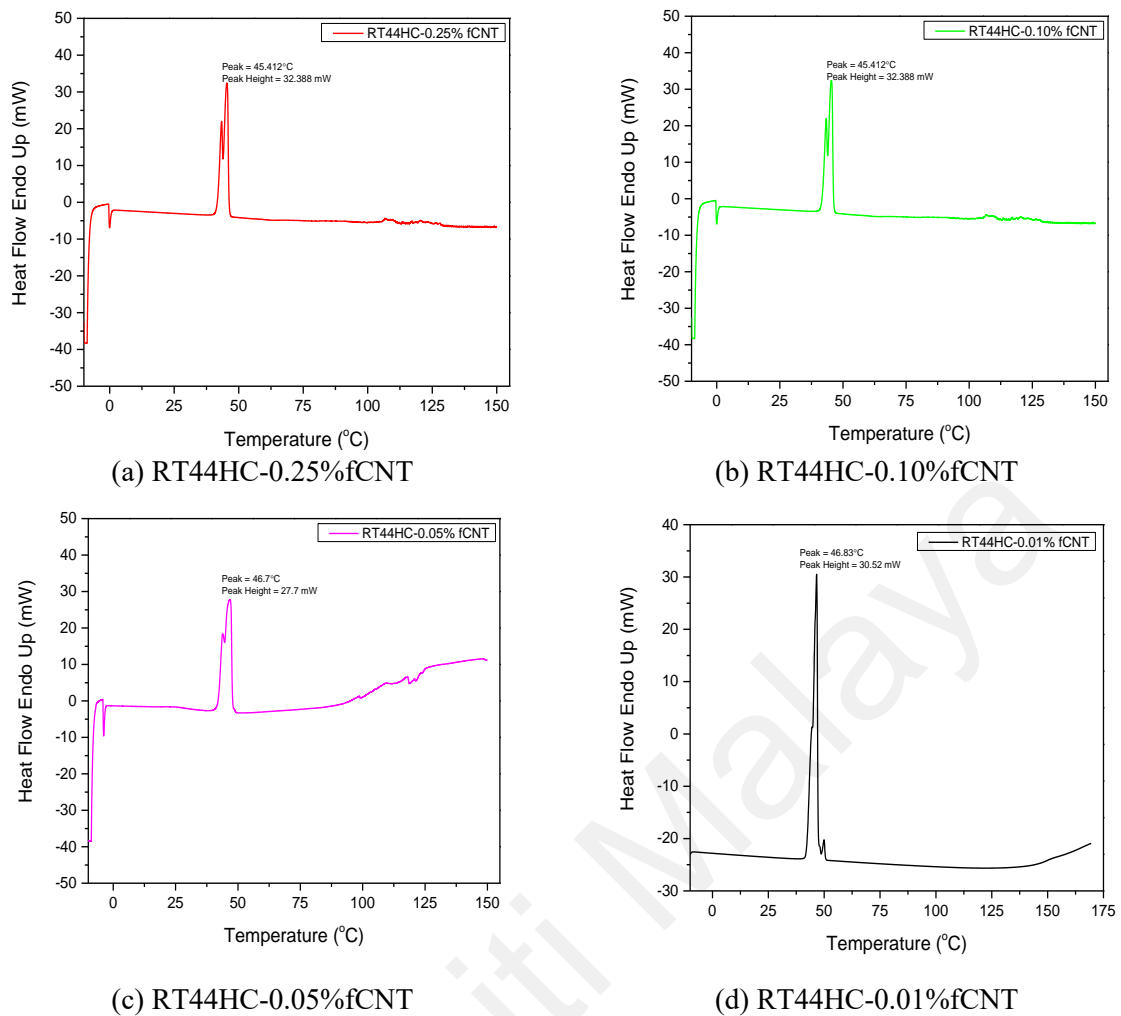
(a) RT44HC-0.25%fCNT   (b) RT44HC-0.10%fCNT

(c) RT44HC-0.05%fCNT   (d) RT44HC-0.01%fCNT

Figure 4.10: DSC heating curve of four synthesized NePCMs

4.2.2.2 TGA analysis

Occurrence of no oxidation (or other reactions) can be understood by the no (or very minor) loss of the original weight of the sample, which is also the indicator of thermal stability. All four NePCMs exhibit no oxidation, at least, up to 200°C (Figure 4.11). Therefore, thermal stability of each of the NePCM is satisfactory for PVT application.
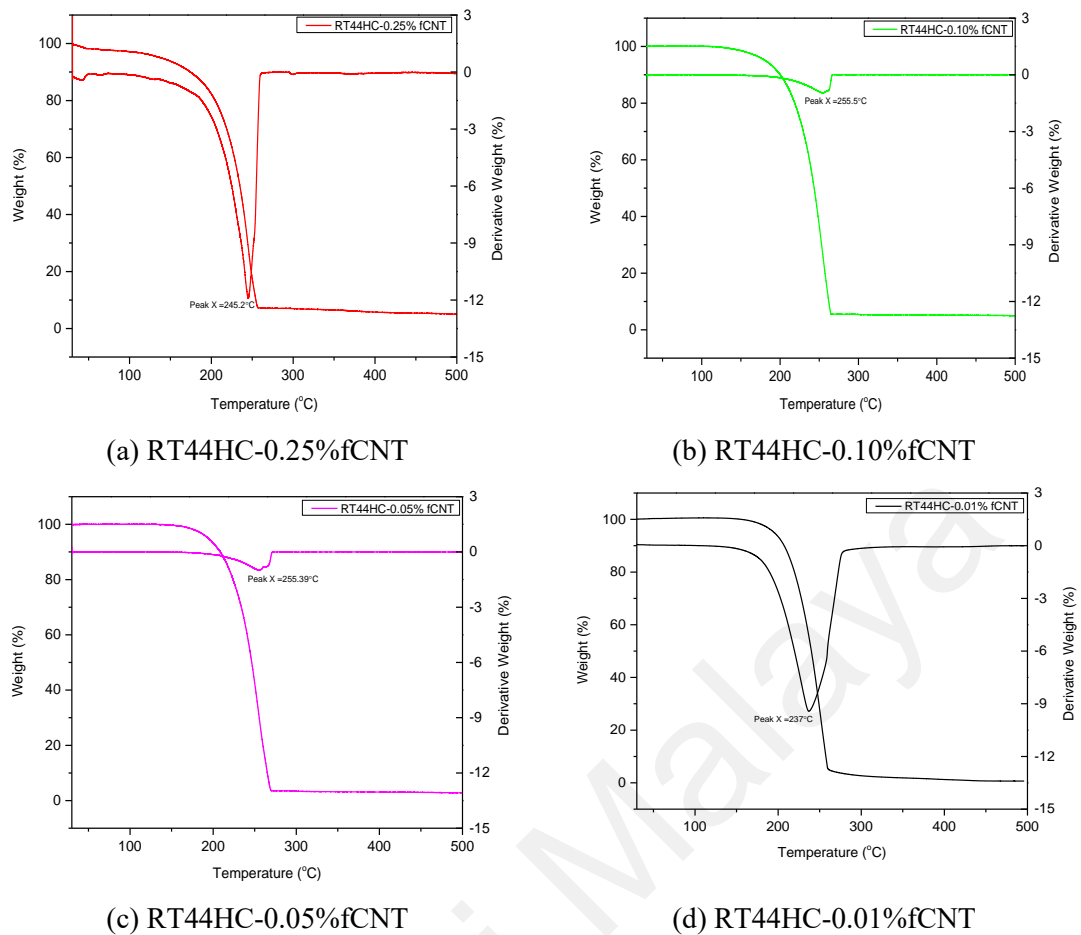
(a) RT44HC-0.25%fCNT

(b) RT44HC-0.10%fCNT

(c) RT44HC-0.05%fCNT

(d) RT44HC-0.01%fCNT

Figure 4.11: TGA curves of four synthesized NePCMs

4.2.2.3 FTIR analysis

The characteristic peaks in the FTIR spectra of all four NePCMs have been presented in Figure 4.12. In all the materials, there can be observed C–H stretching almost in the same region of 3500–3000 cm −1, C–H symmetric & bending near 1477 cm−1, a C–H rocking near 750 cm−1. However, in each case of RT44HC-0.01%fCNT the peaks are greater as compared to other three NePCMs, which indicates the presence of the similar functional groups in greater amount. This may be attributed to the interactions between the base hydrocarbon and inserted nano carbon, which may produce hydrogen bridge bonds and create capillary and surface tension forces (Sari et al., 2018). Formation of no new functional groups shows that no chemical reaction has been occurred between PCM and MWNT.
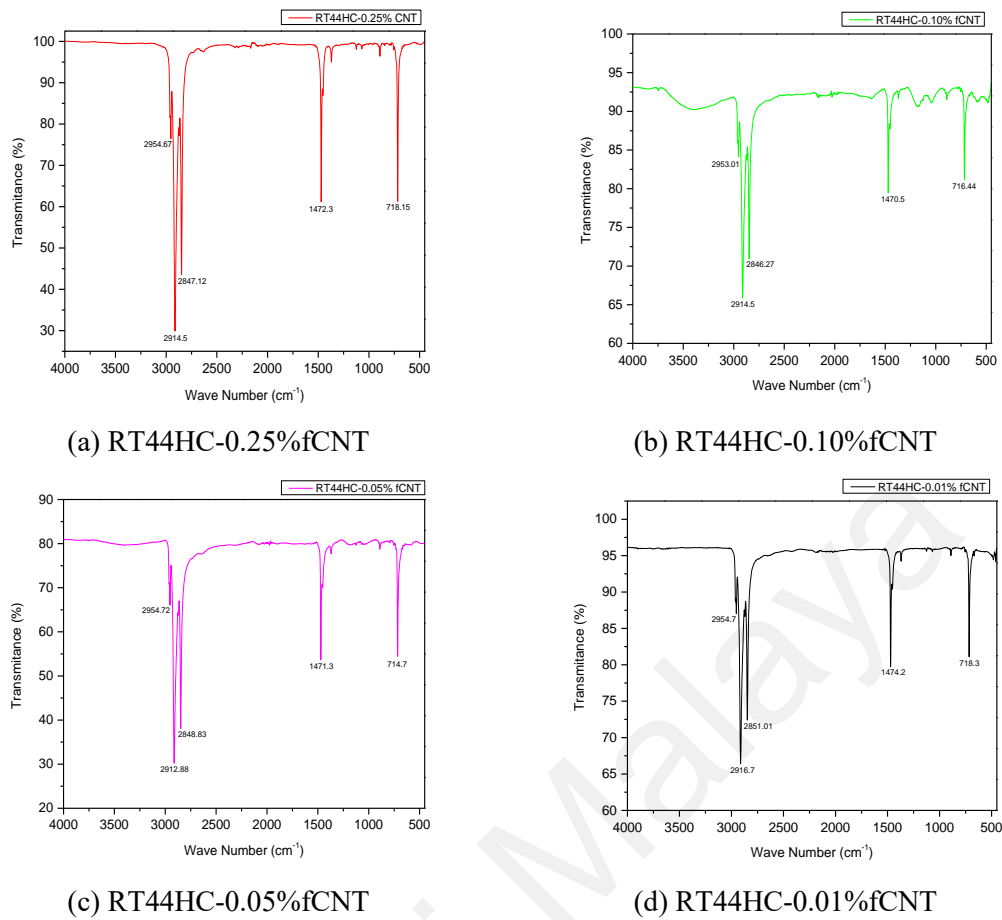
(a) RT44HC-0.25%fCNT (b) RT44HC-0.10%fCNT

(c) RT44HC-0.05%fCNT (d) RT44HC-0.01%fCNT

Figure 4.12: FTIR spectra of four synthesized NePCMs

4.2.2.4 FESEM analysis

The FESEM micrographs of four NePCMs have been shown in Figure 4.13. It is apparent from Figure (d) that in case of RT44HC-0.01%fCNT carbon nanotubes have been incorporated more uniformly into the pores of RT44HC as compared to other three NePCMs. The mutual effect of capillary action and surface tension force help uniform distribution of MWNT into the pores of PCM, thereby increasing the compactness of composite material. In addition, the tubular structure of MWNT has almost disappeared into the base material matrix. No delamination is observed in the composite material.
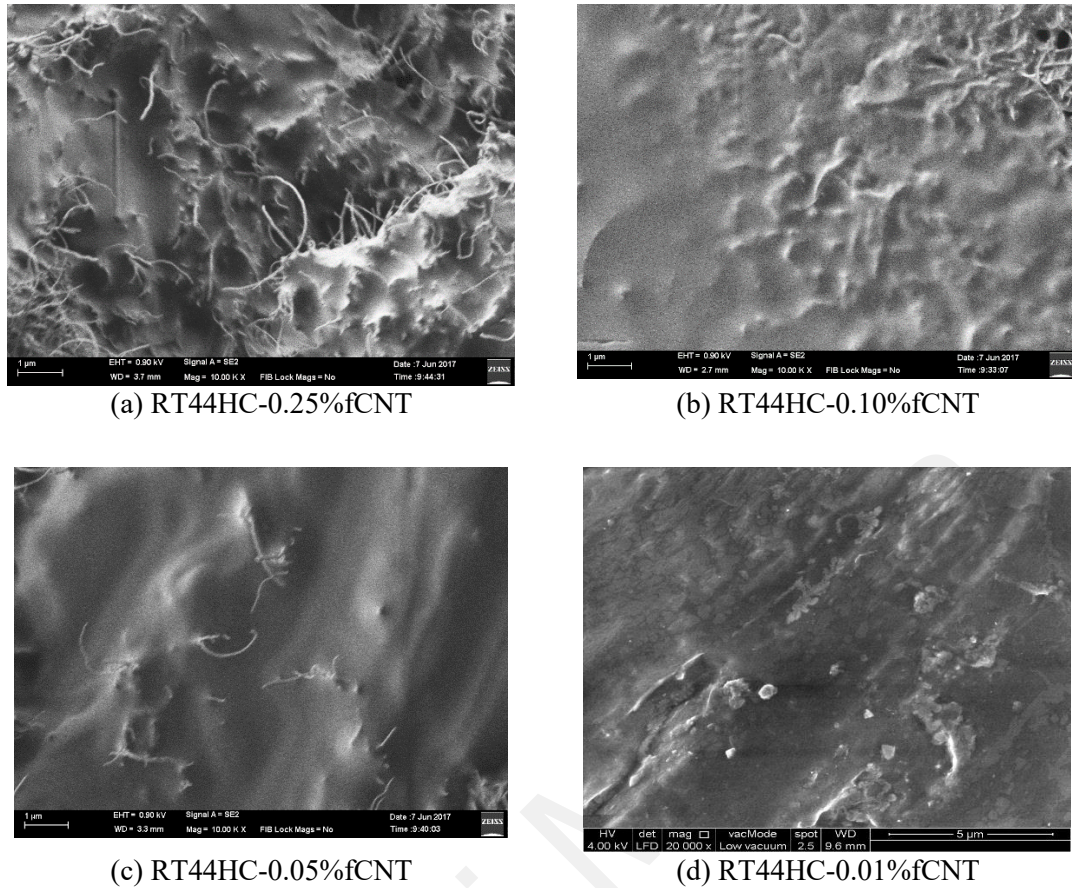
(a) RT44HC-0.25%fCNT (b) RT44HC-0.10%fCNT

(c) RT44HC-0.05%fCNT (d) RT44HC-0.01%fCNT

Figure 4.13: FESEM micrographs of four NePCMs

4.2.2.5 Thermal conductivity analysis

A comparative portrayal of thermal conductivity values of the pure PCM RT44HC and the four synthesized NePCM has been shown in Figure 4.14 and a summary of the thermal conductivity values is given in Table 4.2. It is quite apparent from the figure that insertion of nanoparticle brought about satisfactory enhancement in thermal conductivity of PCM. Thermal conductivity value reached as high as 0.32634 W/m.K in for NePCM RT44HC-0.25%fCNT as against 0.27954 W/m.K for pure PCM RT44HC, which is a 16.74% upsurge. It is also evident from the figure that although thermal conductivity gets augmented with the concentration of nanoparticle in PCM matrix the divergence not that significant, especially below 0.10%fCNT.
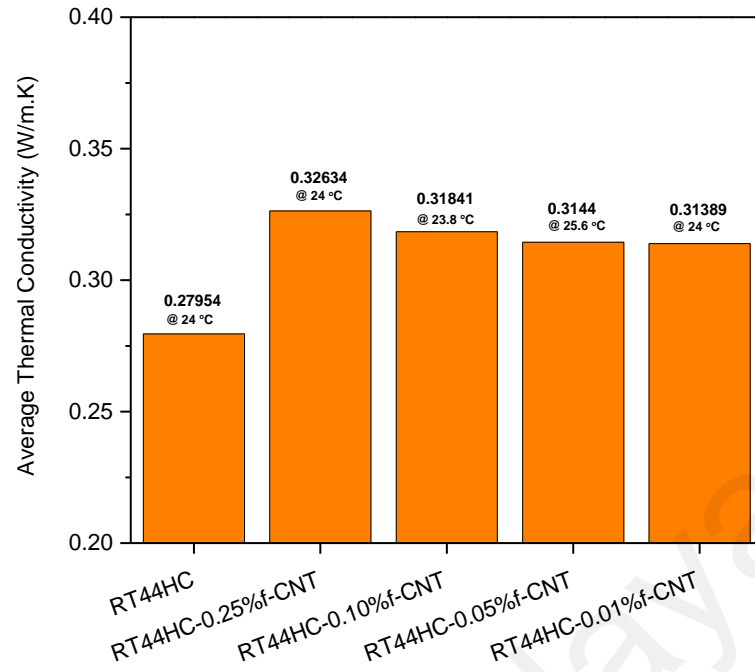
Figure 4.14: Average thermal conductivity of the pure PCM and four NePCMs

Table 4.2: Summary of thermal conductivity results

Material	Thermal conductivity (W/m.K)	Average thermal conductivity (W/m.K)	Transition temperature range (°C)	Average transition temperature (°C)
RT44HC	0.2783 – 0.281407	0.279541	23.78 – 25.14	24.0
RT44HC-0.25%f-CNT	0.325051 – 0.323576	0.326342	23.77 – 24.20	24.0
RT44HC-0.10%f-CNT	0.310005 – 0.320003	0.318407	23.72 – 23.95	23.8
RT44HC-0.05%f-CNT	0.315505 – 0.312315	0.314405	24.63 – 26.89	25.6
RT44HC-0.01%f-CNT	0.313641– 0.317987	0.313887	23.93 – 24.18	24.0

The above inferences reveal that with the highest heat storage capacity and superior phase transition properties RT44HC-0.01%f-CNT exhibits better traits among the four NePCMs. Also, the thermal conductivity of RT44HC-0.01%f-CNT is satisfactory and comparable with other NePCMs even though the value is not the highest. Hence, this NePCM has been selected as thermal storage material for PVT in the present experimental investigation.

4.2.3 Detailed Characterization of RT44HC-0.01%f-CNT

Detailed characterization of RT44HC-0.01%f-CNT including its microstructural analysis, functional group analysis, phase transition behavior has been delineated in the subsequent sections. Characterization was performed through FESEM microscopy, FTIR spectroscopy and some macroscopic testing including DSC and TGA.

4.2.3.1 Microstructural analysis

Internal configuration of any material determines its physical and thermal properties. Analyzing FESEM micrographs is one of the best ways to examine the complete minutiae of microstructure (Karaipekli et al., 2017).

Figure 4.15 (a, b, c) are the field emission scanning electron micrographs of f-CNT, pure PCM RT44HC and NePCM RT44HC-0.01%f-CNT. While the tube-like f-CNTs are clearly visible from Figure 4.15 (a) visible pores (1.441 to 7.131 µm) in pure PCM are evident from Figure 4.15 (b). Such porous structure of pure paraffin wax is evident from earlier works (Silakhori et al., 2013). Figure 4.15 (c) shows the close-packed structure of NePCM wherein f-CNT has been merged evenly into the pores of RT44HC by means of the collective action of capillarity and surface tension. The evanesced tubular structure of f-CNT into PCM matrix ascertains its uniform integration that makes a compact structure of NePCM. No delamination is detected in the synthesized material.
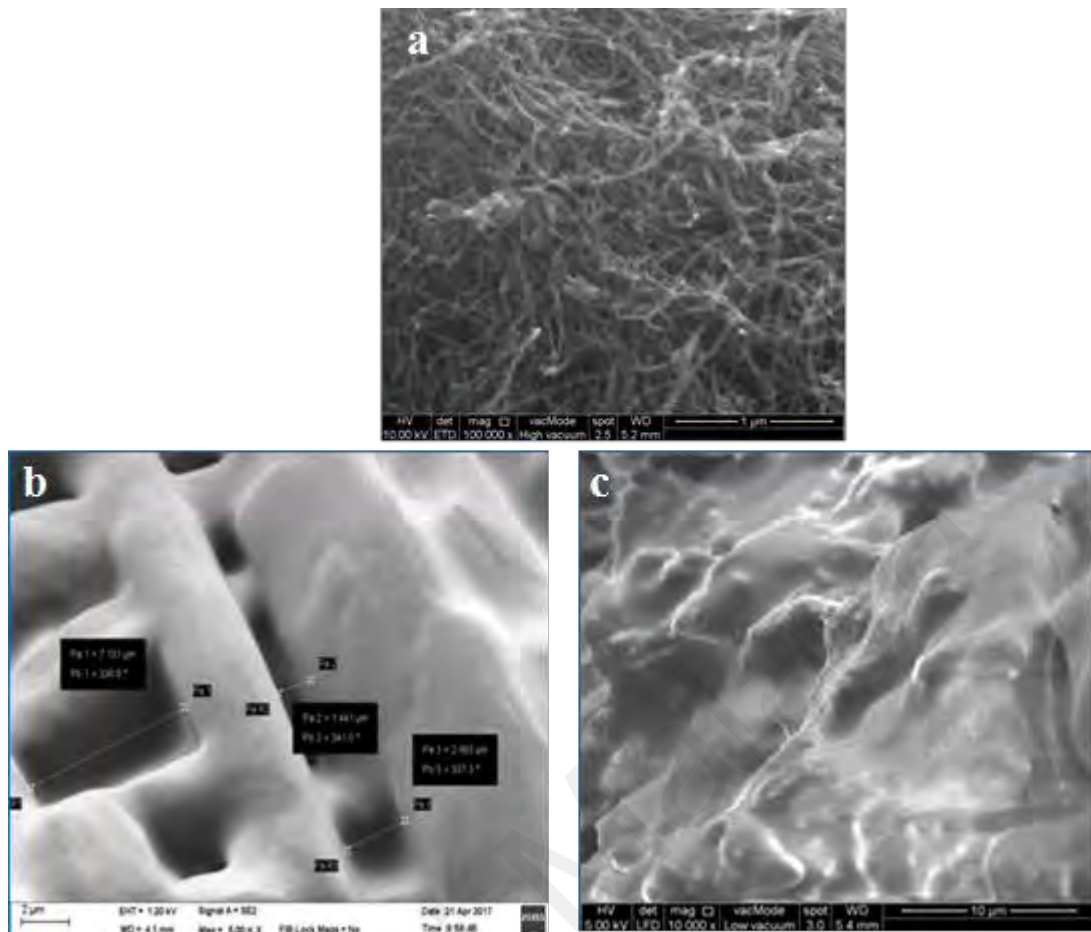
Figure 4.15: FESEM micrographs of (a) Functionalized MWNT (f-CNT), (b) Pure RT44HC and (c) RT44HC-0.01%f-CNT

4.2.3.2 Functional group analysis

Comprehending functional groups is decisive for depicting the precise structure of organic compounds as occurrence of a functional group essentially impacts their physical and chemical properties. Figure 4.16 shows the FTIR spectrum of pure PCM RT44HC (lower curve) and NePCM RT44HC-0.01%f-CNT (upper curve) for the wave number between $4000 - 500$ cm-[1]. The FTIR spectrum of both pure PCM and NePCM shows almost similar peak signifying only physical interaction between the f-CNT nanotubes and PCM. This may be attributed to the interactions between the base hydrocarbon and inserted nano carbon, which may produce hydrogen bridge bonds and also create capillary and surface tension forces (Sari et al., 2018). Formation of no new functional groups shows that no chemical reaction has been occurred between PCM and

MWNT. It can be concluded that the dispersion between f-CNT nanoparticles and the PCM is chemically stable.
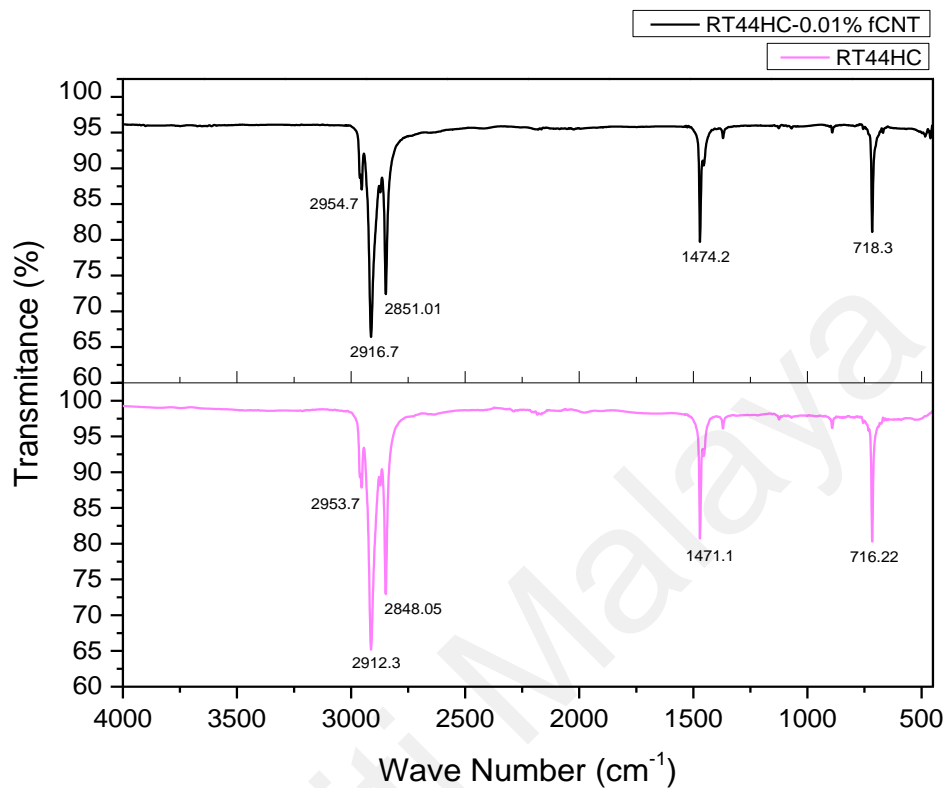

Figure 4.16: FTIR curves of pure RT44HC and RT44HC-0.01%f-CNT

4.2.3.3 Phase transition properties

The impact of inclusion of f-CNT into pure PCM matrix on the thermal characteristics like melting point and latent heat capacity of the latter has been portrayed in Figure 4.17. The principal phase change peak of the NePCM (46.63°C) is nearly one degree Celsius over that of RT44HC (45.69°C). The discrepancy between onset and endset temperature of fusion of nanocomposite material is 2.28°C (onset at 44.32°C; endset at 46.60°C), which is a bit superior than that for the pure PCM. The reason behind this widening of phase transition temperatures can be attribute to the denser formation of NePCM as confirmed in Figure 4.15 (c). However, DSC test results (Table 4.3) confirm that latent heat of fusion of NePCM (248.6505 kJ/kg) is just about 7.06

kJ/kg greater than that of RT44HC (241.5839 kJ/kg), which evidently confirms the efficacy of incorporating carbon nanotubes into pure PCM.
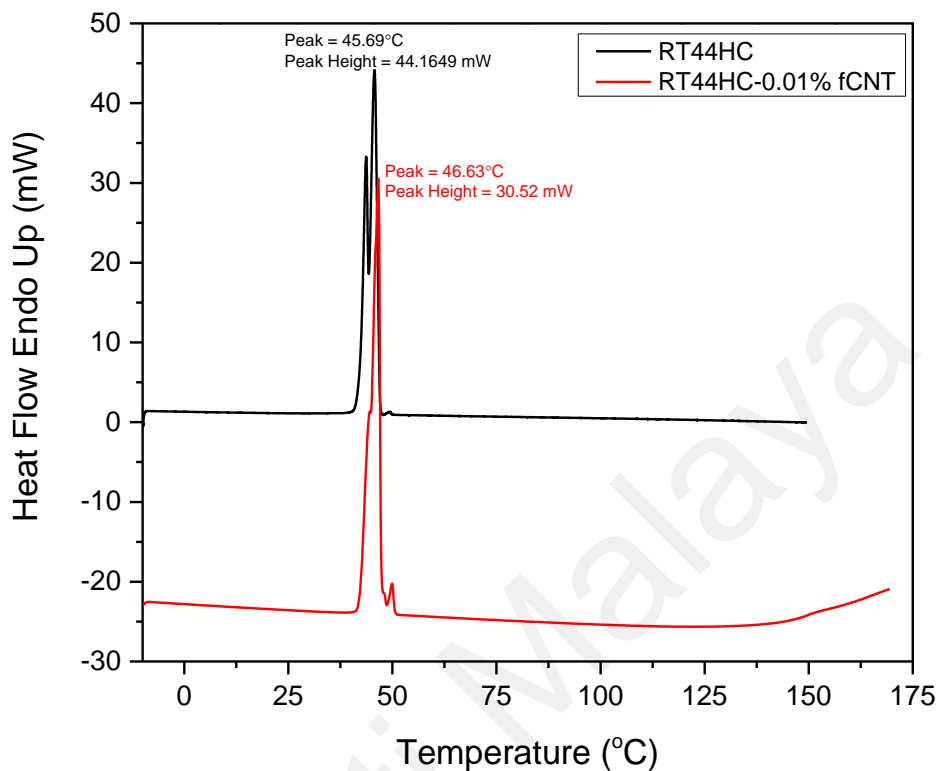

Figure 4.17: Heating DSC curves of RT44HC and RT44HC-0.01%f-CNT

Table 4.3: Comparative DSC test results of pure and composite material

Material	Onset temperature (ºC)	Peak temperature (ºC)	End temperature (ºC)	Latent heat (kJ/kg)
Pure RT44HC	44.55	45.69	45.90	241.5839
RT44HC-0.01%f-CNT	44.32	46.63	46.60	248.6505

It is evident from the TGA curve in Figure 4.18 that with the insertion of f-CNT nanoparticles, the degradation step becomes smoothed compared with pure PCM. While the onset temperatures for mass decay is almost identical for both pure PCM and NePCM the early inflection point (peak of the first derivative curve) indicates slightly faster degradation of NePCM than the pure material.
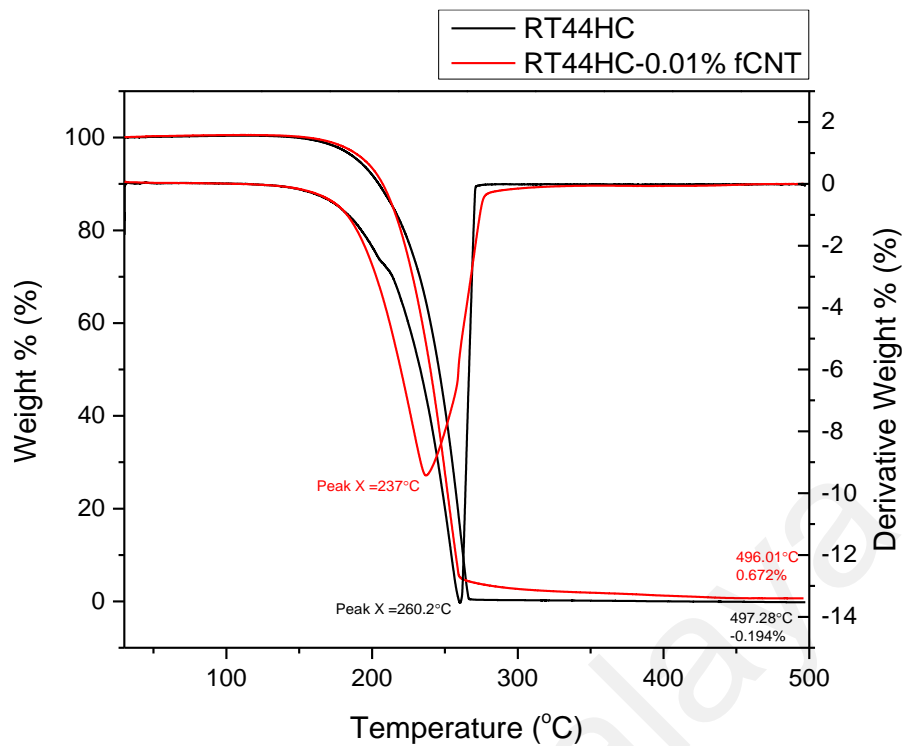
Figure 4.18: TGA curves of RT44HC and RT44HC-0.01%f-CNT

4.2.3.4 Thermal cycling

Since the NePCM RT44HC-0.01%f-CNT has been synthesized for solar thermal application its thermal properties need to be conserved intact over a substantial melt-freeze cycles. Figure 4.19 presents the DSC heating curves for NePCM RT44HC-0.01%f-CNT at zero, 750 and 1000 melt-freeze cycles. Upon cycling, very negligible drop in the peak of the phase transition temperature is evident from the figure which less than 0.5°C. On the other hand, almost no alternation in FTIR spectra is detected upon thermal cycling (Figure 4.20). Furthermore, FESEM micrographs (Figure 4.21) of the NePCM after 750 and 1000 melt-freeze cycles demonstrates no major deterioration in the microstructure.

Therefore, it may be concluded that the newly synthesized NePCM is capable of withstanding substantial melt-freeze cycles and can perform as a robust heat storage material.
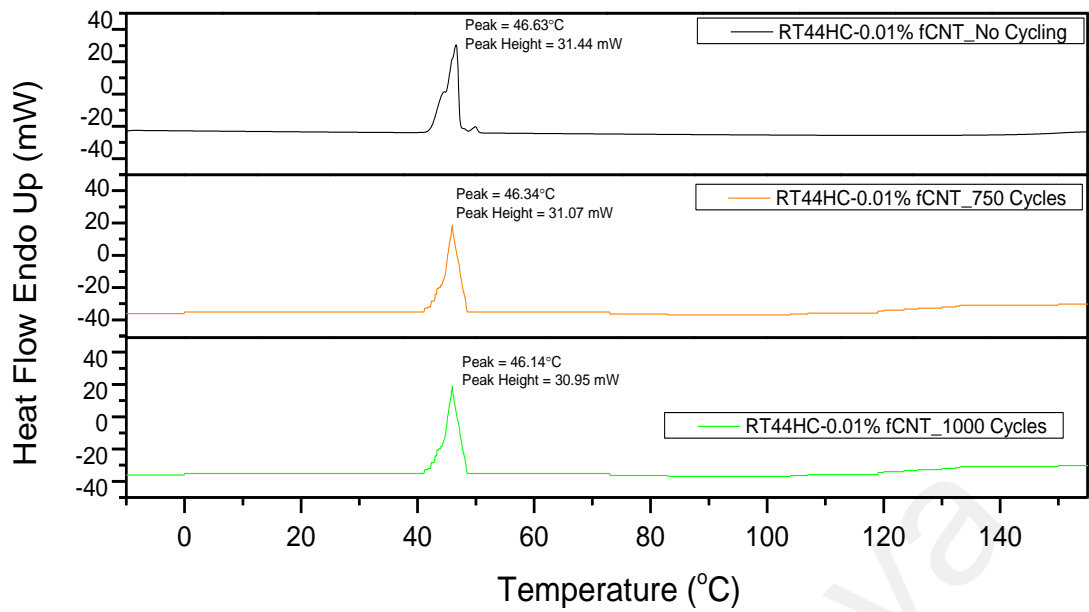
Figure 4.19: DSC heating curve for RT44HC-0.01%f-CNT at zero, 750 and 1000 melt-freeze cycles
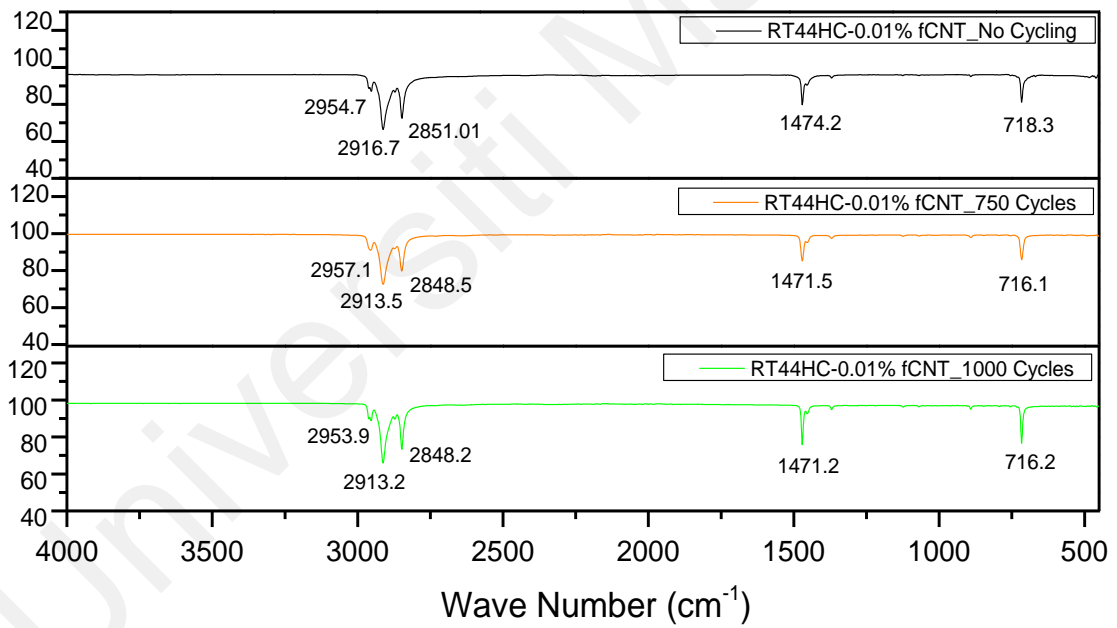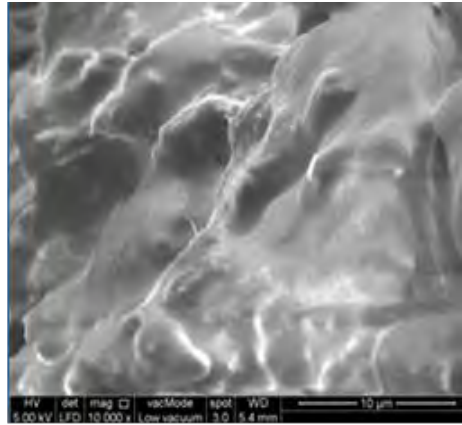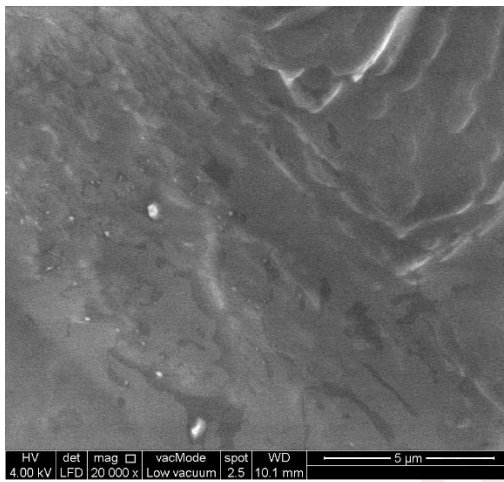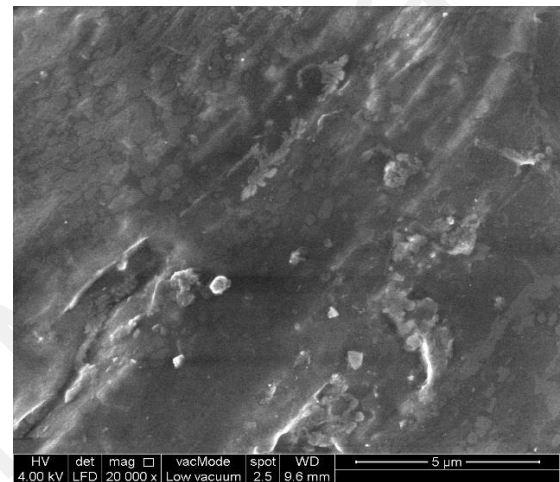

Figure 4.20: FTIR spectra for RT44HC-0.01%f-CNT at zero, 750 and 1000 melt-freeze cycles

(a)

(b)

(c)

Figure 4.21: FESEM micrograph of RT44HC-0.01%f-CNT at (a) zero, (b) 750 and (c) 1000 melt-freeze cycles

4.3 Performance Analysis of PVT-NePCM System

4.3.1 Weather Profile of the Experimental Site

The outdoor experimentations were performed in Kuala Lumpur, Malaysia during June to November 2019. The diurnal solar irradiance and air temperature of a representative day have been depicted in Figure 4.22. It may be perceived from the figure that solar radiation reaches its peak of around $1000 - 1050$ W/m^2 between 1:30 to 2:30 pm when air temperature also touches its maximum of $30^\circ - 30.5^\circ$C.
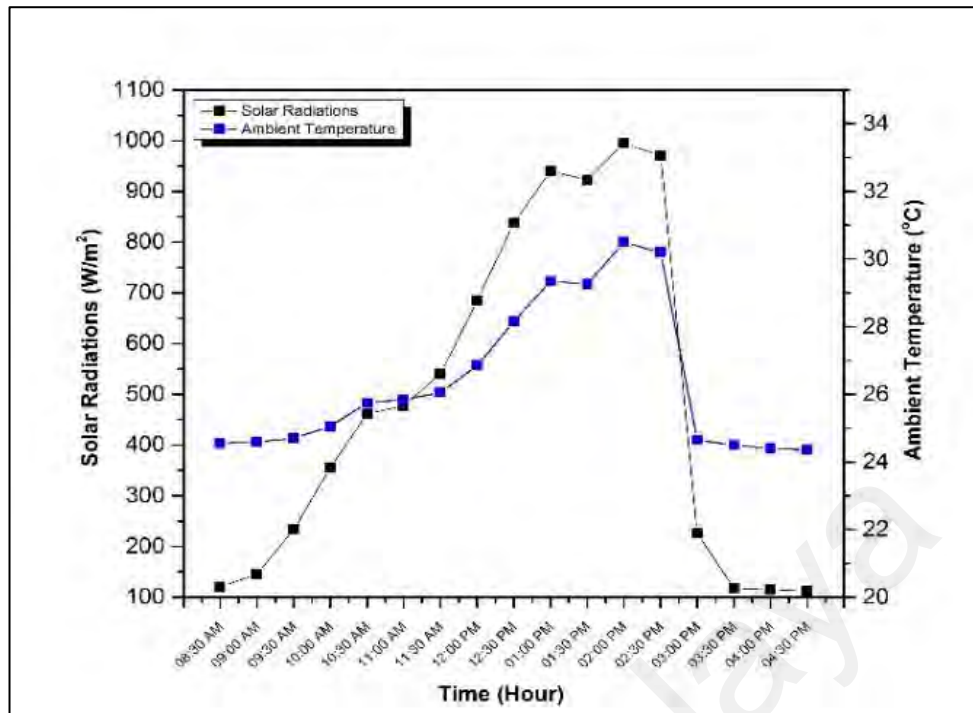
Figure 4.22: Solar irradiance and ambient temperature trend on the experiment site on a typical day

### 4.3.2 Daily Performance Analysis

Performance of the novel PVT-NePCM system has been compared with PV, PV-PCM, PVT-only and PVT-PCM systems. Experimental investigations have been carried out at flow rates ranging from 0.5 to 4.0 litre per minute (L/min or LPM). In order to identify the most efficient system daily performance of all five systems has been evaluated in the first place to have an exhaustive representation. Then performance of the systems has been examined on average basis employing the first and the second laws of thermodynamics.

4.3.2.1 Cell temperature

Figure 4.23 (a) and (b) show the upshots of altering of flow rate and solar irradiance on the average cell temperature, respectively. Mass flow rate is seen to have very little impact on cell temperature as the variation is negligible (Figure 4.23 (a)). In the case of PVT-NePCM system, it varies from 47.5°C at 0.5 l/min to 47.6°C at 4.0 l/min. In

contrast, cell temperature increases substantially with the solar radiation (Figure 4.23 (b)). PVT exhibits the best performance in reducing cell temperature. While the maximum diminution in cell temperature attained is almost $18^{\circ}C$ (at 500 W/m^2) with PVT this value is around $15^{\circ}C$ for both PVT-NePCM and PV-NePCM systems and $11^{\circ}C$ with PVT-PCM system.

The above upshots point out two important facts; firstly, though PCM and NePCM have many long-term vantage points direct integration of these material plays a negative role in assuaging cell temperature on short-term basis as PCM/NePCM layers hinders heat dissipation from PV backside to ambience. Secondly, employing NePCM in PV or PVT can reduce cell temperature better than PCM. In the present case, $4^{\circ}C$ additional retrenchment is attained, which is due to the assimilation of highly conductive MWNT nanotubes into PCM matrix.
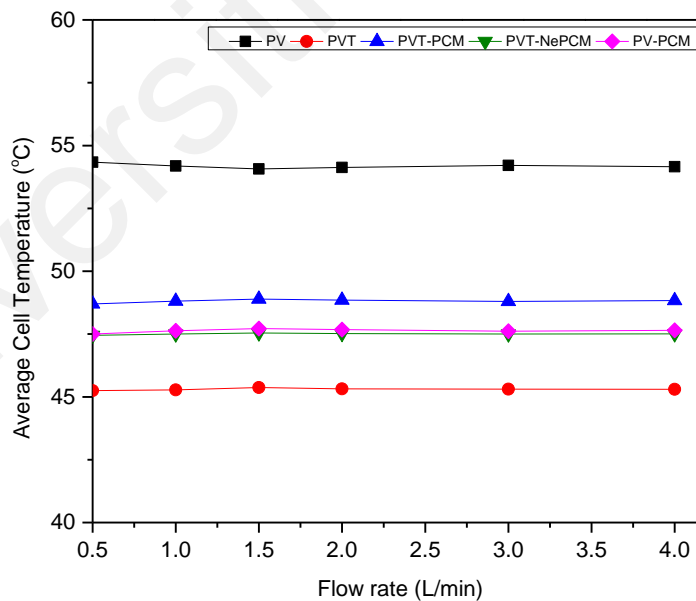

(a)

Figure 4.23: Effect of (a) flow rate (b) solar irradiance on average cell temperature.
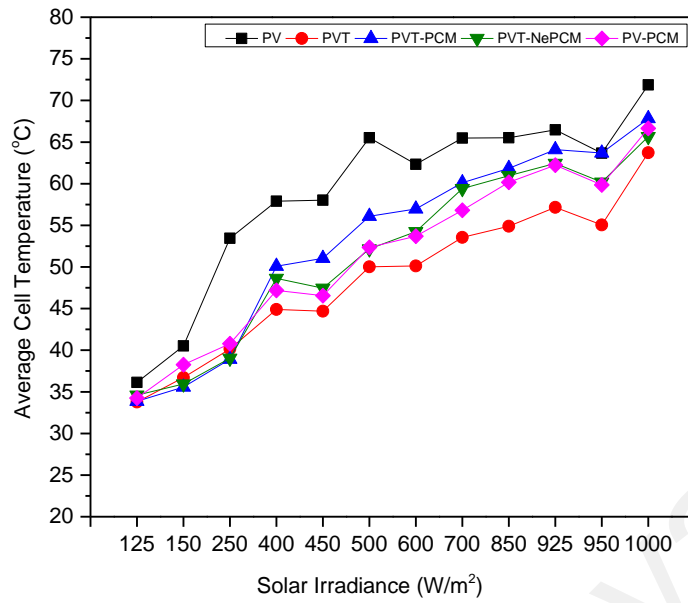
(b)

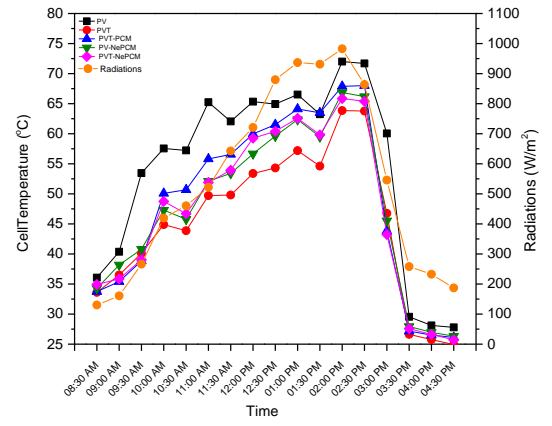**Figure 4.23,** continued

Hourly variation of cell temperatures obtained with flow rates 0.5, 1.0, 1.5, 2.0, 3.0 and 4.0 L/min are shown in Figure 4.24 (a to f). It is evident from these plots that cell temperature of PVT-NePCM module is almost always lower than that of the other modules for all the flow rates, establishing the reasoning of integrating NePCM with PVT.
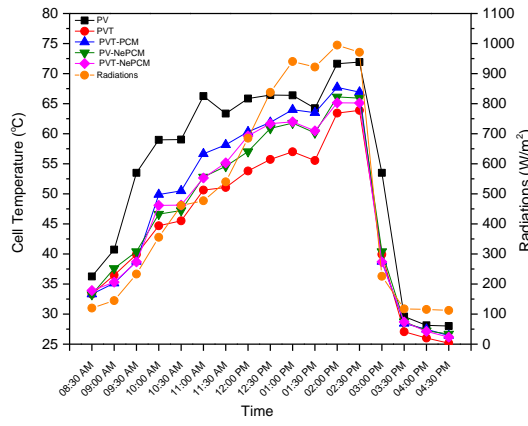
(a) 0.5 L/min

(b) 1.0 L/min
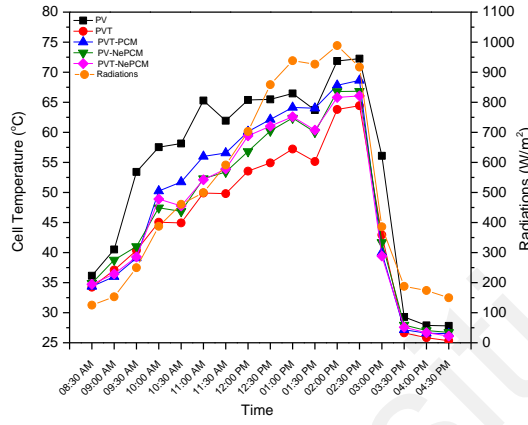
(c) 1.5 L/min
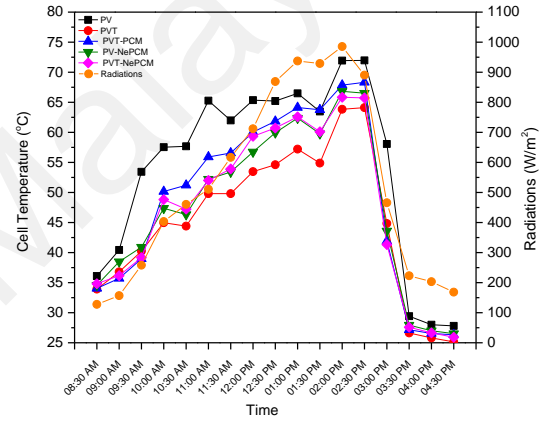
(d) 2.0 L/min
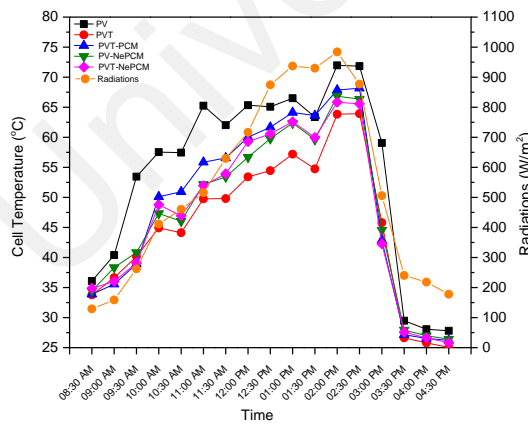
(e) 3.0 L/min
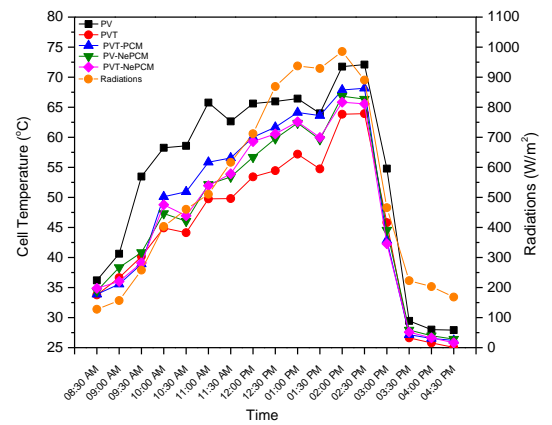
(f) 4.0 L/min

Figure 4.24: Daily variation of cell temperature

4.3.2.2 Water outlet temperature

Hourly change in water outlet temperature at 0.5, 1.0, 1.5, 2.0, 3.0 and 4.0 L/min flow rate have been displayed in Figure 4.25 (a to f). Each of the figure manifests that water outlet temperature of PVT-NePCM module is always higher than other systems. Water outlet temperatures steadily rise with daytime and touches the peak near 2:00 pm before it drops again. It is also noticeable that higher water outlet temperatures are attained at low flow rates since heat transfer fluid (water) gets time enough to acquire heat due to poor convection heat transfer rate. In fact, the lowest flow rate of 0.5 L/min gives rise to the maximum water outlet temperature of 46°C with PVT-NePCM system, which is clearly 1.1°C higher than that with PVT only system at the same flow rate. Interestingly, effect of integrating PCM or NePCM capsules with PVT is substantial only up to 1.5 L/min; from 2.0 L/min such integration seemingly less effective or even a barrier in raising water outlet temperature.

(a) 0.5 L/min
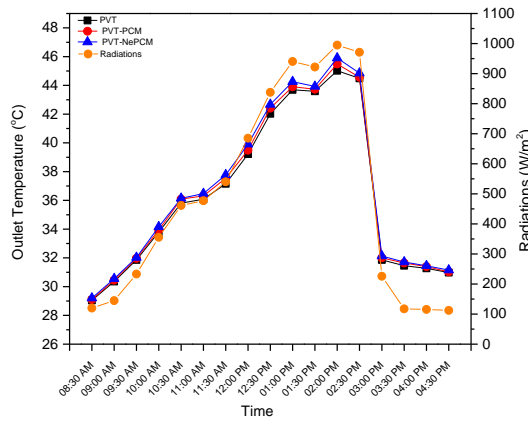
(b) 1.0 L/min
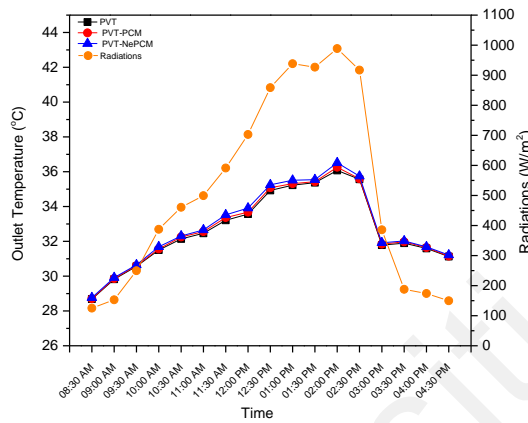
(c) 1.5 L/min
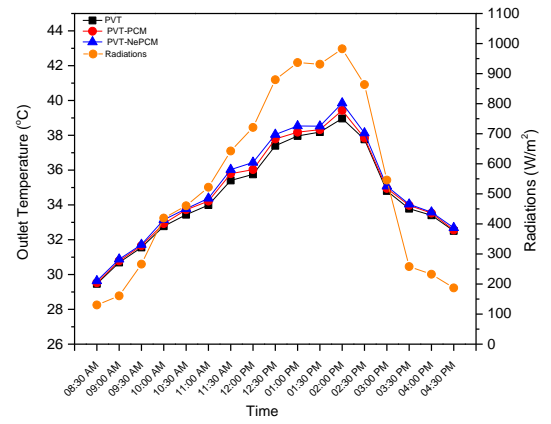
(d) 2.0 L/min

(e) 3.0 L/min
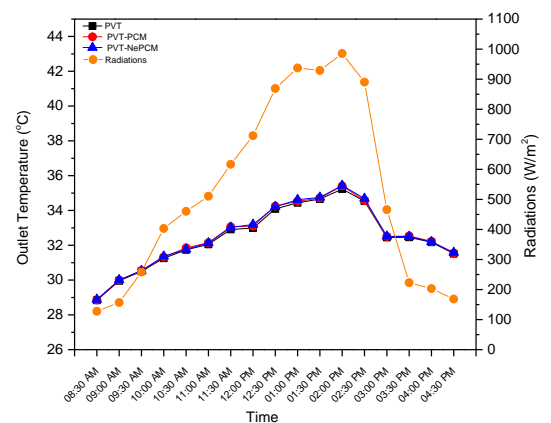
(f) 4.0 L/min

Figure 4.25: Daily variation of water outlet temperature

4.3.3   Energy Analysis
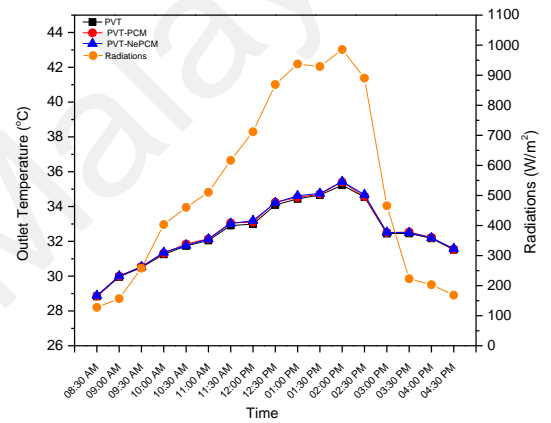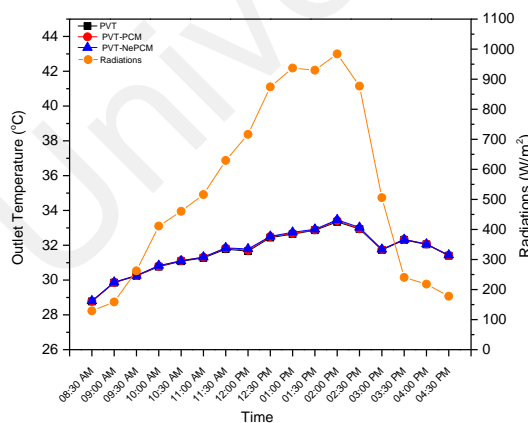
Energetic performance of any PVT system basically includes heat gain by the collector and its thermal efficiency, both estimated applying the first law of thermodynamics or energy balance equation. However, in parallel to thermal energy PVT modules co-generates electricity; that is why, electrical efficiency comes off as an inalienable energetic performance parameter. And, as the generation of heat and electricity from PVT module is a parallel assignment (co-generation) rather than a sequential one so overall system efficiency is calculated by adding up electrical efficiency with thermal efficiency.

4.3.3.1 Heat gain

Adeptness to heat gain by the three photovoltaic thermal collectors under experimental investigation, viz., PVT only, PVT-PCM and PVT-NePCM have been manifested as a function of flow rate in Figure 4.26 (a) and as a function of solar radiation in Figure 4.26 (b). Figure 4.26 (a) shows that the highest heat gain is obtained with PVT-NePCM system which ascertains its pre-eminence over the other two systems for heat supply. The maximum heat gain of 279 W is observed at a lower flow rate of 1.0 L/min and then with rising flow rate it subsides gently to 233 W at 4.0 L/min. On the other hand, heat gain upsurges just about linearly with solar irradiance (Figure 4.26 (b)), wherein PVT-NePCM exceeds other four systems in rate of augmentation. The maximum heat gain by PVT-NePCM system (accomplished at 1000 W/m^2) is around 8.5% greater than that of PVT only system. It is divulged from Figure 4.26 (a) and (b) that heat gain of a photvoltaic thermal system solar radiation influence more markedly than mass flow rate in.
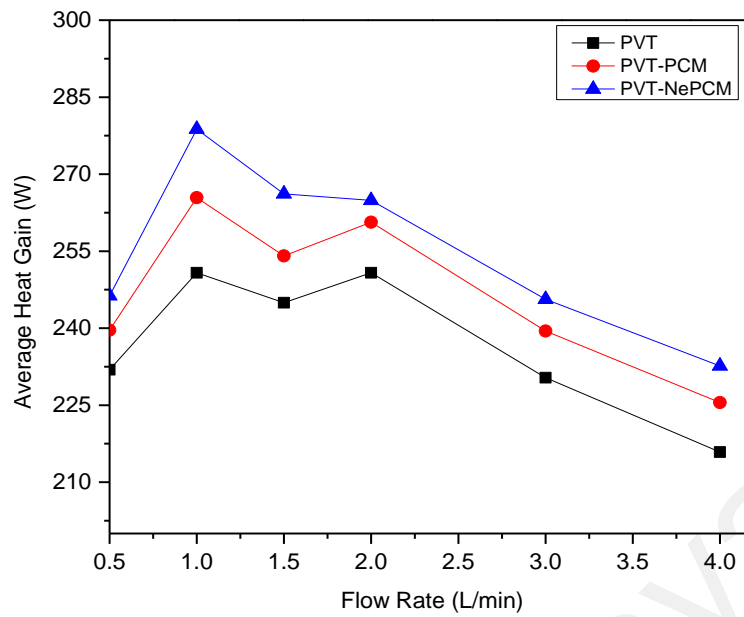
(a)
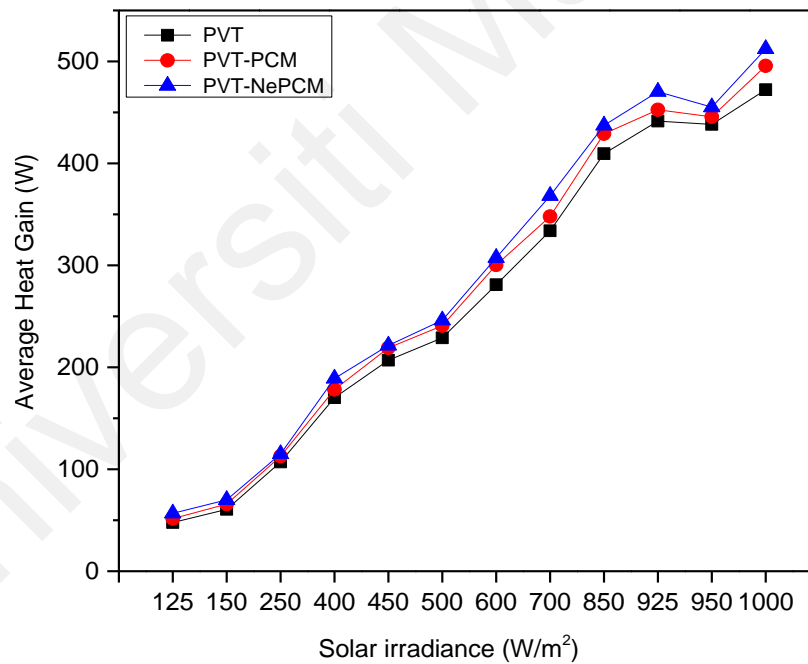
(b)

Figure 4.26: Effect of (a) flow rate (b) solar irradiance on average heat gain

4.3.3.2 Thermal efficiency

Propensity of thermal efficiency of PVT, PVT-PCM and PVT-NePCM systems as functions of flow rate and solar radiations have been shown in Figure 4.27 (a) and (b),

respectively. Figure 4.27 (a) shows that thermal efficiency of PVT-NePCM rises with increase in flow rate till it reaches to the maximum of 75% at 1.5 L/min. However, further rise in flow rate causes a steady decline in thermal efficiency, which is because with greater flow rate less time is available for heat accumulation. Nevertheless, the thermal efficiency of PVT-NePCM at all flow rates is superior. PVT-NePCM system exhibits better thermal efficiency against solar irradiance, too. From irradiation viewpoint, Figure 4.27 (b) shows that even under pretty low irradiance (125 W/m^2), PVT-NePCM works with 66% thermal efficiency, whereas under similar conditions PVT and PVT-PCM systems barely reaches around 55% thermal efficiency. Thermal efficiency of PVT-NePCM carries on growing with irradiation intensity and the highest 76% efficiency is achieved at 1000 W/m^2. Although the rate of increment in thermal efficiency becomes feeble after 50 W/m^2 utility of NePCM persists relatively longer. While thermal efficiency of PVT with and without PCM is noticed to vary within a wide range of 25% and 73% (Al-Waeli et al., 2017; Eisapour et al., 2020; Fayaz et al., 2019; Gaur et al., 2017; Hazami et al., 2016; Hossain et al., 2019; Hosseinzadeh et al., 2018; Nahar et al., 2017), the PVT-NePCM system is capable of maintaining a better mean thermal efficiency level throughout the day: 66% at 125 W/m^2 to 75% at 1000 W/m^2.
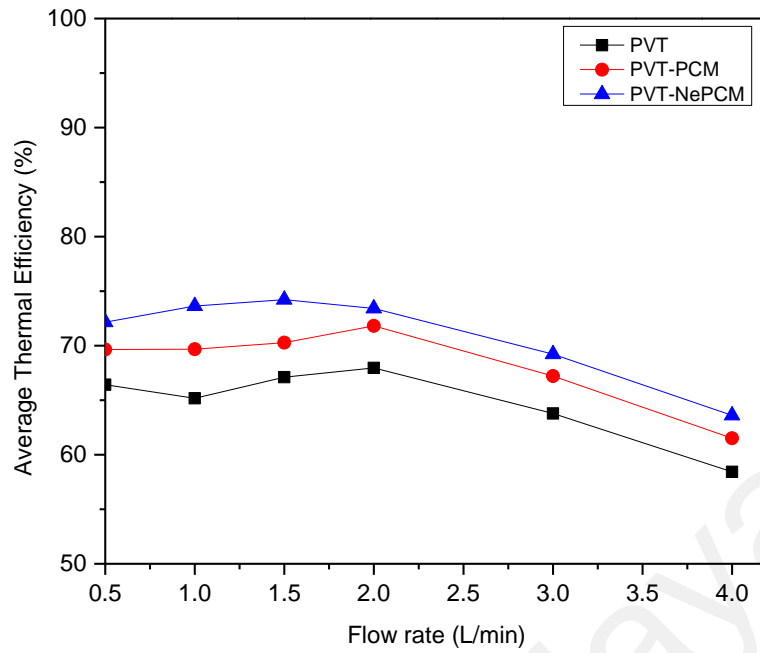
(a)
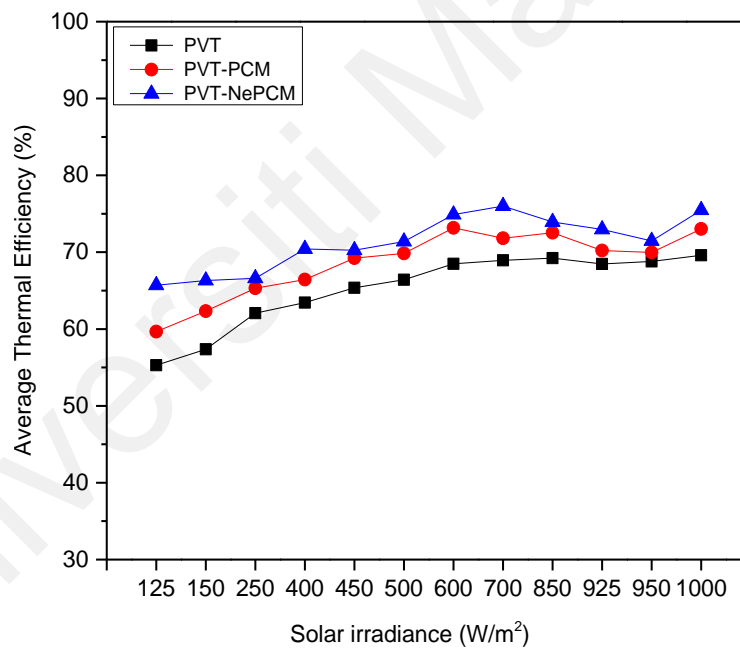
(b)

Figure 4.27: Effect of (a) flow rate (b) solar irradiance on thermal efficiency

Hourly variation of thermal efficiency at 0.5, 1.0, 1.5, 2.0, 3.0 and 4.0 L/min flow rates have been shown in Figure 4.28 (a to f). All these graphs evince the superiority of PVT-NePCM module in terms of thermal efficiency as compared with other four systems at all flow rates.

(a) 0.5 L/min

(b) 1.0 L/min
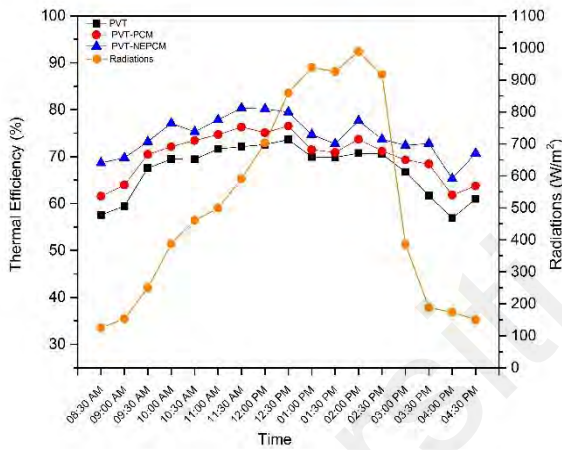
(c) 1.5 L/min
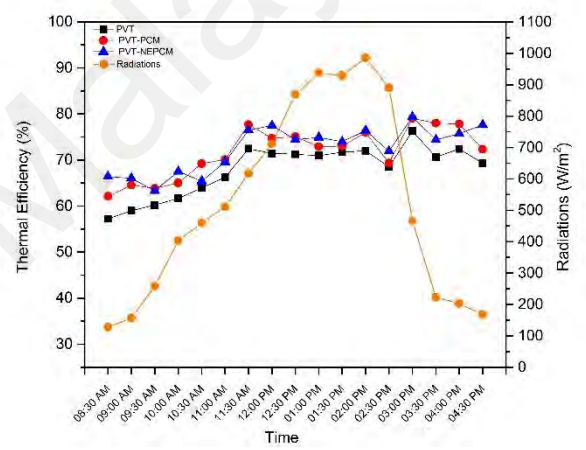
(d) 2.0 L/min
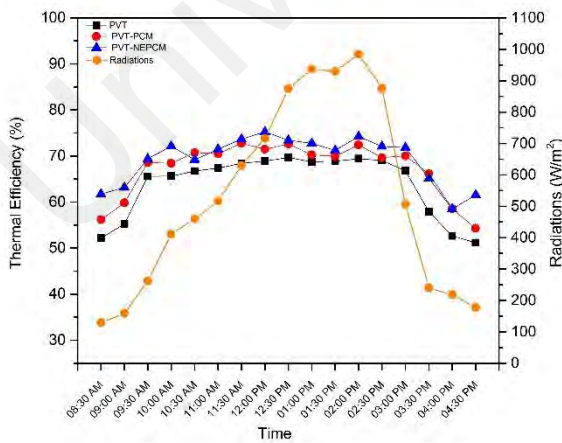
(e) 3.0 L/min
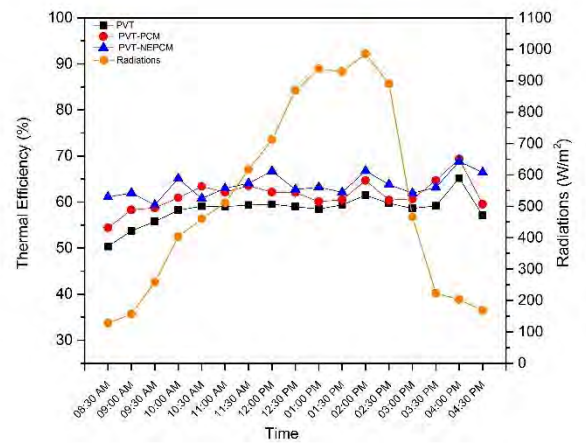
(f) 4.0 L/min

Figure 4.28: Daily variation of thermal efficiency

4.3.3.3 Electrical efficiency

Electrical efficiency is one of the most important performance indicators for PV and PVT modules. As evident from Figure 4.29 (a), influence of HTF flow rate on electrical efficiency is not that salient. In contrast, electrical efficiency of both PV and PVT modules is remarkably affected by solar radiation intensity. Figure 4.29 (b) shows that electrical efficiency of all the systems remains almost unaltered until 250 W/m^2 but then it starts increasing sharply until 500 W/m^2 and then after 600 W/m^2 maintains a steady trend. Hence, it may be concluded that PV and PVT modules deliver better electrical performance near 500 W/m^2 irradiation level.

Another important fact manifested in both Figure 4.29 (a) and (b) is that PVT-NePCM system's electrical efficiency is always significantly higher than all other systems. Figure 4.29 (a) displays an average absolute efficiency headway of 2.5% between PV and PVT-NePCM systems. Likewise, Figure 4.29 (b) corroborates that even under pretty low irradiances like 100 W/m^2, while PVT-NePCM system delivers nearly 4.0% electrical efficiency the PV system hardly reaches 0.5%. In fact, PVT-NePCM system accomplishes a marked margin of 12.75% under 500 W/m^2 realizing a 34.2% enhancement as compared with PV under the same irradiation level. All these consequences indubitably establish the pre-eminence of PVT-NePCM system over other conventional systems.

In literature, electrical efficiency of PVT-PCM systems is reportedly between 8% and 13% (Al-Waeli et al., 2017; Fayaz et al., 2019; Hossain et al., 2019; Hosseinzadeh et al., 2018; Nahar et al., 2017). Onsite solar experimentations are affected by the real-time ambient conditions, especially air temperature and wind speed. Thus, an electrical efficiency of 12.75% for the PVT-NePCM system can be considered up to the mark as compared to those reported in literature.

(a)

(b)

Figure 4.29: Effect of (a) flow rate (b) solar irradiance on electrical efficiency

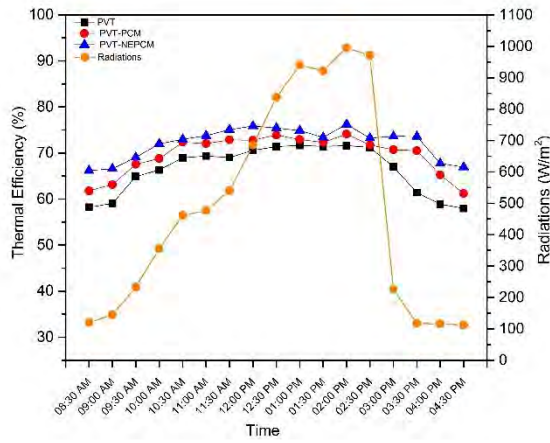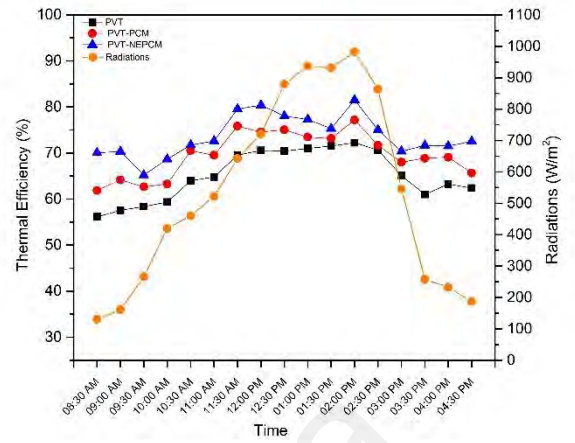Hourly variation of electrical efficiency at 0.5, 1.0, 1.5, 2.0, 3.0 and 4.0 L/min are shown in Figure 4.30 (a to f), wherein PVT-NePCM system is always seen to deliver the highest efficiency.
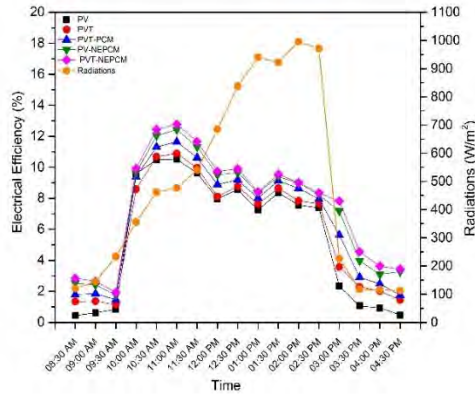
(a) 0.5 L/min
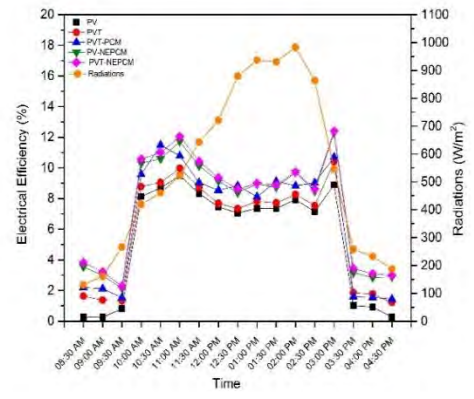
(b) 1.0 L/min
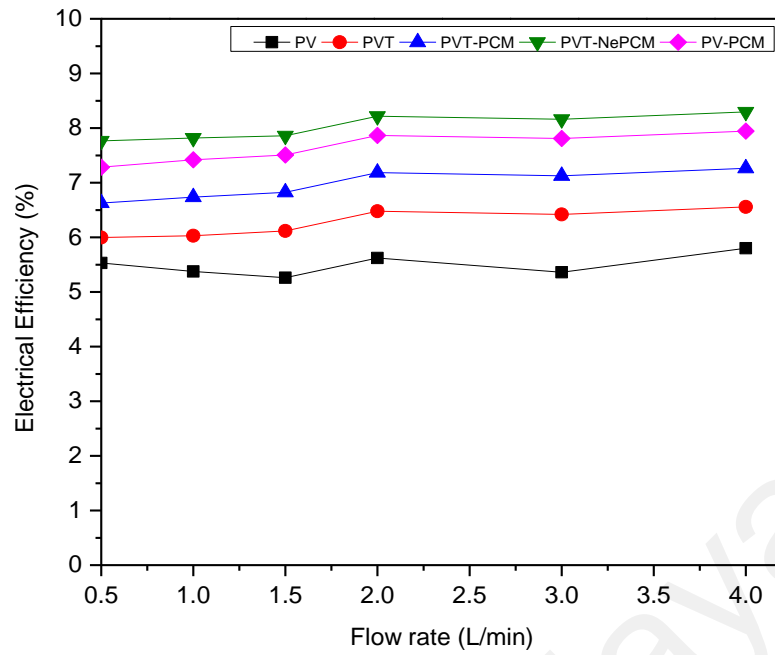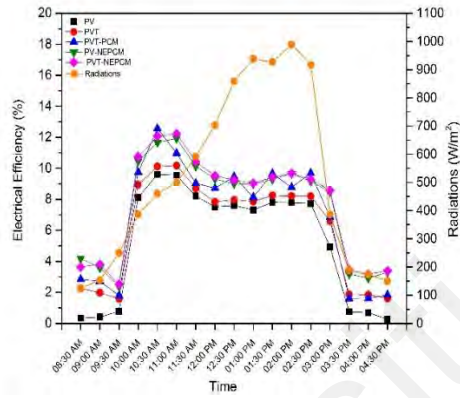
(c) 1.5 L/min
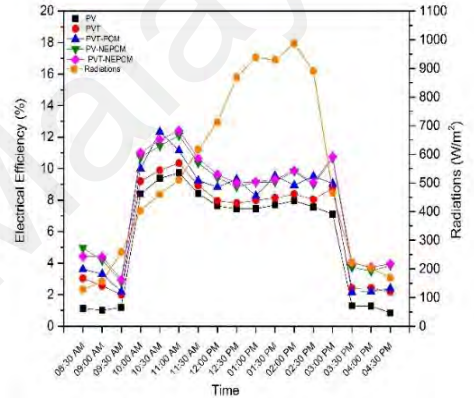
(d) 2.0 L/min
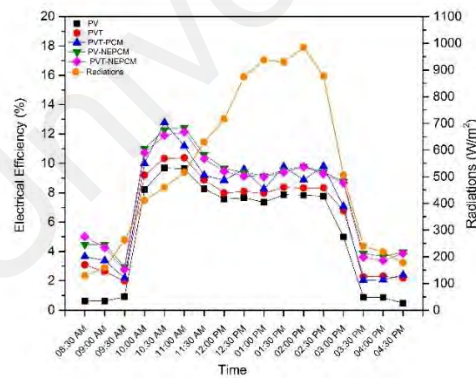
(e) 3.0 L/min
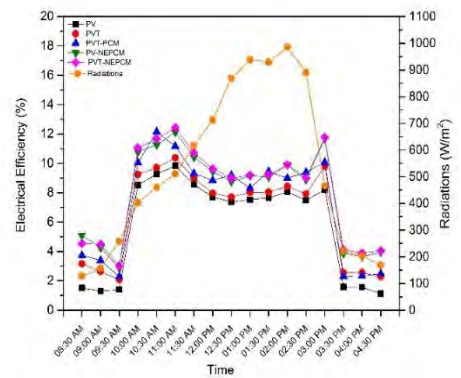
(f) 4.0 L/min

Figure 4.30: Daily variation of electrical efficiency

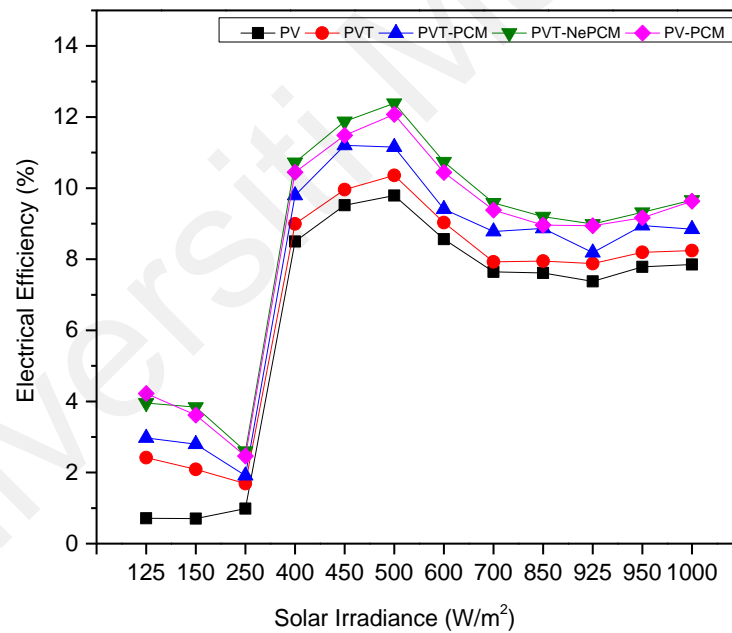### 4.3.3.4 Overall efficiency

Overall efficiency of an energy co-generation system is the sum of the individual efficiency segments. At 1.5 L/min, PVT-NePCM system reaches its maximum overall efficiency of 80.4%, which is 8.1% higher than that of PVT only system and 1.8% higher than PVT-PCM system (Figure 4.31 (a)). From irradiation context (Figure 4.31 (b)), it is interesting to observe that irradiance below 250 W/m^2 and above 500 W/m^2 has trivial effect on overall efficiency, whereas it increases sharply within this band. Overall efficiency touches its peak near 600 – 750 W/m^2 and after that it does not improve markedly. At high solar irradiances, temperature of the NePCM (as well as PCM) remains above its phase transition temperature; as a result, it stays in liquid phase for quite long time. Consequently, latent heat absorption phenomenon becomes inefficient in this chunk stalling further efficiency augmentation.

The maximum overall efficiency of 85.3% is achieved with PVT-NePCM near 600 W/m^2. In literature, a PVT system using nano-PCM and SiC-water nanofluid coolant has been reported to deliver a maximum overall efficiency of 85.7% (Al-Waeli et al., 2019). This little discrepancy in efficiency value consists in the type HTF employed for heat removal. Moreover, since an intermediate heat exchanger is required to heat up water, the net overall efficiency at the application end will be less. On the other hand, in the present research water is used as the HTF that would directly be used in application end with a net overall efficiency of 85.3%.
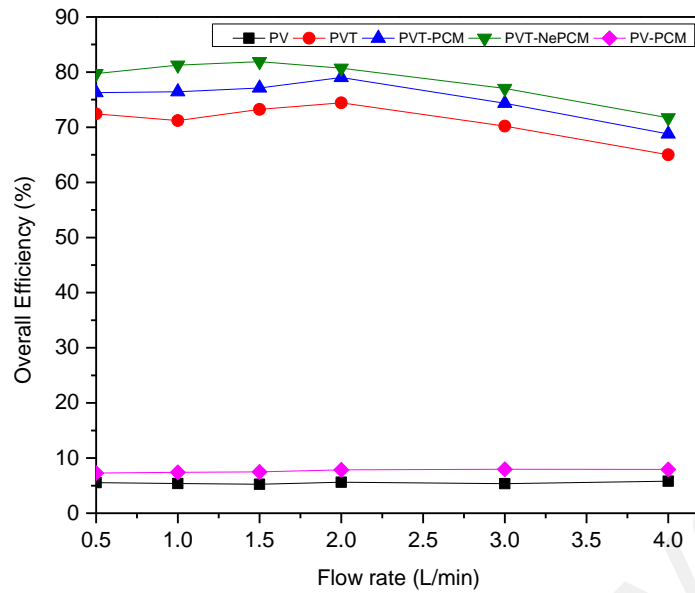
(a)
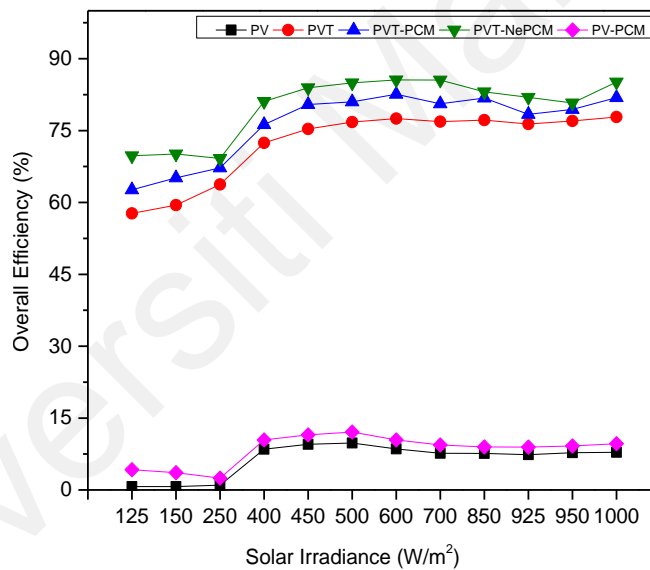
(b)

Figure 4.31: Effect of (a) flow rate (b) solar irradiance on overall efficiency

4.3.4 Exergy Analysis

Thermodynamic processes (and devices) intrinsically comprise a certain type of inefficiency derived as a result irreversibilities involved in various steps as well as mechanisms. Second law of thermodynamics can be sagely used to identify the roots, locations and extents of these process inefficiencies leading to exergetic performance

analysis. This section aims to analyze the performance of the newly developed PVT-NePCM system from exergy viewpoint.

4.3.4.1 Overall exergy efficiency

Overall exergy efficiency consists of thermal and electrical exergy components, wherein contribution of the latter is greater as electricity is intrinsically a high-grade energy. Though the share of thermal exergy in overall exergy is less it strongly influence overall exergy efficiency and the response is not alike against mass flow rate and solar irradiance. Overall exergy efficiency of PV, PVT, PVT-PCM, PV-PCM and PVT-NePCM systems as a function of flow rate (Figure 4.32 (a)) and as a function of solar irradiance (Figure 4.32 (b)) evince the precedence of PVT-NePCM over other four systems. Interestingly, at higher flow rates (after 1.0 L/min) exergy efficiencies of PVT and PV-NePCM are almost identical. Exergy efficiency maintains a steady uniform trend with an overall exergy efficiency of 8.5% for PVT-NePCM system over the entire range of flow (Figure 4.32 (a)). On the contrary, as a function of irradiation intensity, as shown in Figure 4.32 (b), exergy efficiency behaves in a quite peculiar and random manner: at low irradiance of 125 to 250 W/m^2 this variation is very insignificant, while between 250 and 500 W/m^2 exergy efficiency of the system rises to its peak, hence after 700 W/m^2 increase in irradiance have no significant effect on system exergy efficiency. The highest exergy efficiency of PVT-NePCM system is about 13% at 525 W/m^2, which is comparable with the values reported in literature (Chen et al., 2018; Chow et al., 2009; Eisapour et al., 2020; Kazemian et al., 2020).
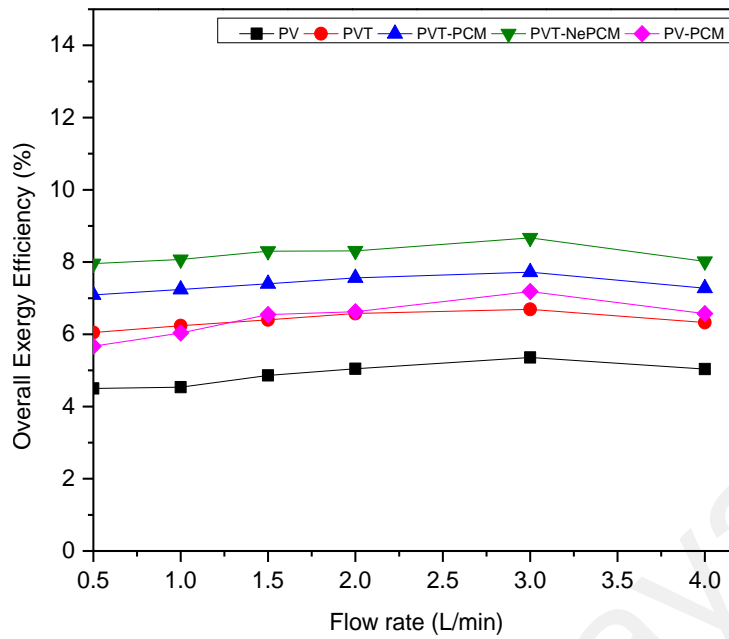
(a)
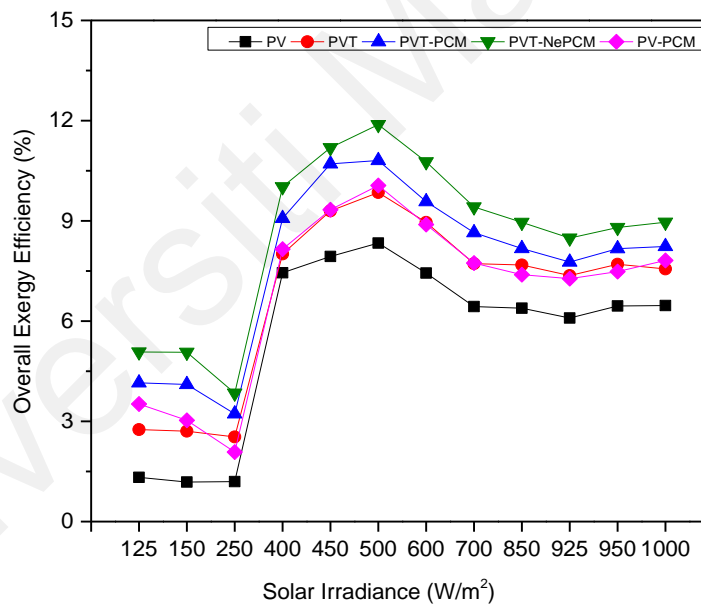
(b)

Figure 4.32: Effect of (a) flow rate (b) solar irradiance on overall exergy efficiency

4.3.4.2 Improvement potential

All thermodynamic processes are irreversible that involve ineptitude to release useful work. While irreversibilities associated with a process cannot entirely be eliminated, these can be lessened up to a certain extent thus enhancing the improvement potential.

Exergetic improvement potential illustrates the potential thermodynamic performance that could be attained upon adopting specific actions (Guarracino et al., 2019). Improvement potential of the five systems (PV, PVT, PV-PCM, PVT-PCM, PVT-NePCM) under experimental investigation has been shown as a function of mass flow rate in Figure 4.33 (a) and as a function solar radiation in Figure 4.33 (b). It quite apparent from the figures that while mass flow has little impact on improvement potential, solar irradiance includes a near-to-linear rising trend. The highest potential value from flow rate context (312 W at 1.0 L/min) is much lower than that with irradiance (550 W at 1000 W/m^2). Both observations reveal the fact that substantial improvements in thermal performance of PV and PVT systems can be best exploited at higher irradiation levels, whereas altering flow rate have minor impact in performance enhancement. As might be anticipated, PV shows the highest improvement potential among all the systems revealing its wide scopes to harvest more energy. Conversely, the lowest improvement potential values with PVT-NePCM systems directs to fact that integrating NePCM with conventional PVT is the best option to increase the yield from such systems.
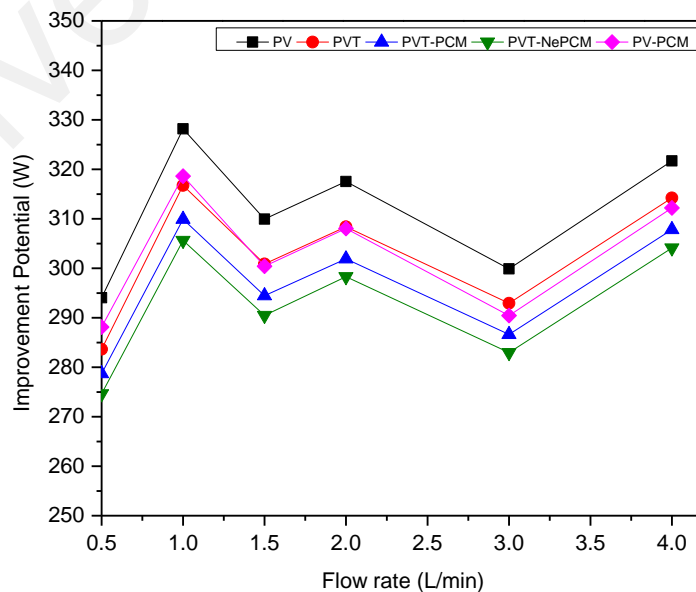
(a)

Figure 4.33: Effect of (a) flow rate (b) solar irradiance on improvement potential
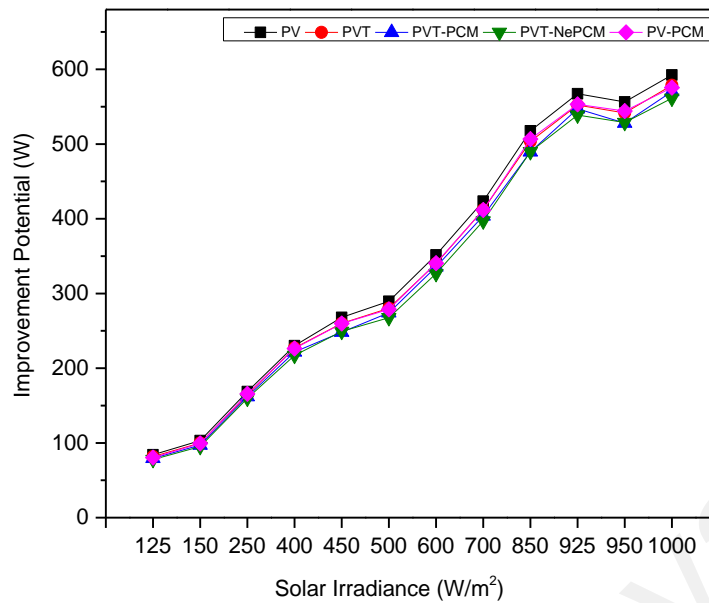
(b)

Figure 4.33, continued

4.3.4.3 Exergy destruction and entropy generation

Exergy analysis of thermodynamic systems not only measures the exergetic efficiency but also identifies the locus, nature and degree of availability destruction.

Figure 4.34 (a) shows the exergy destruction with respect to HTF flow rate, from where it obvious that mass flow rate has pretty little influence on exergy destruction. From the perspective of mass flow rate, a mean exergy destruction of about 320 W is sustained without notable variation over the entire range. Then again, from irradiance context (Figure 4.34 (b)), exergy destruction upsurge sharply with irradiance and the maximum destruction occurs 1000 W/m^2. The reason behind this rising trend of exergy destruction with irradiance consists in the higher electrical and optical obliterations under high solar irradiance (Mehmet et al., 2017). The above findings suggest a paradoxical fact about irradiance and PV power output: despite of being the only fuel increase in solar irradiance destroys exergy of a PV or PVT system.

Figure 4.34 (a) also divulges that exergy destruction of PVT-NePCM module is about 15 W less than that of PV module on average evincing the design superiority of the former one from thermodynamic viewpoint.
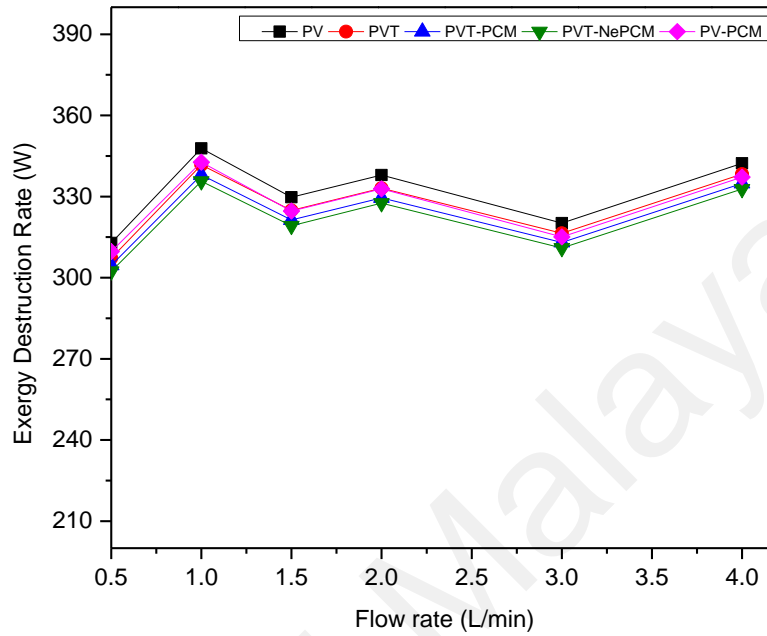
(a)
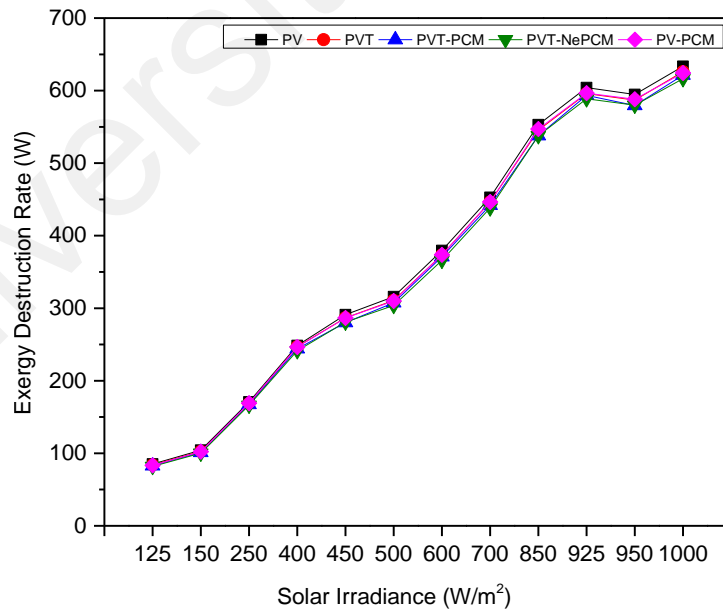
(b)

Figure 4.34: Effect of (a) flow rate (b) solar irradiance on exergy destruction

Entropy generation is the sum of entropy generated during an irreversible heat and mass transfer processes (e.g., heat exchange, fluid flow, etc.) as well as irreversible thermodynamic cycles. Entropy generation analysis judges how much energy is unexploited per unit increase in temperature.

Figure 4.35 (a) shows that variation in flow rate has an insignificant impact on entropy generation of PVT systems and about 1 W entropy is increased for every Kelvin increase in module temperature. On the contrary, as a function of irradiation entropy is generated in a near-to-linear fashion as shown in

Figure 4.35 (b). This figure demonstrates that entropy generation increases from a insignificant value 0.2 W/K at 125 W/m^2 irradiation to the highs of 2.0 W/K at 1000 W/m^2. That is, for every 100 W/m^2 increase in irradiance level a PV or PVT system experiences an augmentation of 0.22 W of entropy per unit Kelvin.
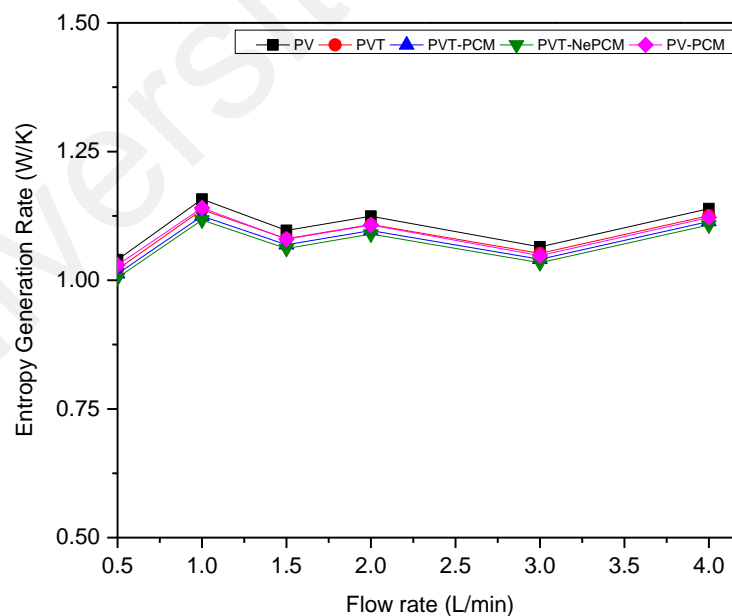
(a)

Figure 4.35: Effect of (a) flow rate (b) solar irradiance on entropy generation
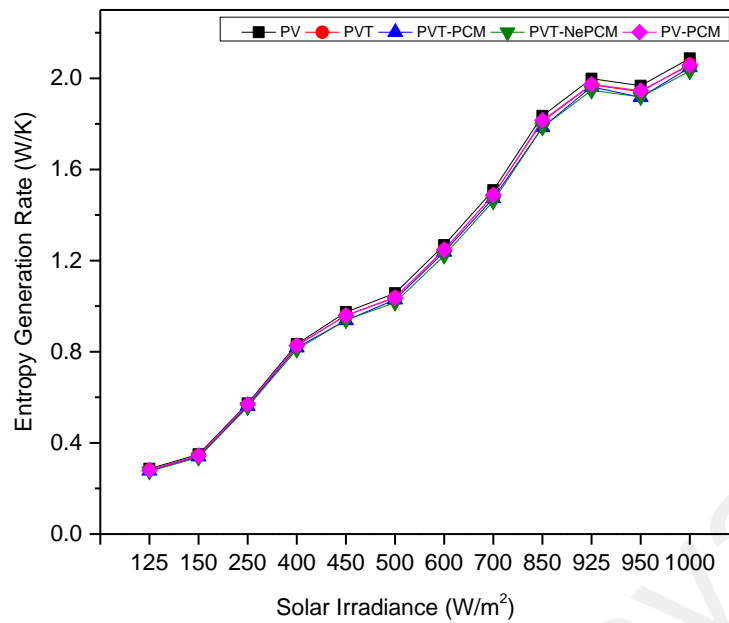
(b)

Figure 4.35, continued

4.3.5 Performance Mapping

Performance mapping is a technique to find out the trade-off point or area of the operating parameters in order to ensure the optimum performance of a system. Thermal and electrical performance maps of the PVT-NePCM system have been plotted as functions of two control parameters, viz., flow rate of the HTF (water) and irradiance level with a view to ascertain the ideal operating point of the newly devised system.

Thermal efficiency map (Figure 4.36 (a)) shows the highest thermal efficiency (represented in maroon color) occurs between 0.5 – 1.0 L/min flow rate and 700 – 850 W/m^2 irradiance level. Maximum electrical efficiency, in contrast, is attainable over a wider range of flow rate within the same solar irradiance level (Figure 4.36 (b)). Likewise, exergy efficiency remains at its peak over a broader range of flow rate but at a narrow irradiance level near 800 W/m^2 (Figure 4.36 (c)). On the other hand, cell temperature map (Figure 4.36 (d)) dictates that to keep the cell temperature within an operable limit (near 45ºC) it is important to maintain flow rate as high as possible.

Hence, based on the efficiency requirement operating points for the PVT-NePCM system can be determined from these performance maps, where one parameter would be traded-off to boost the other.
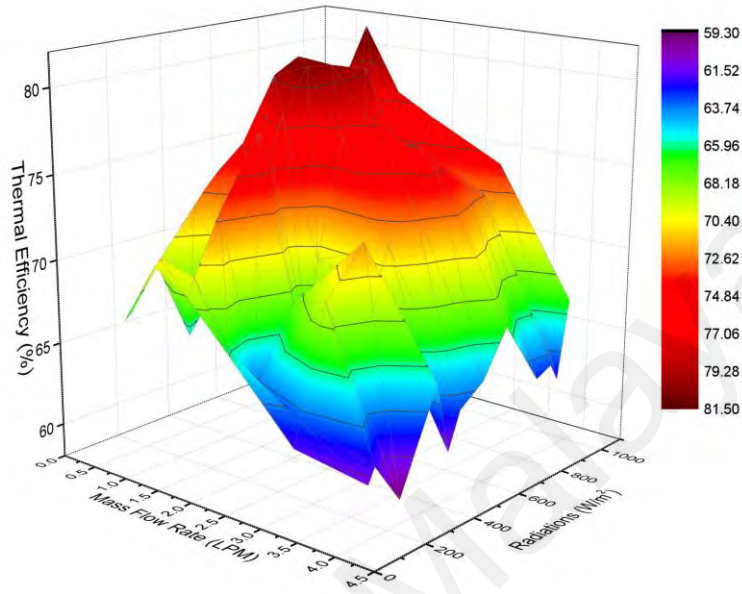
(a)
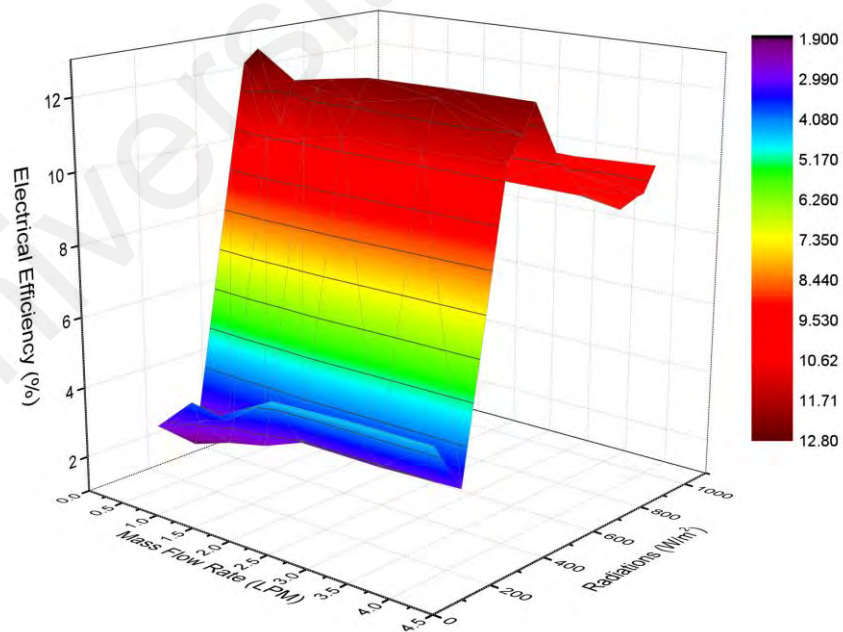
(b)

Figure 4.36: (a) Thermal efficiency map, (b) electrical efficiency map, (c) exergy efficiency map and (d) cell temperature map for the PVT-NePCM system
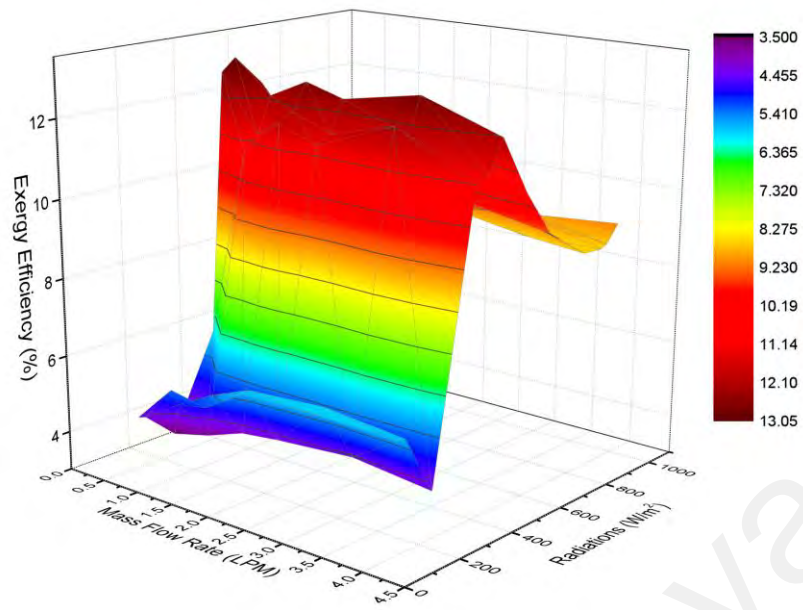
(c)
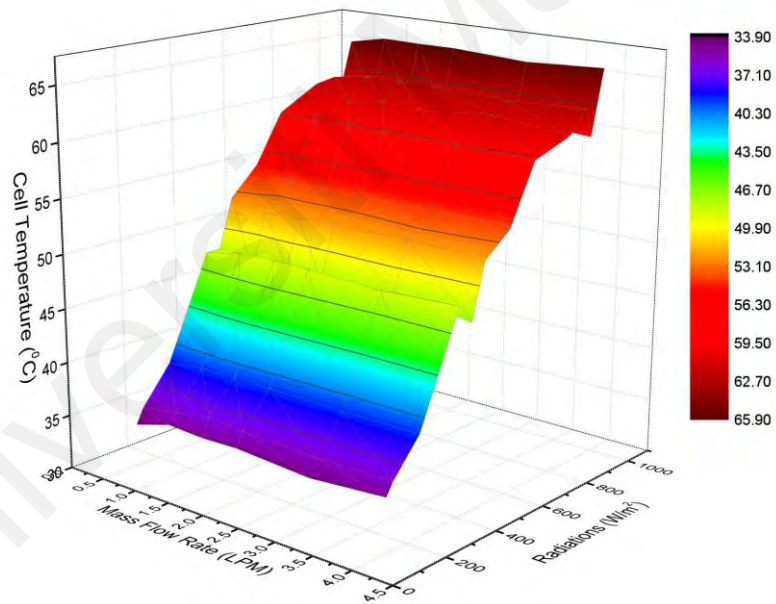
(d)

Figure 4.36, continued

4.3.6   Cooling Period

Cooling period refers to the time span that a PVT system helps to retain the cell temperature below certain specified limit. Figure 4.37 shows that PVT-NePCM system

ensures a cooling period of 2.75 hours (165 minutes) over an 8-hour days' operation, which is about 45 minutes (i.e., 37.5%) longer than the conventional PVT only system. It is also evident from the figure that PVT-NePCM system is superior to PV-PCM and PVT-PCM systems in sustaining extended cooling period. This portrays the efficacy of the newly synthesized NePCM in augmenting latent heat storage capacity and its ability to charge and discharge under a narrow temperature range.
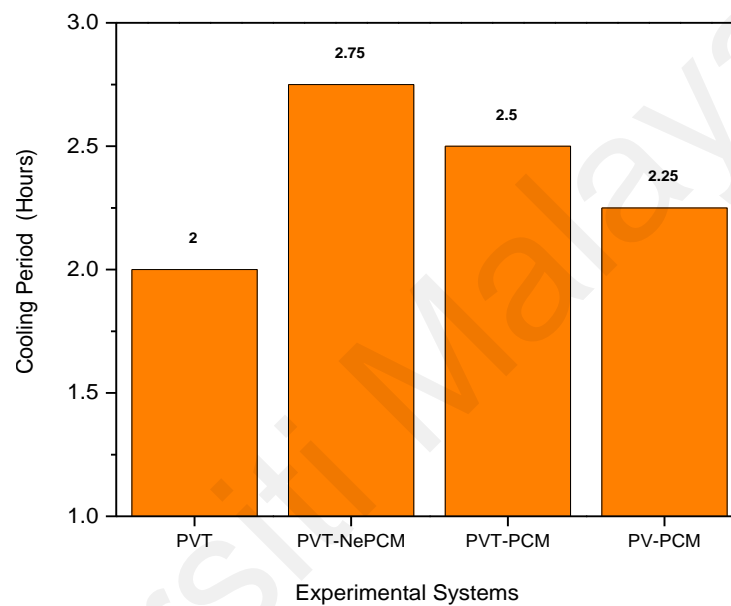
Figure 4.37: Cooling period recorded for different PVT systems

4.4   Chapter Summary

From comparative characterization, it has been confirmed that RT44HC-0.01%f-CNT is the best NePCM for photovoltaic thermal application among the four newly developed nano composite materials. Real-time outdoor performance investigation among five different PV and PVT systems confirms that PVT-NePCM system renders the best performance in enhancing system efficiency and reducing cell temperature as well.

CHAPTER 5: CONCLUSIONS AND RECOMMENDATIONS FOR FUTURE WORKS

5.1 Conclusions

The present research deals with developing a novel material for photovoltaic thermal application and comparative performance assessment of a novel PVT-NePCM system with PV, PV-PCM, PVT and PVT-PCM systems under typical Malaysian conditions. Both the first and the second laws of thermodynamics have been employed to examine the performance. Research findings confirm that NePCM is a better option in enhancing the thermal performance of PVT systems. The key findings of the material synthesis, characterization and experimental performance investigation are enumerated in subsequent sections.

5.1.1 Development of NePCM for Photovoltaic Thermal Application

The primary objective of this research was to develop a novel nanocomposite material that suits the best in photovoltaic thermal applications. For this purpose, four samples of nano enhanced phase change material (NePCM) have been synthesized and characterized to select the best one. The major inferences of the characterization process and properties of the newly developed material is enumerated as below:

- Among the four synthesized NePCMs RT44HC-0.01%f-CNT is characterized as the best material for photovoltaic thermal application.

- FESEM micrographs of the NePCM clearly demonstrates the evanescence of nanoparticles into PCM matrix settling a uniform assimilation between the two materials, which confirms the compact structure of the new nanocomposite. No delamination is detected in the nanocomposite material.

- Phase transition range of the NePCM slightly widens as compared to pure PCM

- Although NePCM decomposes a little faster than the pure material it is thermally stable within operating temperature.

- Almost identical FTIR spectra of pure PCM and NePCM confirms formation of no new functional groups and no chemical reaction has been between PCM and MWNT. Hence, dispersion between f-CNT nanoparticles and the PCM is chemically stable.

- Insertion of functionalized MWNT into PCM matrix upsurges its thermal conductivity by around 16.74%.

- The newly synthesized NePCM is capable of withstanding substantial melt-freeze cycles (more than 1000 cycles), which ensures an unswerving performance for long time.

5.1.2 Energetic and Exergetic Performance of PVT-NePCM System

A novel PVT-NePCM system has been developed by integrating the newly synthesized NePCM with PVT and comparative performance investigation at outdoor conditions has been carried out with four other systems, viz., PV, PVT, PV-PCM and PVT-PCM. Performance of the systems have been analyzed applying both the first and the second laws of thermodynamics. The major implications of the analysis are as follows:

- PVT-NePCM system attained 4°C more diminution in cell temperature as compared with PVT-PCM system.

- The highest water outlet temperature raised by PVT-NePCM system is 46°C. This value is superior to those obtained by both PVT and PVT-PCM systems.

- The maximum overall energy efficiency of PVT-NePCM system is 85.3%, while this system attained a maximum exergy efficiency of 13%. For PVT and PVT-PCM systems, the maximum overall energy efficiency values are 75.1% and 82.6%, while the maximum overall exergy efficiency values are 10.4% and 11.0%.

- For every 100 W/m^2 increase in irradiation level, improvement potential of PVT-NePCM system increases by 54.3 W.

- Increasing solar radiation intensity plays the major role in exergy destruction and entropy generation.

- Cooling period of PVT-NePCM system is 37.5% extended as compared with PVT only system.

5.2   Contribution of the Present Research

This research has some specific contributions in PVT and thermal storage research and development (R&D) works. The major three contributions can be enumerated as below:

1) Development of novel nanocomposite materials suited for solar thermal applications.

2) Remarkable thermal property enhancement using very low amount nanoparticles (MWNT) of the order 1/100th in wt% of the base material (PCM). This will substantially reduce the cost of nanocomposites.

3) Significant extension of heat availability period will facilitate night time usage of solar energy.

5.3 Recommendations for Future Work

In the present research, a novel NePCM based PVT system has been developed and its real-time performance is evaluated from both energy and exergy approach. The newly devised photovoltaic thermal system exhibited notable performance in reducing the cell temperature and enhancing the system efficiency as well. The following points might be considered in future work:

1) Newer nano composite materials may be synthesized for solar application, especially using eutectic PCMs and nano powdered metals.

2) Apart from integrating NePCMs on PV or PVT backside, isolated NePCM batteries may be developed to store large amount of heat harvested from the PV panel and improve the heat storage potential of the system.

3) Leakproof containment of PCM and NePCM in lightweight ampules and their operative integration with PV module still needs thorough focus.

4) In order to ensure effective heat removal from the module, heat transfer equipment such as microchannels or heat-pipe maybe used in conjunction with NePCM ampules.

5) The nighttime behavior of the PVT-NePCM system may be studied to see how these systems use radiant cooling at night to regenerate the NePCM.

REFERENCES

Abdelrahman, H. E., Wahba, M. H., Refaey, H. A., Moawad, M., and Berbish, N. S. (2019). Performance enhancement of photovoltaic cells by changing configuration and using PCM (RT35HC) with nanoparticles Al$_2$O$_3$. *Solar Energy, 177*: 665-671.

Aelenei, L., Pereira, R., Gonçalves, H., and Athienitis, A. (2014). Thermal Performance of a Hybrid BIPV-PCM: Modeling, Design and Experimental Investigation. *Energy Procedia, 48*: 474-483.

Akbarzadeh, A., and Wadowski, T. (1996). Heat pipe-based cooling systems for photovoltaic cells under concentrated solar radiation. *Applied Thermal Engineering, 16*(1): 81-87.

Akrami, E., Nemati, A., Nami, H., and Ranjbar, F. (2018). Exergy and exergoeconomic assessment of hydrogen and cooling production from concentrated PVT equipped with PEM electrolyzer and LiBr-H2O absorption chiller. *International Journal of Hydrogen Energy*, 43(2): 622-633.

Al-Waeli, A. H., Chaichan, M. T., Sopian, K., Kazem, H. A., Mahood, H. B., and Khadom, A. A. (2019). Modeling and experimental validation of a PVT system using nanofluid coolant and nano-PCM. *Solar Energy, 177*: 178-191.

Al-Waeli, A. H., Sopian, K., Chaichan, M. T., Kazem, H. A., Ibrahim, A., Mat, S., and Ruslan, M. H. (2017). Evaluation of the nanofluid and nano-PCM based photovoltaic thermal (PVT) system: An experimental study. *Energy Conversion and Management, 151*: 693-708.

Alizadeh, H., Ghasempour, R., Shafii, M. B., Ahmadi, M. H., Yan, W. M., and Nazari, M. A. (2018). Numerical simulation of PV cooling by using single turn pulsating heat pipe. *International Journal of Heat and Mass Transfer*, 127: 203-208.

Alkan, C., Sarı, A., Karaipekli, A., and Uzun, O. (2009). Preparation, characterization, and thermal properties of microencapsulated phase change material for thermal energy storage. *Solar Energy Materials and Solar Cells, 93*(1): 143-147.

Anderson, W. G., Dussinger, P. M., Sarraf, D. B., and Tamanna, S. *Heat pipe cooling of concentrating photovoltaic cells*. In 33rd IEEE Photovoltaic Specialists Conference (pp. 1-6). May 2008, IEEE.

Araki, K., Uozumi, H., and Yamaguchi, M. *A simple passive cooling structure and its heat analysis for 500/spl times/concentrator PV module.* Paper presented at the Conference Record of the 29th IEEE Photovoltaic Specialists Conferenc (pp. 1568-1571). May 2002, IEEE.

Aste, N., Chiesa, G., and Verri, F. (2008). Design, development and performance monitoring of a photovoltaic-thermal (PVT) air collector. *Renewable Energy*, *33*(5): 914-927.

Aste, N., Leonforte, F., and Del Pero, C. (2015). Design, modeling and performance monitoring of a photovoltaic–thermal (PVT) water collector. *Solar Energy*, *112*: 85-99.

Badescu, V. (2018). How much work can be extracted from diluted solar radiation? *Solar Energy, 170*: 1095-1100.

Bambrook, S. M., and Sproul, A. B. (2012). Maximising the energy output of a PVT air system. *Solar Energy*, *86*(6): 1857-1871.

Beach, R. T., and White, R. M. (1981). *Heat pipe for passive cooling of concentrator solar cells.* Paper presented at the 15th IEEE Photovoltaic Specialists Conference (pp. 75-80), IEEE.

Bergene, T., and Løvvik, O. M. (1995). Model calculations on a flat-plate solar heat collector with integrated solar cells. *Solar Energy*, *55*(6): 453-462.

Biwole, P. H., Eclache, P., and Kuznik, F. (2013). Phase-change materials to improve solar panel's performance. *Energy and Building, 62*: 59-67.

Borkar, D. S., Prayagi, S. V., and Gotmare, J. (2014). Performance evaluation of photovoltaic solar panel using thermoelectric cooling. *International Journal of Engineering Research*, *3*(9): 536-539.

Bosanac, M., Sorensen, B., Katic, I., Sorensen, H., Nielsen, B., and Badran, J. (2003). Photovoltaic/thermal solar collectors and their potential in Denmark. *Final Report EEP Project*, 1713, 00-0014.

Brano, V. L., Ciulla, G., Piacentino, A., and Cardona, F. (2014). Finite difference thermal model of a latent heat storage system coupled with a photovoltaic device: Description and experimental validation. *Renewable Energy, 68*: 181-193.

Brinkworth, B. J., Cross, B. M., Marshall, R. H., and Yang, H. (1997). Thermal regulation of photovoltaic cladding. *Solar Energy*, *61*(3): 169-178.

Brinkworth, B. J., Marshall, R. H., and Ibarahim, Z. (2000). A validated model of naturally ventilated PV cladding. *Solar Energy, 69*(1): 67-81.

Browne, M. C., Quigley, D., Hard, H. R., Gilligan, S., Ribeiro, N. C., Almeida, N., and McCormack, S. J. (2016). Assessing the thermal performance of phase change material in a photovoltaic/thermal system. *Energy Procedia*, *91*: 113-121.

Cabeza, L. F., Castell, A., Barreneche, C., De Gracia, A., and Fernández, A. I. (2011). Materials used as PCM in thermal energy storage in buildings: A review. *Renewable and Sustainable Energy Reviews, 15*(3): 1675-1695.

Cellura, M., Brano, V. L., and Marvuglia, A. (2008). *A Photovoltaic panel coupled with a phase changing material heat storage system in hot climates.* Paper presented at the 25th Conference on Passive and Low Energy Architecture, PLEA 2008, Dublin, Ireland.

Chen, J., Zhang, L., & Dai, Y. (2018). Performance analysis and multi-objective optimization of a hybrid photovoltaic/thermal collector for domestic hot water application. *Energy, 143*: 500-516.

Chen, P., Gao, X., Wang, Y., Xu, T., Fang, Y., and Zhang, Z. (2016). Metal foam embedded in SEBS/paraffin/HDPE form-stable PCMs for thermal energy storage. *Solar Energy Materials and Solar Cells, 149*: 60-65.

Chen, Y., Luo, W., Wang, J., and Huang, J. (2017). Enhanced Thermal Conductivity and Durability of a Paraffin Wax Nanocomposite Based on Carbon-Coated Aluminum Nanoparticles. *The Journal of Physical Chemistry C, 121*: 12603–12609.

Chen, Y., Zhang, Q., Wen, X., Yin, H., and Liu, J. (2018). A novel CNT encapsulated phase change material with enhanced thermal conductivity and photo-thermal conversion performance. *Solar Energy Materials and Solar Cells, 184*: 82-90.

Chieruzzi, M., Miliozzi, A., Crescenzi, T., Torre, L., and Kenny, J. M. (2015). A New Phase Change Material Based on Potassium Nitrate with Silica and Alumina Nanoparticles for Thermal Energy Storage. *Nanoscale Research Letters, 10*(1): 273.

Choi, D. H., Lee, J., Hong, H., and Kang, Y. T. (2014). Thermal conductivity and heat transfer performance enhancement of phase change materials (PCM) containing carbon additives for heat storage application. *International Journal of Refrigeration, 42*: 112-120.

Chow, T. T. (2010). A review on photovoltaic/thermal hybrid solar technology. *Applied Energy, 87*(2): 365-379.

Chow, T. T., Pei, G., Fong, K., Lin, Z., Chan, A., and Ji, J. (2009). Energy and exergy analysis of photovoltaic–thermal collector with and without glass cover. *Applied Energy, 86*(3): 310-316.

Clarke, J. A., Hand, J. W., Janak, M., Johnstone, C. M., and Strachan, P. A. (1998). PV-HYBRID-PAS Final report: modelling annex report 6 on simulation case study: Elsa Building, Ispra, Italy. *JOULE III, PASLINK EEIG contract JOR3-CT96-0092*.

Colla, L., Fedele, L., Mancin, S., Danza, L., and Manca, O. (2017). Nano-PCMs for enhanced energy storage and passive cooling applications. *Applied Thermal Engineering, 110*: 584–589.

Cooper, P. (1969). The absorption of radiation in solar stills. *Solar Energy, 12*(3): 333-346.

Cuce, E., and Cuce, P. M. (2014). Improving thermodynamic performance parameters of silicon photovoltaic cells via air cooling. *International Journal of Ambient Energy*, 35(4): 193-199.

Cui, T., Xuan, Y., and Li, Q. (2016). Design of a novel concentrating photovoltaic–thermoelectric system incorporated with phase change materials. *Energy Conversion and Management, 112*: 49-60.

Cui, Y., Liu, C., Hu, S., and Yu, X. (2011). The experimental exploration of carbon nanofiber and carbon nanotube additives on thermal behavior of phase change materials. *Solar Energy Materials and Solar Cells, 95*(4): 1208-1212.

Demirbas, M. F. (2006). Thermal energy storage and phase change materials: An overview. *Energy Sources, Part B: Economics, Planning, and Policy, 1*(1): 85-95.

Dorobanțu, L., Popescu, M. O., Popescu, C. L., & Crăciunescu, A. *Experimental assessment of PV panels front water cooling strategy*. In International Conference on Renewable Energies and Power Quality, ICREPQ'13 (pp. 2172-038), March 20 – 22, 2013, Bilbao, Spain.

Ebbesen, T. W., Lezec, H. J., Hiura, H., Bennett, J. W., Ghaemi, H. F., and Thio, T. (1996). Electrical conductivity of individual carbon nanotubes. *Nature, 382*(6586): 54-56.

Eisapour, M., Eisapour, A. H., Hosseini, M., and Talebizadehsardari, P. (2020). Exergy and energy analysis of wavy tubes photovoltaic-thermal systems using microencapsulated PCM nano-slurry coolant fluid. *Applied Energy, 266*: 114849.

El Khadraoui, A., Bouadila, S., Kooli, S., Guizani, A., and Farhat, A. (2016). Solar air heater with phase change material: An energy analysis and a comparative study. *Applied Thermal Engineering*, 107: 1057-1064.

Elmir, M., Mehdaoui, R., and Mojtabi, A. (2012). Numerical simulation of cooling a solar cell by forced convection in the presence of a nanofluid. *Energy Procedia, 18*: 594-603.

Elsafi, A. M., and Gandhidasan, P. (2015). Comparative study of double-pass flat and compound parabolic concentrated photovoltaic–thermal systems with and without fins. *Energy Conversion and Management*, *98*: 59-68.

Fayaz, H., Nasrin, R., Rahim, N. A., and Hasanuzzaman, M. (2018). Energy and exergy analysis of the PVT system: Effect of nanofluid flow rate. *Solar Energy*, *169*: 217-230.

Fayaz, H., Rahim, N. A., Hasanuzzaman, M., Rivai, A., and Nasrin, R. (2019). Numerical and outdoor real time experimental investigation of performance of PCM based PVT system. *Solar Energy, 179*: 135-150.

Feldman Jr, K. T., Kenney, D. D., and Edenburn, M. W. *A passive heat pipe cooled photovoltaic receiver*. Paper presented at the 15th Photovoltaic Specialists Conference (pp. 165-172), May 12 – 15, 1981, IEEE, Kissimmee, Florida, USA.

Florschuetz, L. (1979). Extension of the Hottel-Whillier model to the analysis of combined photovoltaic/thermal flat plate collectors. *Solar Energy, 22*(4): 361-366.

Florschuetz, L. W. *On heat rejection from terrestrial solar cell arrays with sunlight concentration.* Paper presented at the 11th Photovoltaic Specialists Conference, May 6 – 8, 1975, IEEE, Scottsdale, Arizona, USA .

Fudholi, A., Zohri, M., Jin, G. L., Ibrahim, A., Yen, C. H., Othman, M. Y., . . . Sopian, K. (2018). Energy and exergy analyses of photovoltaic thermal collector with∇-groove. *Solar Energy, 159*: 742-750.

Gao, D., and Deng, T. (2013). Energy storage: Preparations and physicochemical properties of solid-liquid Phase change materials for thermal energy storage. *Material Process Energy Communication: Current Research Technology Development*, *1*: 32-44.

Garg, H. P., and Adhikari, R. S. (1997). Conventional hybrid photovoltaic/thermal (PV/T) air heating collectors: steady-state simulation. *Renewable Energy, 11*(3): 363-385.

Garg, H. P., and Adhikari, R. S. (1998). Transient simulation of conventional hybrid photovoltaic/thermal (PV/T) air heating collectors. *International Journal of Energy Research, 22*(6): 547-562.

Garg, H. P., and Adhikari, R. S. (1999). System performance studies on a photovoltaicithermal (PV/T) air heating collector. *Renewable Energy, 16*(1-4): 725-730.

Garg, H. P., and Agarwal, R. K. (1995). Some aspects of a PV/T collector/forced circulation flat plate solar water heater with solar cells. *Energy Conversion and Management, 36*(2): 87-99.

Garg, H. P., Agarwal, R. K., and Joshi, J. C. (1994). Experimental study on a hybrid photovoltaic-thermal solar water heater and its performance predictions. *Energy Conversion and Management, 35*(7): 621-633.

Gaur, A., Ménézo, C., and Giroux, S. (2017). Numerical studies on thermal and electrical performance of a fully wetted absorber PVT collector with PCM as a storage medium. *Renewable Energy, 109*: 168-187.

Ghadiri, M., Sardarabadi, M., Pasandideh-fard, M., and Moghadam, A. J. (2015). Experimental investigation of a PVT system performance using nano ferrofluids. *Energy Conversion and Management, 103*: 468-476.

Groenewoud, W. M. (2001). *Chapter 1: Differential scanning calorimetry - characterisation of polymers by thermal analysis* (pp. 10-60). Amsterdam, Netherlands: Elsevier Science B.V.

Guarracino, I., Freeman, J., Ramos, A., Kalogirou, S. A., Ekins-Daukes, N. J., and Markides, C. N. (2019). Systematic testing of hybrid PV-thermal (PVT) solar

collectors in steady-state and dynamic outdoor conditions. *Applied Energy, 240*: 1014-1030.

Gustafsson, S. E. (1991). Transient plane source techniques for thermal conductivity and thermal diffusivity measurements of solid materials. *Review of Scientific Instruments, 62*: 797–804.

Hajare, V. S., and Gawali, B. S. (2015). Experimental study of latent heat storage system using nano-mixed phase change material. *International Journal of Engineering Technology Management and Applied Science*, 3(8): 37-44.

Hajare, V. S., Narode, A. R., Gawali, B. S., & Bamane, S. R. (2014). Experimental investigation of enhancement in heat transfer using nano-mixed PCM. *International Journal of Engineering Research & Technology*, 3(11): 843-848.

Harish, S., Orejon, D., Takata, Y., and Kohno, M. (2015). Thermal conductivity enhancement of lauric acid phase change nanocomposite with graphene nanoplatelets. *Applied Thermal Engineering, 80*: 205-211.

Hasan, A., McCormack, S. J., Huang, M. J., and Norton, B. (2010). Evaluation of phase change materials for thermal regulation enhancement of building integrated photovoltaics. *Solar Energy, 84*(9): 1601-1612.

Hasan, A., McCormack, S. J., Huang, M. J., and Norton, B. (2014a). Characterization of phase change materials for thermal control of photovoltaics using Differential Scanning Calorimetry and Temperature History Method. *Energy Conversion Management, 81*: 322-329.

Hasan, A., McCormack, S. J., Huang, M. J., and Norton, B. (2014b). Energy and cost saving of a photovoltaic-phase change materials (PV-PCM) system through temperature regulation and performance enhancement of photovoltaics. *Energies, 7*(3): 1318-1331.

Hasan, A., McCormack, S. J., Huang, M. J., Sarwar, J., and Norton, B. (2015). Increased photovoltaic performance through temperature regulation by phase change materials: Materials comparison in different climates. *Solar Energy, 115*: 264-276.

Hassan, A., Nouman, H., Assi, A., and Norton, B. (2014,). *Temperature Regulation and Thermal Energy Storage Potential of Phase Change Materials Layer Contained at the Back of a Building Integrated Photovoltaic Panel.* Paper presented at the 30th International PLEA 2014 Conference, CEPT University, Ahmedabad.

Häusler, T., and Rogaß, H. (1998). *Photovoltaic Module with Latent Heat-Storage-Collector*. Proceedings of 2nd World Conference on Photovoltaic Solar Energy Conversion, vol. 1, 6 - 10 July 1998, Vienna, Austria.

Hazami, M., Riahi, A., Mehdaoui, F., Nouicer, O., and Farhat, A. (2016). Energetic and exergetic performances analysis of a PV/T (photovoltaic thermal) solar system tested and simulated under to Tunisian (North Africa) climatic conditions. *Energy, 107*: 78-94.

He, Y. (2005). Rapid thermal conductivity measurement with a hot disk sensor: Part 1. Theoretical considerations. *Thermochimica Acta, 436*(1): 122-129.

Hendricks, J. H. C., and Van Sark, W. G. J. H. M. (2013). Annual performance enhancement of building integrated photovoltaic modules by applying phase change materials. *Progress in Photovoltaics: Research and Applications*, *21*(4): 620-630.

Hendrie, S. D. (1979). *Evaluation of combined photovoltaic/thermal collectors.* Paper presented at the International Solar Energy Society Meeting (No. COO-4577-8; CONF-790541-54), Lincoln Lab, Massachusetts Institute. of Technology, Atlanta, USA.

Ho, C. J., Chou, W. L., and Lai, C. M. (2015). Thermal and electrical performance of a water-surface floating PV integrated with a water-saturated MEPCM layer. *Energy Conversion and Management, 89*: 862-872.

Ho, C. J., and Gao, J. Y. (2009). Preparation and thermophysical properties of nanoparticle-in-paraffin emulsion as phase change material. *International Communications in Heat and Mass Transfer, 36*(5): 467-470.

Ho, C. J., Jou, B. T., Lai, C. M., and Huang, C. Y. (2013). Performance assessment of a BIPV integrated with a layer of water-saturated MEPCM. *Energy and Buildings, 67*: 322-333.

Horne, W. (1993). Solar energy system, patent US5269851. In: USA.

Hossain, M., Pandey, A., Selvaraj, J., Rahim, N. A., Islam, M., and Tyagi, V. (2019). Two side serpentine flow based photovoltaic-thermal-phase change materials (PVT-PCM) system: Energy, exergy and economic analysis. *Renewable Energy, 136*: 1320-1336.

Hossain, M., Pandey, A., Selvaraj, J., Rahim, N. A., Rivai, A., and Tyagi, V. J. (2019). Thermal performance analysis of parallel serpentine flow based photovoltaic/thermal (PV/T) system under composite climate of Malaysia. *Applied Thermal* Engineering,*153*: 861-871.

Hosseinzadeh, M., Sardarabadi, M., and Passandideh-Fard, M. (2018). Energy and exergy analysis of nanofluid based photovoltaic thermal system integrated with phase change material. *Energy, 147*: 636-647.

Huang, M., Eames, P., and Norton, B. (2007). Comparison of predictions made using a new 3D phase change material thermal control model with experimental measurements and predictions made using a validated 2D model. *Heat Transfer Engineering, 28*(1): 31-37.

Huang, M. J. (2011). The effect of using two PCMs on the thermal regulation performance of BIPV systems. *Solar Energy Material and Solar Cells, 95*(3): 957-963.

Huang, M. J., Eames, P. C., and Norton, B. (2004). Thermal regulation of building-integrated photovoltaics using phase change materials. *International Journal of Heat Mass Transfer, 47*(12–13): 2715-2733.

Huang, M. J., Eames, P. C., and Norton, B. (2006). Phase change materials for limiting temperature rise in building integrated photovoltaics. *Solar Energy, 80*(9): 1121-1130.

Huang, M. J., Eames, P. C., Norton, B., and Hewitt, N. J. (2011). Natural convection in an internally finned phase change material heat sink for the thermal management of photovoltaics. *Solar Energy Material and Solar Cells, 95*(7): 1598-1603.

Huang, M. J. (2011). The effect of using two PCMs on the thermal regulation performance of BIPV systems. *Solar Energy Materials and Solar Cells*, 95(3): 957-963.

Huang, X., Lin, Y., Alva, G., and Fang, G. (2017). Thermal properties and thermal conductivity enhancement of composite phase change materials using myristyl alcohol/metal foam for solar thermal storage. *Solar Energy Materials and Solar Cells, 170*: 68–76.

Ibrahim, A., Othman, M. Y., Ruslan, M. H., Alghoul, M., Yahya, M., Zaharim, A., and Sopian, K. (2009). Performance of photovoltaic thermal collector (PVT) with different absorbers design. *WSEAS Transactions on Environment and Development*, 5(3): 321-330.

Ivanov, S. (2012). *Multiferroic complex metal oxides: main features of preparation, structure, and properties*. Science and Technology of Atomic, Molecular, Condensed Matter & Biological Systems (vol. 2), 163-238, Elsevier B.V.

Javani, N., Dincer, I., and Naterer, G. F. (2014). New latent heat storage system with nanoparticles for thermal management of electric vehicles. *Journal of Power Sources, 268*: 718-727.

Jing, D., Hu, Y., Liu, M., Wei, J., and Guo, L. (2015). Preparation of highly dispersed nanofluid and CFD study of its utilization in a concentrating PV/T system. *Solar Energy, 112*: 30-40.

Kabeel, A. E., Khalil, A., Shalaby, S. M., and Zayed, M. E. (2017). Improvement of thermal performance of the finned plate solar air heater by using latent heat thermal storage. *Applied Thermal Engineering, 123*: 546-553.

Kalogirou, S. A., and Tripanagnostopoulos, Y. (2006). Hybrid PV/T solar systems for domestic hot water and electricity production. *Energy Conversion and Management, 47*: 3368–3382.

Kane, A., Verma, V., and Singh, B. (2017). Optimization of thermoelectric cooling technology for an active cooling of photovoltaic panel. *Renewable and Sustainable Energy Reviews*, 75: 1295-1305.

Kant, K., Anand, A., Shukla, A., and Sharma, A. (2020). Heat transfer study of building integrated photovoltaic (BIPV) with nano-enhanced phase change materials. *Journal of Energy Storage*, *30*: 101563.

Kant, K., Shukla, A., Sharma, A., and Henry Biwole, P. (2017). Heat transfer study of phase change materials with graphene nano particle for thermal energy storage. *Solar Energy*, *146*: 453-463.

Karaipekli, A., Biçer, A., Sarı, A., and Tyagi, V. V. (2017). Thermal characteristics of expanded perlite/paraffin composite phase change material with enhanced thermal conductivity using carbon nanotubes. *Energy Conversion and Management*, *134*: 373-381.

Karami, N., and Rahimi, M. (2014). Heat transfer enhancement in a PV cell using Boehmite nanofluid. *Energy Conversion Management, 86*: 275-285.

Karthik, M., Faik, A., Blanco-Rodríguez, P., Rodríguez-Aseguinolaza, J., and D'Aguanno, B. (2015). Preparation of erythritol–graphite foam phase change composite with enhanced thermal conductivity for thermal energy storage applications. *Carbon*, *94*: 266-276.

Kazemian, A., Taheri, A., Sardarabadi, A., Ma, T., Passandideh-Fard, M., and Peng, J. (2020). Energy, exergy and environmental analysis of glazed and unglazed PVT system integrated with phase change material: An experimental approach. *Solar Energy*, *201*: 178-189.

Kenisarin, M., and Mahkamov, K. (2007). Solar energy storage using phase change materials. *Renewable and Sustainable Energy Review*, *11*(9): 1913-1965.

Kern Jr, E. C., and Russell, M. C. (1978). *Combined photovoltaic and thermal hybrid collector systems*. IEEE photovoltaic specialists conference, 5 Jun 1978, Washington DC, USA.

Khalid, S. I. (2013). Carbon nanotubes–properties and applications: a review. *Carbon Letters*, *14*(3), 131-144

Khodadadi, J. M., and Hosseinizadeh, S. F. (2007). Nanoparticle-enhanced phase change materials (NEPCM) with great potential for improved thermal energy storage. *International Communications in Heat and Mass Transfer*, *34*(5): 534-543.

Kim, P., Shi, L., Majumdar, A., and McEuen, P. L. (2001). Thermal transport measurements of individual multiwalled nanotubes. *Physical Review Letters*, *87*(21): 215502.

Kline, S. J. (1953). Describing uncertainty in single sample experiments. *Journal of Mechanical Engineering, 75*: 3-8.

Kumar, A., Baredar, P., and Qureshi, U. (2015). Historical and recent development of photovoltaic thermal (PVT) technologies. *Renewable and Sustainable Energy Review*, *42*: 1428-1436.

Kumar, L., Hasanuzzaman, M., Rahim, N., and Islam, M. (2021). Modeling, simulation and outdoor experimental performance analysis of a solar-assisted process heating system for industrial process heat. *Renewable Energy*, *164*: 656-673.

Lee, H. J., Cho, M. K., Jo, Y. Y., Lee, K. S., Kim, H. J., Cho, E., . . . Jang, J. H. (2012). Application of TGA techniques to analyze the compositional and structural degradation of PEMFC MEAs. *Polymer Degradation and Stability*, *97*(6): 1010-1016.

Li, M. (2013). A nano-graphite/paraffin phase change material with high thermal conductivity. *Applied Energy*, *106*: 25-30.

Li, M., Zhong, D., Ma, T., Kazemian, A., and Gu, W. (2020). Photovoltaic thermal module and solar thermal collector connected in series: Energy and exergy analysis. *Energy Conversion and Management*, *206*: 112479.

Li, Y., Li, J., Deng, Y., Guan, W., Wang, X., and Qian, T. (2016). Preparation of paraffin/porous TiO_2 foams with enhanced thermal conductivity as PCM, by covering the TiO_2 surface with a carbon layer. *Applied Energy*, *171*: 37-45.

Li, Y., Witharana, S., Cao, H., Lasfargues, M., Huang, Y., and Ding, Y. (2014). Wide spectrum solar energy harvesting through an integrated photovoltaic and thermoelectric system. *Particuology*, *15*: 39-44.

Li, Z., Ahmed, S., and Ma, T. (2021). Investigating the Effect of Radiative Cooling on the Operating Temperature of Photovoltaic Modules. *Solar RRL*, 5(4): 2000735.

Li, Z., Ma, T., Zhao, J., Song, A., and Cheng, Y. (2019). Experimental study and performance analysis on solar photovoltaic panel integrated with phase change material. *Energy*, *178*: 471-486.

Lillo, B. I., Silva, P. M., and Larraneta, G. C. M. (2011). *Use of phase change materials in photovoltaic modules with solar concentration of up to 2X.* In European Photovoltaic Solar Energy Conference and Exhibition (EUPVCEC), pp. 634-639, Hamburg, Germany.

Ling, Z., Chen, J., Xu, T., Fang, X., Gao, X., and Zhang, Z. (2015). Thermal conductivity of an organic phase change material/expanded graphite composite across the phase change temperature range and a novel thermal conductivity model. *Energy Conversion and Management*, *102*: 202-208.

Lo, B. V., Ciulla, G., Piacentino, A., and Cardona, F. (2013). On the efficacy of PCM to shave peak temperature of crystalline photovoltaic panels: an FDM model and field validation. *Energies*, *6*(12): 6188-6210.

Luque, A., Sala, G., Arboiro, J. C., Bruton, T., Cunningham, D., and Mason, N. (1997). Some results of the EUCLIDES photovoltaic concentrator prototype. *Progress in Photovoltaics: Research and Applications*, *5*(3): 195-212.

Luque, A., Sala, G., and Arboiro, J. C. (1998). Electric and thermal model for non-uniformly illuminated concentration cells. *Solar Energy Materials and Solar Cells*, *51*(3): 269-290.

Machniewicz, A., Knera, D., and Heim, D. (2015). Effect of Transition Temperature on Efficiency of PV/PCM Panels. *Energy Procedia*, *78*: 1684-1689.

Mahian, O., Kianifar, A., Kalogirou, S. A., Pop, I., and Wongwises, S. (2013). A review of the applications of nanofluids in solar energy. *International Journal of Heat and Mass Transfer*, *57*(2): 582-594.

Mahmoud, S., Tang, A., Toh, C., Al-Dadah, R., and Soo, S. L. (2013). Experimental investigation of inserts configurations and PCM type on the thermal performance of PCM based heat sinks. *Applied Energy*, *112*: 1349-1356.

Maiti, S., Banerjee, S., Vyas, K., Patel, P., & Ghosh, P. K. (2011). Self regulation of photovoltaic module temperature in V-trough using a metal–wax composite phase change matrix. *Solar Energy*, *85*(9): 1805-1816.

Malvi, C. S., Dixon-Hardy, D. W., and Crook, R. (2011). Energy balance model of combined photovoltaic solar-thermal system incorporating phase change material. *Solar Energy*, *85*(7): 1440-1446.

Matuska, T. (2012). Simulation study of building integrated solar liquid PV-T collectors. *International Journal of Photoenergy*, *2012*: 1-8.

Mazón-Hernández, R., García-Cascales, J. R., Vera-García, F., Káiser, A. S., and Zamora, B. (2013). Improving the Electrical Parameters of a Photovoltaic Panel by Means of an Induced or Forced Air Stream. *International Journal of Photoenergy*, 2013: 1-10.

Mehmet Ö. Z., Mutlucan B., and Ulukaya, C. (2017). *Exergetic Improvement Potential Analysis of a Solar Photovoltaic Module Considering Irreversibilities and Loses.* 9th International Exergy, Energy and Environment Symposium (IEEES-9), Split, Croatia.

Mehrotra, S., Rawat, P., Debbarma, M., and Sudhakar, K. (2014). Performance of A Solar panel with Water Immersion Cooling Technique. *International Journal of Science Environment and Technology*, *3*: 1161-1172.

MetMalaysia. (2020). *MET Malaysia Annual Report 2019*. Retrieved from Malaysia: https://www.met.gov.my/content/pdf/penerbitan/laporantahunan/laporantahunan2019.pdf

Mills, A., Farid, M., Selman, J. R., and Al-Hallaj, S. (2006). Thermal conductivity enhancement of phase change materials using a graphite matrix. *Applied Thermal Engineering*, *26*(14): 1652-1661.

Mishra, R. K., and Tiwari, G. N. (2013). Energy and exergy analysis of hybrid photovoltaic thermal water collector for constant collection temperature mode. *Solar Energy*, *90*, 58-67.

Moharram, K. A., Abd-Elhady, M. S., Kandil, H. A., and El-Sherif, H. (2013). Enhancing the performance of photovoltaic panels by water cooling. *Ain Shams Engineering Journal*, *4*(4): 869-877.

Moshfegh, B., and Sandberg, M. (1998). Flow and heat transfer in the air gap behind photovoltaic panels. *Renewable and Sustainable Energy Review*, *2*(3): 287-301.

Mozes, G. (1982). *Paraffin Products: Properties, Technologies, Applications. Developments in Petroleum Science*: Elsevier Scientific Publishing Co., New York, USA.

Murugan, P., Ganesh K. P., Kumaresan, V., Meikandan, M., Malar M., K., and Velraj, R. (2018). Thermal energy storage behaviour of nanoparticle enhanced PCM during freezing and melting. *Phase Transitions*, 91(3): 254-270.

Nagano, K., Mochida, T., Iwata, K., Hiroyoshi, H., and Domanski, R. (2000). *Thermal performance of Mn(NO₃)₂·6H₂O as a new PCM for cooling system.* 5th Workshop of the IEA ECES IA Annex

Nagano, K., Mochida, T., Takeda, S., Domański, R., and Rebow, M. (2003). Thermal characteristics of manganese (II) nitrate hexahydrate as a phase change material for cooling systems. *Applied Thermal Engineering*, *23*(2): 229-241.

Nahar, A., Hasanuzzaman, M., and Rahim, N. A. (2017). Numerical and experimental investigation on the performance of a photovoltaic thermal collector with parallel plate flow channel under different operating conditions in Malaysia. *Solar Energy*, *144*: 517-528.

Najafi, H., and Woodbury, K. A. (2013). Optimization of a cooling system based on Peltier effect for photovoltaic cells. *Solar Energy*, *91*: 152-160.

Nasrin, R., Rahim, N. A., Fayaz, H., and Hasanuzzaman, M. (2018). Water/MWCNT nanofluid based cooling system of PVT: Experimental and numerical research. *Renewable Energy*, *121*: 286-300.

Natarajan, S. K., Mallick, T. K., Katz, M., and Weingaertner, S. (2011). Numerical investigations of solar cell temperature for photovoltaic concentrator system with and without passive cooling arrangements. *International Journal of Thermal Sciences*, *50*(12): 2514-2521.

Ngo, C. L., Le, Q. T., Ngo, T. T., Nguyen, D. N., and Vu, M. T. (2013). Surface modification and functionalization of carbon nanotube with some organic compounds. Advances in Natural Sciences: *Nanoscience and Nanotechnology*, *4*(3): 035017.

Oró, E., Barreneche, C., Farid, M. M., and Cabeza, L. F. (2013). Experimental study on the selection of phase change materials for low temperature applications. *Renewable Energy*, *57*: 130-136.

Pakrouh, R., Hosseini, M. J., and Ranjbar, A. A. (2015). A parametric investigation of a PCM-based pin fin heat sink. *Mechanical Sciences*, *6*(1): 65-73.

Park, S. R., Pandey, A. K., Tyagi, V. V., and Tyagi, S. K. (2014). Energy and exergy analysis of typical renewable energy systems. *Renewable and Sustainable Energy Reviews*, *30*: 105-123.

Pielichowska, K., and Pielichowski, K. (2014). Phase change materials for thermal energy storage. *Progress in Materials Science*, *65*: 67-123.

Qian, T., Li, J., Min, X., Guan, W., Deng, Y., and Ning, L. (2015). Enhanced thermal conductivity of PEG/diatomite shape-stabilized phase change materials with Ag nanoparticles for thermal energy storage. *Journal of Materials Chemistry A*, *3*: 8526-8536.

Qiu, L., Ouyang, Y., Feng, Y., and Zhang, X. (2019). Review on micro/nano phase change materials for solar thermal applications. *Renewable Energy*, *140*: 513-538.

Qiu, Z., Ma, X., Zhao, X., Li, P., and Ali, S. (2016). Experimental investigation of the energy performance of a novel Micro-encapsulated Phase Change Material (MPCM) slurry based PV/T system. *Applied Energy*, *165*: 260-271.

Qiu, Z., Zhao, X., Li, P., Zhang, X., Ali, S., and Tan, J. (2015). Theoretical investigation of the energy performance of a novel MPCM (Microencapsulated Phase Change Material) slurry based PV/T module. *Energy*, *87*: 686-698.

Radziemska, E. (2003a). The effect of temperature on the power drop in crystalline silicon solar cells. *Renewable Energy*, *28*: 1-12.

Radziemska, E. (2003b). The effect of temperature on the power drop in crystalline silicon solar cells. *Renewable Energy*, *28*(1): 1-12.

Rahman, M. M., Hasanuzzaman, M., and Rahim, N. A. (2015). Effects of various parameters on PV-module power and efficiency. *Energy Conversion and Management*, *103*: 348-358.

Reddy, K. S., Lokeswaran, S., Agarwal, P., and Mallick, T. K. (2014). Numerical investigation of micro-channel based active module cooling for solar CPV system. *Energy Procedia*, *54*: 400-416.

Rejeb, O., Sardarabadi, M., Ménézo, C., Passandideh-Fard, M., Dhaou, M. H., and Jemni, A. (2016). Numerical and model validation of uncovered nanofluid sheet and tube type photovoltaic thermal solar system. *Energy Conversion and Management*, *110*: 367-377.

Rodgers, P., & Eveloy, V. (2013). *An integrated thermal management solution for flat-type solar photovoltaic modules.* 14th International Conference on Thermal, Mechanical and Multi-Physics Simulation and Experiments in Microelectronics and Microsystems (EuroSimE), (pp. 1-7) IEEE.

Rosen, M. A., Tang, R., and Dincer, I. (2004). Effect of stratification on energy and exergy capacities in thermal storage systems. *International Journal of Energy Research*, *28*(2): 177–193.

Royne, A., and Dey, C. J. (2007). Design of a jet impingement cooling device for densely packed PV cells under high concentration. *Solar Energy*, *81*(8): 1014-1024.

Rubitherm. (2020). RT44HC Data Sheet. Retrieved from https://www.rubitherm.eu/media/products/datasheets/Techdata_-RT44HC_EN_09102020.PDF

Safi, T. S., and Munday, J. N. (2015). Improving photovoltaic performance through radiative cooling in both terrestrial and extraterrestrial environments. *Optics Express*, *23*(19): A1120-A1128..

Şahan, N., Fois, M., and Paksoy, H. (2015). Improving thermal conductivity phase change materials—A study of paraffin nanomagnetite composites. *Solar Energy Materials and Solar Cells*, *137*: 61-67.

Saito, T., Matsushige, K., and Tanaka, K. (2002). Chemical treatment and modification of multi-walled carbon nanotubes. *Physica B: Condensed Matter*, *323*(1-4): 280-283.

Sardarabadi, M., Hosseinzadeh, M., Kazemian, A., and Passandideh-Fard, M. (2017). Experimental investigation of the effects of using metal-oxides/water nanofluids on a photovoltaic thermal system (PVT) from energy and exergy viewpoints. *Energy*, *138*: 682-695.

Sardarabadi, M., Passandideh-Fard, M., and Heris, S. Z. (2014). Experimental investigation of the effects of silica/water nanofluid on PV/T (photovoltaic thermal units). *Energy*, *66*: 264-272.

Sardarabadi, M., and Passandideh-Fard, M. (2016). Experimental and numerical study of metal-oxides/water nanofluids as coolant in photovoltaic thermal systems (PVT). *Solar Energy Materials and Solar Cells*, *157*: 533-542.

Sari, A., Bicer, A., Al-Sulaiman, F., Karaipekli, A., and Tyagi, V. (2018). Diatomite/CNTs/PEG composite PCMs with shape-stabilized and improved thermal conductivity: Preparation and thermal energy storage properties. *Energy and Buildings*, *164*: 166-175.

Sari, A., and Kaygusuz, K. (2002). Thermal performance of a eutectic mixture of lauric and stearic acids as PCM encapsulated in the annulus of two concentric pipes. *Solar Energy*, *72*(6): 493-504.

Sharma, A., and Shukla, A. (2015). Thermal cycle test of binary mixtures of some fatty acids as phase change materials for building applications. *Energy and Buildings*, *99*: 196-203.

Sharma, A., Tyagi, V. V., Chen, C. R., and Buddhi, D. (2009). Review on thermal energy storage with phase change materials and applications. *Renewable and Sustainable Energy Reviews*, *13*(2): 318-345.

Sharma, R. K., Ganesan, P., Tyagi, V. V., and Mahlia, T. M. I. (2016). Accelerated thermal cycle and chemical stability testing of polyethylene glycol (PEG) 6000 for solar thermal energy storage. *Solar Energy Materials and Solar Cells*, *147*: 235-239.

Sharma, S., Tahir, A., Reddy, K. S., and Mallick, T. K. (2016). Performance enhancement of a Building-Integrated Concentrating Photovoltaic system using phase change material. *Solar Energy Materials and Solar Cells*, *149*: 29-39.

Silakhori, M., Naghavi, M. S., Metselaar, H. S. C., Mahlia, T. M. I., Fauzi, H., and Mehrali, M. (2013). Accelerated thermal cycling test of microencapsulated paraffin wax/polyaniline made by simple preparation method for solar thermal energy storage. *Materials*, *6*(5): 1608-1620.

Solar Master (2020) Hybrid PVT solar panel, https://www.solarmastertech.com/

Sopian, K., Liu, H. T., Kakac, S., and Veziroglu, T. N. (2000). Performance of a double pass photovoltaic thermal solar collector suitable for solar drying systems. *Energy Conversion and Management*, *41*(4): 353-365.

Sopian, K., Yigit, K. S., Liu, H. T., Kakac, S., and Veziroglu, T. N. (1996). Performance analysis of photovoltaic thermal air heaters. *Energy Conversion and Management*, *37*(11): 1657-1670.

Stultz, J. W., and Wren, L. C. (1978). *Thermal performance testing and analysis of photovoltaic modules in natural sunlight*. Retrieved from LSA Task Report 5101, (pp. 31), Jet Propulsion Laboratory: Pasadena,California, USA.

Sun, Y., Wang, Y., Zhu, L., Yin, B., Xiang, H., and Huang, Q. (2014). Direct liquid-immersion cooling of concentrator silicon solar cells in a linear concentrating photovoltaic receiver. *Energy*, 65: 264-271.

Taylor, J. (1997). *Introduction to error analysis, the study of uncertainties in physical measurements*. 2nd ed., University Science Books, New York, USA.

Telkes, M. (1980). Thermal energy storage in salt hydrates. *Solar Energy Materials*, *2*(4): 381-393.

Teo, H. G., Lee, P. S., and Hawlader, M. N. A. (2012). An active cooling system for photovoltaic modules. *Applied Energy*, *90*(1): 309-315.

Tina, G. M., Rosa-Clot, M., Rosa-Clot, P., and Scandura, P. F. (2012). Optical and thermal behavior of submerged photovoltaic solar panel: SP2. *Energy*, *39*(1): 17-26.

Tiwari, A., and Sodha, M. S. (2006). Performance evaluation of solar PV/T system: An experimental validation. *Solar Energy*, *80*(7): 751-759.

Tiwari, A., Sodha, M. S., Chandra, A., and Joshi, J. C. (2006). Performance evaluation of photovoltaic thermal solar air collector for composite climate of India. *Solar Energy Materials and Solar Cells*, *90*(2): 175-189.

Treacy, M. J., Ebbesen, T. W., and Gibson, J. M. (1996). Exceptionally high Young's modulus observed for individual carbon nanotubes. *Nature*, *381*(6584): 678-680.

Tripanagnostopoulos, Y. (2007). Aspects and improvements of hybrid photovoltaic/thermal solar energy systems. *Solar Energy*, *81*(9): 1117-1131.

Tripanagnostopoulos, Y., Souliotis, M., Battisti, R., and Corrado, A. (2006). Performance, cost and life-cycle assessment study of hybrid PVT/AIR solar systems. *Progress in Photovoltaics: Research and applications*, *14*(1): 65-76.

Trisaksri, V., and Wongwises, S. (2007). Critical review of heat transfer characteristics of nanofluids. *Renewable and Sustainable Energy Review*, *11*(3): 512-523.

Tyagi, V., Panwar, N., Rahim, N., and Kothari, R. (2012). Review on solar air heating system with and without thermal energy storage system. *Renewable and Sustainable Energy Review, 16*(4): 2289-2303.

Tyagi, V. V., and Buddhi, D. (2008). Thermal cycle testing of calcium chloride hexahydrate as a possible PCM for latent heat storage. *Solar Energy Materials and Solar Cells*, *92*(8): 891-899.

Tyagi, V. V., Pandey, A. K., Giridhar, G., Bandyopadhyay, B., Park, S. R., and Tyagi, S. K. (2012a). Comparative study based on exergy analysis of solar air heater collector using thermal energy storage. *International Journal of Energy Research*, *36*(6): 724-736.

Valeh-e-Sheyda, P., Rahimi, M., Parsamoghadam, A., and Masahi, M. M. (2014). Using a wind-driven ventilator to enhance a photovoltaic cell power generation. *Energy and Buildings*, 73: 115-119.

van Helden, W. G. J., van Zolingen, R. J. C., and Zondag, H. A. (2004). PV Thermal Systems: PV Panels Supplying Renewable Electricity and Heat. *Progress in Photovoltaics: Research and Applications*, *12*: 415–426.

Vera, J. T., Laukkanen, T., and Sirén, K. (2014). Performance evaluation and multi-objective optimization of hybrid photovoltaic–thermal collectors. *Solar Energy*, *102*: 223-233.

Wang, C., Lin, T., Li, N., and Zheng, H. (2016). Heat transfer enhancement of phase change composite material: Copper foam/paraffin. *Renewable Energy*, *96*: 960-965.

Wang, F., Zhang, C., Liu, J., Fang, X., and Zhang, Z. (2017). Highly stable graphite nanoparticle-dispersed phase change emulsions with little supercooling and high thermal conductivity for cold energy storage. *Applied Energy*, *188*: 97-106.

Wang, J., Xie, H., Xin, Z., Li, Y., and Chen, L. (2010). Enhancing thermal conductivity of palmitic acid based phase change materials with carbon nanotubes as fillers. *Solar Energy, 84*(2): 339-344.

Wolf, M. (1976). Performance analyses of combined heating and photovoltaic power systems for residences. *Energy Conversion and Management*, *16*(1): 79-90.

Wu, S., & Xiong, C. (2014). Passive cooling technology for photovoltaic panels for domestic houses. *International Journal of Low-Carbon Technologies*, *9*(2): 118-126.

Wu, S., Zhu, D., Zhang, X., and Huang, J. (2010). Preparation and Melting/Freezing Characteristics of Cu/Paraffin Nanofluid as Phase-Change Material (PCM). *Energy & Fuels*, *24*: 1894–1898.

Xiang, H., Wang, Y., Zhu, L., Han, X., Sun, Y., and Zhao, Z. (2012). 3D numerical simulation on heat transfer performance of a cylindrical liquid immersion solar receiver. *Energy Conversion and Management*, *64*: 97-105.

Xiao, X., Zhang, P., and Li, M. (2013). Thermal characterization of nitrates and nitrates/expanded graphite mixture phase change materials for solar energy storage. *Energy Conversion and Management*, *73*: 86-94.

Xu, Z., and Kleinstreuer, C. (2014). Concentration photovoltaic–thermal energy co-generation system using nanofluids for cooling and heating. *Energy Conversion and Management*, *87*: 504-512.

Yang, K., and Zuo, C. (2015). A novel multi-layer manifold microchannel cooling system for concentrating photovoltaic cells. *Energy Conversion and Management*, *89*, 214-221.

Yazdanpanahi, J., Sarhaddi, F., and Adeli, M. M. (2015). Experimental investigation of exergy efficiency of a solar photovoltaic thermal (PVT) water collector based on exergy losses. *Solar Energy*, *118*, 197-208.

Yu, Z. T., Fang, X., Fan, L. W., Wang, X., Xiao, Y. Q., Zeng, Y., . . . Cen, K. F. (2013). Increased thermal conductivity of liquid paraffin-based suspensions in the presence of carbon nano-additives of various sizes and shapes. *Carbon*, *53*: 277-285.

Cui, Y., & Zhu, Q. (2012). *Study of photovoltaic/thermal systems with MgO-water nanofluids flowing over silicon solar cells*. Asia-Pacific Power and Energy Engineering Conference (pp. 1-4), March 2012, IEEE.

Zalba, B., Marín, J. M., Cabeza, L. F., and Mehling, H. (2003). Review on thermal energy storage with phase change: materials, heat transfer analysis and applications. *Applied Thermal Engineering*, *23*(3): 251-283.

Zarma, I., Ahmed, M., and Ookawara, S. (2019). Enhancing the performance of concentrator photovoltaic systems using Nanoparticle-phase change material heat sinks. *Energy Conversion and Management*, *179*: 229-242.

Zeng, J. L., Cao, Z., Yang, D. W., Sun, L. X., and Zhang, L. (2010). Thermal conductivity enhancement of Ag nanowires on an organic phase change material. *Journal of Thermal Analysis and Calorimetry*, *101*(1): 385-389.

Zhang, H., Gao, X., Chen, C., Xu, T., Fang, Y., & Zhang, Z. (2016). A capric–palmitic–stearic acid ternary eutectic mixture/expanded graphite composite phase change material for thermal energy storage. *Composites Part A: Applied Science and Manufacturing*, *87*: 138-145.

Zhang, Q., and Liu, J. (2017). Sebacic acid/CNT sponge phase change material with excellent thermal conductivity and photo-thermal performance. *Solar Energy Materials and Solar Cells*, *179*: 217-222.

Zhang, Z., and Fang, X. (2006). Study on paraffin/expanded graphite composite phase change thermal energy storage material. *Energy Conversion and Management*, *47*(3): 303-310.

Zhu, L., Boehm, R. F., Wang, Y., Halford, C., and Sun, Y. (2011). Water immersion cooling of PV cells in a high concentration system. *Solar Energy Materials and Solar Cells*, *95*(2): 538-545.

Zhu, L., Raman, A., Wang, K. X., Abou Anoma, M., and Fan, S. (2014). Radiative cooling of solar cells. *Optica*, *1*(1): 32-38.

Zhu, Q., and Si, L. (2012). Electrical outputs and thermal outputs of water/air cooled amorphous-silicon photovoltaic modules. Advances in Biomedical Engineering, *8*: 83.

Zou, D., Ma, X., Liu, X., Zheng, P., and Hu, Y. (2018). Thermal performance enhancement of composite phase change materials (PCM) using graphene and carbon nanotubes as additives for the potential application in lithium-ion power battery. *International Journal of Heat and Mass Transfer*, *120*: 33-41.